DTU Mechanical Engineering
Department of Mechanical Engineering

Numerical and experimental study of flow in choanoflagellates and choanocytes

Seyed Saeed Asadzadeh

PhD Thesis

Numerical and experimental study of flow in choanoflagellates and choanocytes

By
Seyed Saeed Asadzadeh

A dissertation submitted to The Technical University of Denmark (DTU)
as partial fulfillment of the requirements for the degree of Ph.D
(Philosophiae Doctor)

Thesis submitted:	Month 08, 2019
PhD Supervisor:	Prof. Jens Honoré Walther
	Technical University of Denmark (DTU)
	ETH Zürich

Preface

This dissertation concludes the work carried out in a Ph.D. project at the Department of Mechanical Engineering at the Technical University of Denmark during the period August 1, 2016 – July 31, 2019. The content of this dissertation is original work where most parts have been published in scientific journals or presented at conferences.

Published journal papers

1. Nielsen, L.T., **Asadzadeh, S.S**., Dölger, J., Walther, J.H., Kiørboe, T. and Andersen, A., 2017. Hydrodynamics of microbial filter feeding. Proceedings of the National Academy of Sciences, 114(35), pp.9373-9378.

2. **Asadzadeh, S.S**., Nielsen, L.T., Andersen, A., Dölger, J., Kiørboe, T., Larsen, P.S. and Walther, J.H., 2019. Hydrodynamic functionality of the lorica in choanoflagellates. Journal of the Royal Society Interface, 16(150), p.20180478.

3. **Asadzadeh, S.S**., Larsen, P.S., Riisgård, H.U. and Walther, J.H., 2019. Hydrodynamics of the leucon sponge pump. Journal of the Royal Society Interface, 16(150), p.20180630.

There are two manuscripts in preparation which I have contributed but are not included in this dissertation:

- Sørensen, S., **Asadzadeh, S.S**., Walther, J.H., Hydrodynamics of prey capturing and transportation in choanoflagellates.

- Larsen, P.S., **Asadzadeh, S.S**., Riisgård, H.U. and Walther, J.H., Hydrodynamics of ascon and sycon sponge pumps.

I gratefully acknowledge funding support from DTU MEK and from VILLUM FONDEN through the research grant (9278).

Personal Acknowledgement

During this work, I had the opportunity to work with many researchers and scientists from different disciplines who I learned a lot from.

I would like to thank my supervisor Jens H. Walther for his excellent supervision along with many useful, constructive and encouraging discussions. He was friendly, patient and always available for discussions. I sincerely enjoyed working with him.

I also would like to thank Poul S. Larsen and Knud E. Mayer for the discussions on the Sponge project. Poul was enthusiastic about the project and we would often discuss and exchange ideas that were very useful and constructive in progress of the thesis. I also would like to thank Sponge project group who during our half-year meetings had many positive biological feedback on this work.

I had also the privilege to work with Thomas Kiørboe and Anders Andersen who were like an inspiring and encouraging teacher to me. Thomas' mature comments and feedback were always to the point with a broad outlook on the work. Anders' meticulous and positive feedback on the mathematical modeling were of a great help to me.

I further want to thank Lasse T. Nielsen, Julia Dölger, and Emily Riley for great discussions during our weekly fluid dynamic meetings.

I would like to thank Mimi A. R. Koehl for hosting me during my external stay in her lab at University of California, Berkeley. It was a great opportunity for me to meet and work closely with her. I learned a lot from her on the experimental side of this thesis. I would also like to thank King lab group for providing us with the culture of choanoflagellates during my stay at UC, Berkeley.

During my external stay, I had also the opportunity to spend some time and work with imaginative scientist Manu Prakash at Stanford. It was a great and fun experience visiting and interacting with Prakash group.

I would like to thank Siv Sørensen for her interest and involvement in the choanoflagellate project and for her great and unique work in accomplishing the project.

Finally, I am very grateful for the support of my friends and family, specially my wife Simin who were always supportive and understanding during this work.

Abstract

The present thesis uses mainly three dimensional computational fluid dynamics (CFD) along with experiments to study hydrodynamics of choanoflagellates and choanocytes of leuconoid sponges. Choanoflagellates are unicellular eukaryotes that are ubiquitous in aquatic habitats. They are morphologically similar to choanocytes of sponges and believed to be sister group to animals. Both chaonoflagellates and choanocytes have a single flagellum that creates a flow toward a collar filter composed of filter strands that extend from the cell. Leuconoid sponges are filter-feeders with a complex system of branching inhalant and exhalant canals leading to and from the close-packed choanocyte chambers. Each of these choanocyte chambers hold many choanocytes that act as pumping units delivering the relatively high pressure needed to overcome the system pressure losses in canals and constrictions. In this thesis, we first study hydrodynamics of choanoflagellates, specifically morphological adaptations for their flagellum to create adequate flow through the collar filter. We show that observed feeding flow is inconsistent with hydrodynamics of choanoflagellates based on a 'naked' flagellum. Instead, addition of a flagellar vane, a wing-like structure sporadically observed in some species of chonaoflagellates, to both CFD and theoretical models reasonably accounts for the observed flow. Next, we explore hydrodynamic functionality of the lorica, an elaborate extra-cellular structure in choanoflagellates the function of which has remained unknown. Our results provide no support for the several previous hypotheses, i.e. an increased flow rate through the collar and slowing down the motion through increasing drag. Instead, we argue that the main function of the lorica is to enhance the capture efficiency, but this happens at the cost of lower encounter rate with motile prey. We subsequently explore hydrodynamics of leucon sponges. We show that simply a collection of choanoflagellates with many flagella cannot account for the relatively high pressure measured and estimated for sponges. Instead, some detailed morphological adaptations and additional design elements, i.e. the minimal gap between flagellar vane and collar, the glycocalyx mesh on the collar, and the secondary reticulum, are crucial to the functionality of the choanocyte pump. Finally, we investigate hydrodynam-

ics of fast swimmer choanoflagellates, a dispersal life form of some species of choanoflagellates, near surfaces and explore the possible hydrodynamic impacts on their trajectory. We find that unless very close to a surface, hydrodynamics does not substantially affect their trajectory, but rather their initial swimming direction (and possible flicks) are the determining factor in directing them toward surfaces. However, we find that hydrodynamics benefit fast swimmers in keeping them close to a surface while they navigate arguably looking for a suitable position to attach themselves to the surface; an attachment that seems purposeful, that is to differentiate into feeding thecate cells, but does not happen in the absence of bacteria.

Resumé

Nærværende afhandling benytter tre-dimensionale computational fluid dynamics (CFD) samt eksperimenter for at studere hydrodynamik af choanoflagellater og choanocytter af leuconoid svampe. Choanoflagellater er encellede eukaryoter, der er allestedsnærværende i akvatiske levesteder. De ligner morfologisk choanocytter af svampe og antages at være søstergruppe til dyr. Både chaonoflagellater og choanocytter har et enkelt flagellum, der skaber en strømning mod et kravefilter, der består af filterstrenge, der strækker sig fra cellen. Leuconoid svape har et komplekst system med forgrenede ind- og udløbskanaler, der fører til og fra de tætpakkede choanocytkamre. Hvert af disse choanocytkamre har mange choanocytter, der fungerer som pumpeenheder, der leverer den relativt høje trykstigning, der er nødvendig for at overvinde systemets tryktab i kanaler og indsnævringer. I denne afhandling studerer vi først hydrodynamik af choanoflagellater, specifikt morfologiske tilpasninger til deres flagellum for at skabe tilstrækkelig strøm gennem kravefilteret. Vi viser, at den observerede fødestrøm er uforenelig med hydrodynamik af choanoflagellater baseret på en 'nøgen' flagellum. I stedet giver tilføjelse af en flagellær vinge, en vinge-lignende struktur sporadisk observeret i nogle arter af chonaoflagellater, god overensstemmelse mellem CFD og teoretiske modeller med den observerede strøm. Dernæst udforsker vi hydrodynamisk funktionalitet af lorica, en detaljeret ekstra-cellulær struktur i choanoflagellater, hvis funktion er forblevet ukendt. Vores resultater giver ingen støtte til de flere tidligere hypoteser, dvs. en øget strømningshastighed gennem kraven og at den skulle bremse bevægelsen gennem stigende vand modstand. I stedet argumenterer vi for, at hovedfunktionen med lorica er at øge fangsteffektiviteten, men dette sker på bekostning af lavere sandsynlighed for fangst af bevægeligt bytte. Vi udforsker efterfølgende hydrodynamik af leuconsvampe. Vi viser, at en samling af choanoflagellater med mange flageller ikke kan redegøre for det relativt høje tryk, der er målt og estimeret for svampe. I stedet er nogle detaljerede morfologiske tilpasninger og yderligere designelementer, dvs. det minimale mellemrum mellem flagellær vinge og krave, glycocalyxnet på kraven og det sekundære retikulum, afgørende for funktionaliteten af choanocytpumpen. Endelig undersøger vi

hydrodynamik af hurtigt svømmende choanoflagellater, en spredningslivsform for nogle arter af choanoflagellater, nær overflader og udforsker de mulige hydrodynamiske påvirkninger på deres bane. Vi finder, at med mindre meget tæt på en overflade, så har hydrodynamik ikke nogen væsentlig indflydelse på deres bane, men snarere deres oprindelige svømmeretning (og mulige flicks) er den afgørende faktor for at lede dem mod overflader. Vi finder dog, at hydrodynamik er til fordel for hurtigt svømmere ved at holde dem tæt på en overflade, mens de navigerer og leder efter en passende position til at fastgøre sig selv til overfladen; en fastgørelse, som synes målrettet, med efterfølgende differentiering til thecatcelle, dog ikke i fraværd af bakterier.

Contents

Part I

Introduction

Introduction

1 Choanoflagellates and choanocytes of sponges

Choanoflagellates are a group of free-living unicellular and colonial flagellate eukaryotes. They are filter feeders and an important component of microbial foodwebs [5, 10]. They share ancestry with animals (Fig. 1) and have remarkably common characteristics with choanocytes of sponges [13]. Sponges are multicellular organisms that have bodies full of pores and channels allowing water to circulate through them with numerous closely packed choanocytes. Choanoflagellates and choancytes are morphologically similar: They both contain a flagellum surrounded by a collar of microvilli which extend from the cell. As the flagella beat, it creates a water flow across the microvilli which can then filter nutrients. Food particles are then phagocytosed by the cell [4]. During the past century, choanoflagellates and choanocytes have been subject to numerous studies with the goal of understanding the evolution of multicellularity in animals [7, 13, 14, 17]. In this report, we study hydrodynamics of choanoflagellates and choanocytes in an attempt to understand how they function and what morphological adaptation has been required to function properly in a flow at small scales.

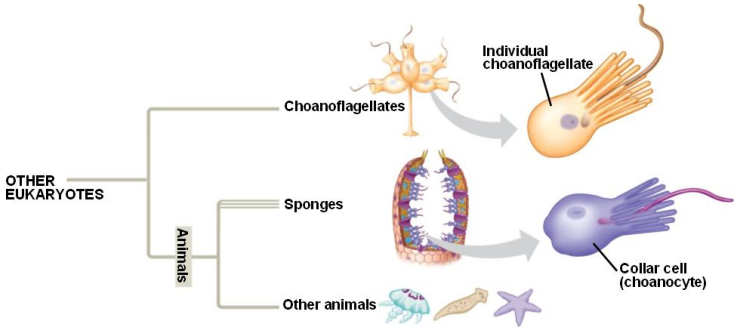

Fig. 1: A simple tree of life, branch of eukaryotes. showing choanoflagellates as sister group to animals. (http://www.bio.miami.edu).

2 Flow at low Reynolds number

The governing equations of an incompressible Newtonian fluid with density ρ and viscosity μ are the continuity and Navier-Stokes equations:

$$\nabla \cdot \mathbf{u} = 0 \tag{1}$$

$$\rho \left(\frac{\partial \mathbf{u}}{\partial t} + (\mathbf{u} \cdot \nabla)\mathbf{u} \right) = -\nabla p + \mu \nabla^2 \mathbf{u} \tag{2}$$

where $\mathbf{u}$ and p denote the velocity and pressure, respectively. In the small scale world of choanoflagellates and choanocytes the Reynolds number, the ratio of inertia to viscous forces, is small, typically $\mathrm{Re} = \rho V L/\mu = 10^{-2}$–$10^{-4}$, employing $L = 5$-$25\,\mu$m the flagellar central length, and $V = \lambda f$ the wave speed, in which $f = 5$-50 Hz is the beat frequency, and $\lambda = 5$-$30\,\mu$m the wavelength [13].

An important consequence of low Re number is that inertia terms are negligible, hence flow motion is reversible. This means that reciprocal motions cannot generate a net flow or locomotion [19]. Therefore, motions employed by large marine organisms would not be beneficial for smaller organisms. In fact, it has been reported that these hydrodynamic constraints on the ubiquitous feeding mechanism using a mouth in the first-feeding larvae fishes result in a hydrodynamic starvation with a mortality rates $> 99\%$ within days of hatching [2]. On the other hand, many of smaller organisms such as filter feeding choanoflagellates and choanocytes have evolved an efficient way of feeding by beating their flagella. The flagellum beat is non-reciprocal and almost a propagating wave which has a direction and always drive the flow through the collar filter where the prey is being captured.

3 Hydrodynamics of choanoflagellates

3.1 Presence of the vane on the flagella

Eukaryotic flagella (and cilia), the body part responsible for driving the flow, have a common characteristic: the cross section of the axoneme, the core of the flagellum, consists of 9 microtubes doublets spaced on the circumference along the flagellum + 2 microtubes along the center (Fig 2). Molecular motors (dynein) between the doublets slide them back and force giving rise to the flagellum deformation. Diameter of the flagellum is typically around 0.2-0.4 μm. Despite this common structure, in some species of choanoflagellates and choancytes it has been observed that their flagellum is not just a 'naked' filament, but also has a hairy wing-like structure called vane that extrudes from two sides of the flagellum [6, 13, 16, 21]. However, these observations

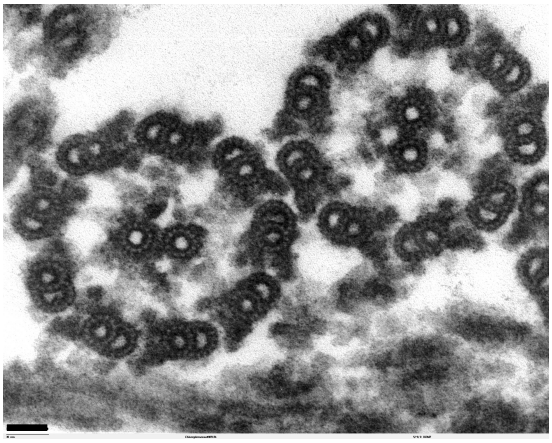

Fig. 2: Flagella (of Chlamydomonas) have the "9+2" structure characteristic of all eukaryotic cells. The axoneme has a central unit containing two single microtubules and nine peripheral doublet microtubules (known as the "9+2"). Scale bar 30 nm. (http://remf.dartmouth.edu/imagesindex.html).

have been sporadic and since the vane appears as a thin and delicate structure (nm), it is notoriously difficult to visualize the vane [9].

In the paper A in this report, we try to address this puzzling presence of the vane in choanoflagellates by studying the hydrodynamics of these microbial filter feeding. Specifically, what is hydrodynamically required for creating adequate flow through the collar? In doing so, the feeding flow around loricate choanoflagellate *Diaphanoeca grandis*, as a model organism, is quantified using particle tracking. A flagellar vane has not been yet reported for this species (Fig 3). CFD then is employed to simulate the generated flow with a naked flagellum and with inclusion of a flagellar vane. The CFD results indicate that simply a naked flagellum cannot generate enough flow (Fig A.2, therein), and the observed high flow rate through the collar filter of *D. grandis* can be explained by the inclusion of the flagellar vane (Fig A.3, therein). The result has been extended to other species of choanoflagellates using a simple theoretical model (Eq. A.3 therein) which predicts the flow rate generated by a naked flagellum (Q_T), and a proposed pumping mechanisms by a flagellar vane ($Q_V = AW\lambda f$, Eq. A.4 therein). In fact, Q_V provides an accurate prediction of the observed clearance rate (Q) in six of the seven species for which the naked flagellum clearance rate estimate Q_T cannot account for Q (Table A.1, therein).

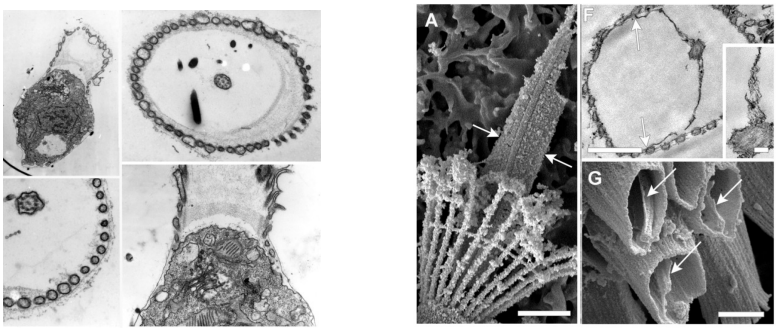

Fig. 3: Left: *Diaphanoeca grandis* (by Helge A. Thomsen). Right: Flagellar vane in choanoflagellate *Monosiga brevicolis* and sponge *Spongilla lacustris* [13].

3.2 Hydrodynamic functionality of the lorica

Some choanoflagellates (over 150 species) construct a very ornate extra-cellular basket-like structure, known as the lorica (Fig. 4), the function of which has remained unknown. Despite extensive research on the morphology, construction, and assembly of the lorica [10], there are only few and limited studies on its functionality, and the presence of this structure has puzzled scientists for almost a century. Beside providing protection, it has been suggested that the lorica acts in a hydrodynamic sense by funneling the inflow through the lorica and increases the water flow through the collar [1].

In paper B, we study the possible hydrodynamic functionality of the lorica in choanoflagellates and test previously proposed functionality. We use *D. grandis* as the model organisms, and analyze the flow around and forces on different parts of the organism with and without its lorica to elucidate its effect. Moreover, modeling the Brownian motion and motility of bacteria-sized prey as a passive scalar field subject to an effective diffusivity representing the size and motility of the prey, we determine the advective-diffusive transport of the passive scalar to the collar filter. Our CFD results show no support for the previous hypotheses: specifically, it does not lead to an increased clearance rate. However, the clearance rate is only a suitable measure of particle encounter and it does not represent the whole feeding process in filter feeding. Filter feeding process is three main steps: prey encounter, retention and handling [20]. Fig. 5 show the process of prey capture and ingestion by thecate non-loricate choanoflagellate *Salpingoeca rosetta*. In this process, it has been often observed that after contact of bacteria with the collar and remaining there for several seconds, they slip off the end of the collar without being phagocytosed [4, 18]. This observation lead us to analyzing the details of flow in between microvilli of *D. grandis* with and without its lorica. The results show a 'back-flow' at the distal part of the collar which could be responsible

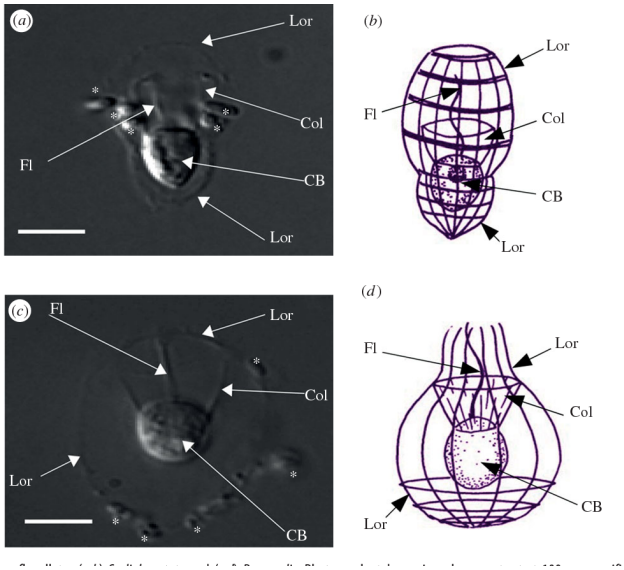

Fig. 4: The loricate choanoflagellates (a,b) *Stephanoeca diplocostata* and (c,d) *Diaphanoeca grandis*. Lor, Lorica; CB, cell body; Fl, flagellum; Col, collar. Bacteria in the photographs are annotated with asterisks (*). Scale bar, 5 mm. Images from [15].

for washing off the prey. However, the lorica reduces the 'back-flow' through the filter (Fig. B.9, therein) and thus may improve prey retention on the collar filter which suggests that the main function of the lorica is to enhance the capture efficiency.

4 Hydrodynamics of leucon sponges

Sponges have three different body structures: Asconoid, Syconoid, and Leuconoid (Fig. 6). Asconoid, the simplest body structure is a tube or vase shape where choanocytes sit in a single layer on the surface of the body wall. Because of limitations in the number of choanocytes in such body structure, they seldom exceed 1 mm in diameter. Syconoid sponges are larger structure, in which the body wall is pleated which allows more choancytes sitting on the inner walls, hence increasing its capacity to pump water. In leuconoid structure, the capacity even increases further, by filling the interior almost completely with a network of chambers lined with choanocytes. These kind of sponges can grow to over 1 m in diameter, since the growth in any directions provides room and the number of choanocyte chambers can increase with the sponge volume. Employing many of these choancyte chambers, this sponge type can generate strong and impressive flow through their body

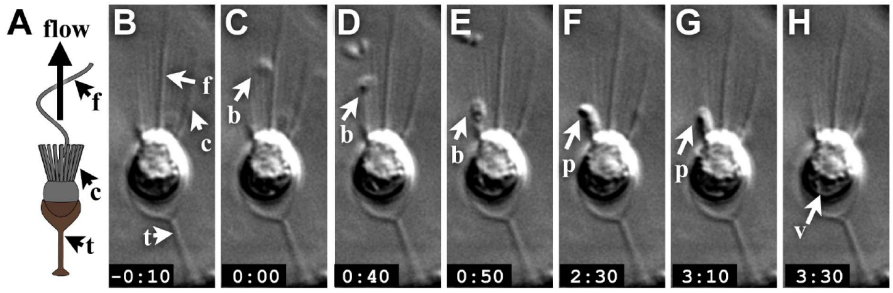

Fig. 5: The process of prey capture and ingestion by thecate cells reported by [4]: (A) Schematic of a thecate cell. (B-G) A time series from a time-lapse movie of a thecate cell shows phagocytosis of a bacterium at the base of the collar. A bacterial cell arrived at the collar at t = 0:00 (C), then moved around the collar and reached the base (E) where it remained for $\sim$ 2 minutes before being phagocytosed (F, G) and transported into the cell (H).

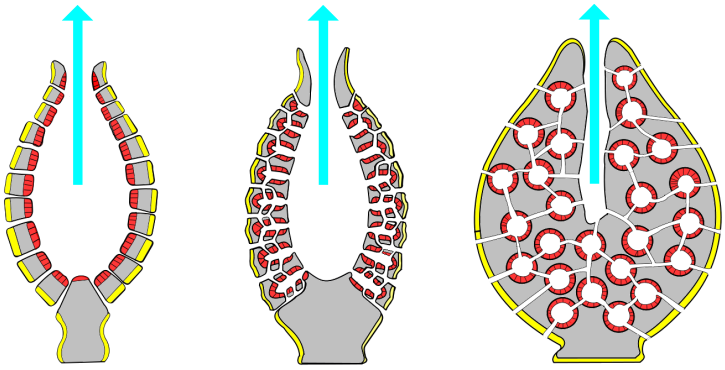

Fig. 6: Three different sponge body structure. From left to right: Asconoid, Syconoid, and Leuconoid. Ascon sponges are the simplest and least common sponge body from. b) Sycon sponges are more complex than ascon sponges but are simpler than leucon sponges. c) leucon sponges are the most complex of the sponge body forms and also most common. Yellow: flat cells pinacocytes, Red: choanocytes, Grey: gelatinous matrix mesohyl Pale, blue: water flow (https://en.wikipedia.org/wiki/Sponge)

Fig. 7: The pumping action of a sponge: A non-toxic yellow dye has been squirted around the base of the sponge and shortly thereafter, the dye is pumped out through the osculum at the top of the sponge. (www.oceanicresearch.org/education/wonders/sponges.html).

(Fig. 7). Figure 8 illustrates the path of water through the sponge body, and different sizes of chaonocyte chambers from different species of sponges. In this thesis, we focus on hydrodynamics of leucon sponges as the most common and complex sponges.

From choanoflagellates to choanocytes

Functionally, choanoflagellates are similar to a ventilation fan as they are operating in free space with a relatively small pressure drop through the collar. The aim for a fan is to optimize the flow rate. However, choanocytes are part of a larger structure and analogous to mechanical pumps, i.e. in addition to creating the flow, they need to deliver a pressure to drive the flow through the narrow channels in the sponge body. From direct measurement performed by Larsen et al. [8] of demosponge *Haliclona urceolus* and estimated values of pressure resistance in canal systems for different species of sponges [11, 12], the required pressure rise is calculated as $\approx$ 1-3 mmH_2O. The fact that many choanocytes (30-80) sit inside one chamber might suggest that this collection of choancytes inside one chamber can give rise to the required high pressure as a result of interaction between the flagella. To test this hypothesis, we simulate an infinite array of choanoflagellates using periodic boundary conditions (Fig. 9A). The CFD results show that the maximum pressure delivered by an infinite array of choanoflagellates (even with a flagellar vane) is two orders of magnitudes smaller than what is required (Fig. 9B).

The similarity between the choanoflagellates and choanocytes of sponges

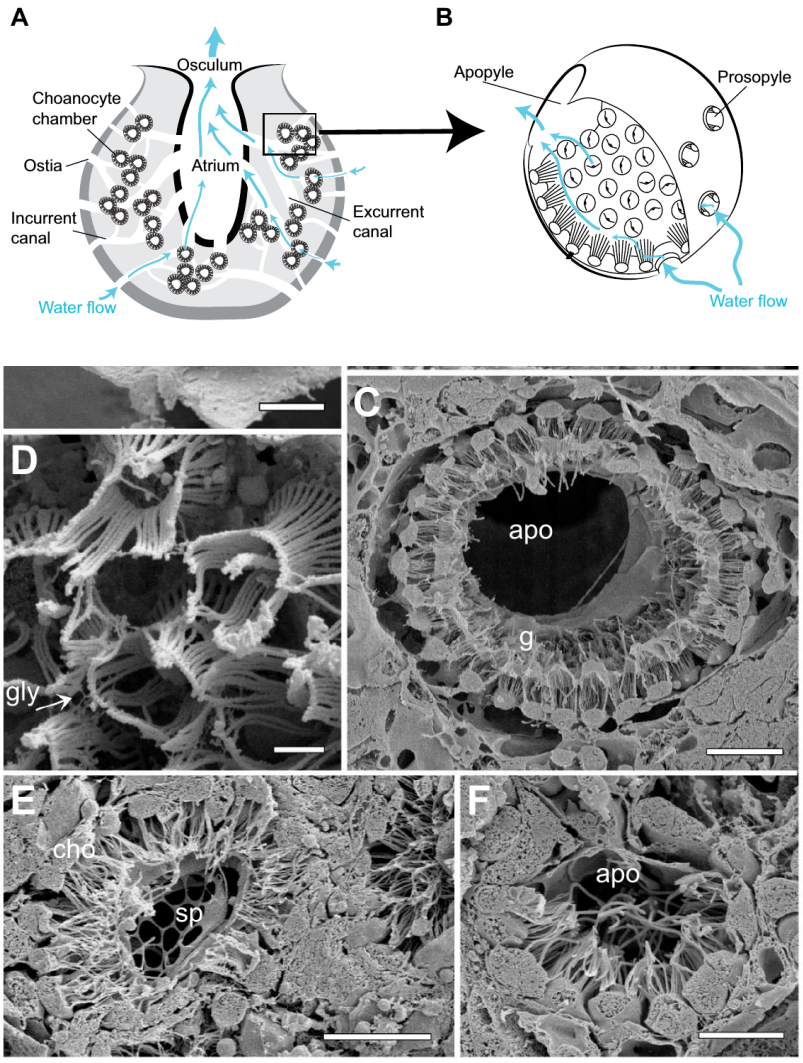

Fig. 8: Schematic illustrating the path of water through the aquiferous system of sponges. (A) Water enters through pores (ostia) on the sponge surface, into incurrent canals to the choanocyte chambers, where the water is filtered, then out through the excurrent canals to the osculum. (B) Water enters the choanocyte chamber through prosopyles and exits via the apopyle. (C-D) Scanning electron micrographs of choanocyte chambers in four species of demosponges. (C) Large choanocyte chamber in *Haliclona mollis* . (D) *Neopetrosia problematica*. (E) *Tethya californiana*. (F) Smaller choanocyte chamber in *Cliona delitrix*. Scale bars: (B) 2 μm; (C,E) 10 μm; (D) 1μm; (F) 5μm. Taken from [12].

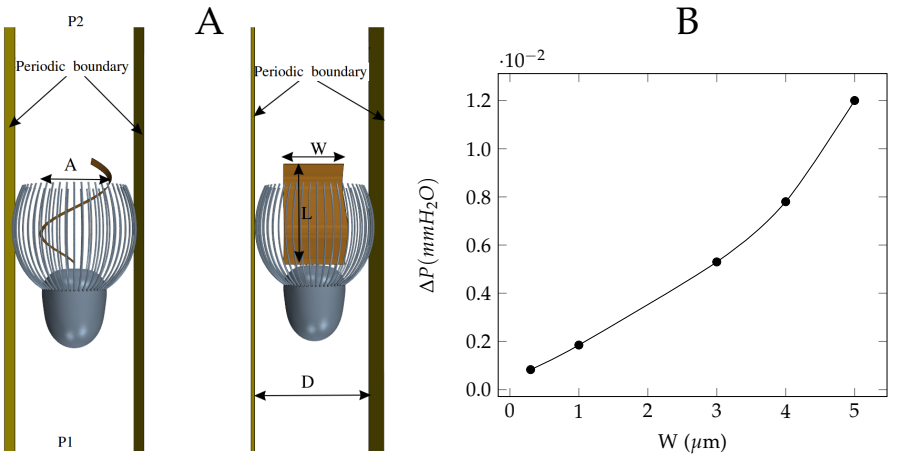

Fig. 9: A) CFD setup for simulations of an infinite array of choanoflagellates using periodic boundary conditions. B) The maximum pressure delivered by an infinite array of choanoflagellates (with a flagellar vane, *W* the width of the vane) is two orders of magnitudes smaller than what is estimated from measurements.

has been discussed for a century [14, 16]. However, few studies have quantified detailed dissimilarities in their morphology. Recently, Mah et al. (2014) found some subtle differences (Fig. 10); First, in choanoflagellates the observed vane spans the width of the collar at the base whereas in choanocytes the vane spans the width of the collar at the most part. Second, in choanoflagellates, spacing between microvilli increases from the bases to the tips, leading to big gaps between the flagellar vane and the collar filter, while in choanocyte, the microvilli are held tightly together by the glycocalyx mesh for the distal two-thirds of the collar. Moreover, edges of the flagellum in choancytes becomes in contact with the collar during the beat cycle. Despite this detailed description, the study fails to relate these differences to the functionality of these two cell types.

In paper C, accounting for above differences, we study hydrodynamics of leucon sponges. The paper demonstrates that all those detailed morphological differences between choanoflagellates and choanocytes are vital to the functionality of choanocytes where they now act as a pumping unit. We derive a simple theoretical model based on a minimal gap between the flagellar vane and the microvilli, which can predict the pump characteristics of sponges and is in a very good agreement with the available experiment data (Fig C.3, therein). In addition, we also simulate one choanocyte inside chamber using appropriate boundary conditions to study the effects of different parts of the the chamber. We find that both the impermeable glycocalyx-mesh covering the upper part of the collar, and the secondary reticulum are

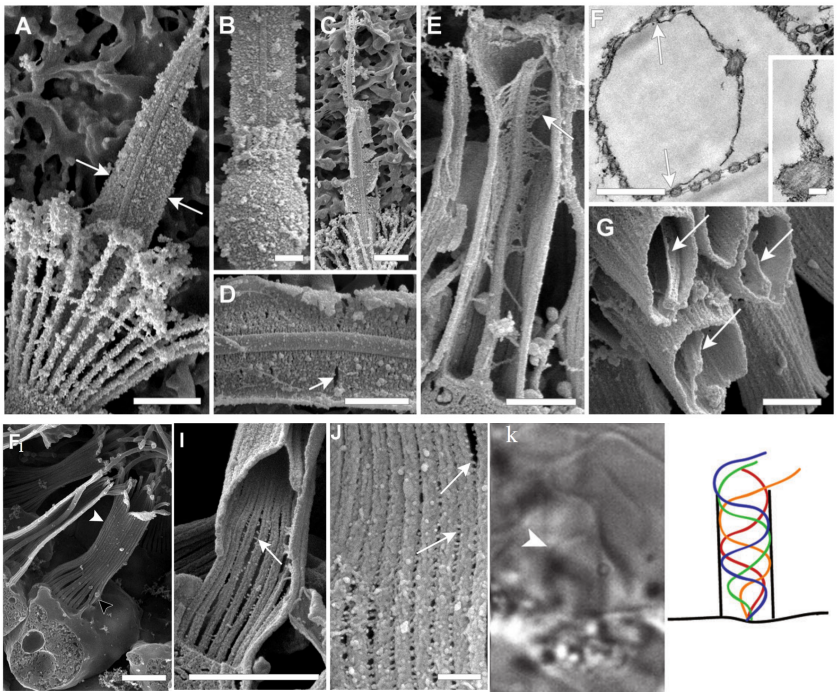

Fig. 10: Morphology differences in Monosiga brevicollis and Spongilla lacustris. A-E, G: Scanning electron microscopy; F: Transmission electron microscopy. (A, C, D) The flagellar vane of M. brevicollis. (B) A short-collared M. brevicollis dispersal cell showing the vane spans the width of the base of the collar. (E) A choanocyte from S. lacustris shows the flagellar vane spans the width of the collar. ((F) Cross-section of a choanocyte showing the vane spans the diameter of the collar with its edges touching the collar wall (arrows). High magnification of the vane in S. lacustris (inset). (G) Fracture of collars in S. lacustris showing the edges of the vane (arrows) in contact with the collar. (F1) An S. lacustris choanocyte. Spacing between microvilli is widest near the collar base, forming a bulge (black arrowhead) that narrows into a tight cylinder (white arrowhead). (I) S. lacustris choanocyte collar showing the glycocalyx mesh fibrils (arrow). (J) In S. lacustris, at higher magnification the glycocalyx mesh appears as small fibers (arrows) closely linking adjacent microvilli. (K) The flagellum beats in a single plane, as shown in the image to the left (double-headed arrows indicate the flagellar wave form). The drawing on the right shows tracings of successive frames of the flagellar beat seen perpendicular to the plane of beat; single-headed arrows and arrowheads mark the progression of peaks in the flagellar waveform. (Scale bars: A, 2 mm; G, 1 mm; F (inset), 100 nm, I, 2 mm; J, 300 nm.) Taken from [13].

indispensable features for the choanocyte pump to deliver the observed high pressures.

5 Fast swimmer choanoflagellates near surfaces

Finally, in the last section, we study fast swimmer choanoflagellates, a different life form of choanoflagellates that lack the collar filter. Fast swimmers are believed to be dispersal life form of choanoflagellates [3], but it remains yet unknown whether (and how) this dispersal form is used in conjunction with physical or chemical sensing.

In paper D (unpublished), both experimentally and numerically we study the possible hydrodynamic effects of nearby surfaces on the trajectory of the fast swimmers and the possible hydrodynamic interaction with nearby surfaces their navigation.

References

[1] P. Andersen, "Functional biology of the choanoflagellate *Diaphanoeca grandis Ellis*," *Marine Microbial Food Webs*, vol. 3, no. 2, pp. 35–50, 1988.

[2] V. China and R. Holzman, "Hydrodynamic starvation in first-feeding larval fishes," *Proc. Natl. Acad. Sci. USA*, vol. 111, no. 22, pp. 8083–8088, 2014.

[3] M. Dayel, R. Alegado, S. Fairclough, T. Levin, S. Nichols, K. McDonald, and N. King, "Cell differentiation and morphogenesis in the colony-forming choanoflagellate *Salpingoeca rosetta*," *Develop. Biol.*, vol. 357, no. 1, pp. 73–82, 2011.

[4] M. Dayel and N. King, "Prey capture and phagocytosis in the choanoflagellate *Salpingoeca rosetta*," *PLoS One*, vol. 9, no. 5, p. e95577, 2014.

[5] T. Fenchel, "Suspended marine bacteria as a food source," in *Flows of energy and materials in marine ecosystems*. Springer, 1984, pp. 301–315.

[6] E. J. Fjerdingstad, "The ultrastructure of choanocyte collars in *Spongilla lacustris* (l.)," *Z. Zellforsch.*, vol. 53, no. 5, pp. 645–657, 1961.

[7] N. King, M. J. Westbrook, S. L. Young, A. Kuo, M. Abedin, J. Chapman, S. Fairclough, U. Hellsten, Y. Isogai, I. Letunic *et al.*, "The genome of the choanoflagellate monosiga brevicollis and the origin of metazoanss," *Nature*, vol. 451, no. 7180, p. 783, 2008.

[8] P. S. Larsen and H. U. Riisgård, "The sponge pump," *J. Theor. Biol.*, vol. 168, pp. 53–63, 1994.

[9] B. S. C. Leadbeater, "The mystery of the flagellar vane in choanoflagellates," *Nova Hedwigia Beiheft*, vol. 130, p. 213, 2006.

[10] B. S. Leadbeater, *The Choanoflagellates: Evolution, Biology and Ecology*, 1st ed. Cambridge: Cambridge University Press, 2015.

[11] S. P. Leys, G. Yahel, A. Reidenbach, V. Tunnicliffe, U. Shavit, and H. Reiswig, "The sponge pump: the role of current induced flow in the design of the sponge body plan," *PLoS One*, vol. 6, no. 12, p. e27787, 2011.

[12] D. A. Ludeman, M. A. Reidenbach, and S. P. Leys, "The energetic cost of filtration by demosponges and their behavioural response to ambient currents," *J. Exp. Biol.*, vol. 220, no. 6, pp. 995–1007, 2017.

[13] J. L. Mah, K. K. Christensen-Dalsgaard, and S. P. Leys, "Choanoflagellate and choanocyte collar-flagellar systems and the assumption of homology," *Evol. & Develop.*, vol. 16, no. 1, pp. 25–37, 2014.

[14] M. Maldonado, "Choanoflagellates, choanocytes, and animal multicellularity," *Invert. Biol.*, vol. 123, no. 1, pp. 1–22, 2004.

[15] A. O. Marron, M. J. Alston, D. Heavens, M. Akam, M. Caccamo, P. W. Holland, and G. Walker, "A family of diatom-like silicon transporters in the siliceous loricate choanoflagellates," *Proceedings of the Royal Society B: Biological Sciences*, vol. 280, no. 1756, p. 20122543, 2013.

[16] D. Mehl and H. M. Reiswig, "The presence of flagellar vanes in choanomeres of Porifera and their possible phylogenetic implications," *J. Zoo. Sys. Evol. Res.*, vol. 29, no. 4, pp. 312–319, 1991.

[17] J. K. Nielsen, H. K. Rasmussen, and O. Hassager, "Stress relaxation of narrow molar mass distribution polystyrene following uniaxial extension," *J. Rheol.*, vol. 52, no. 4, pp. 885–899, 2008.

[18] M. E. Pettitt, B. A. A. Orme, J. R. Blake, and B. S. C. Leadbeater, "The hydrodynamics of filter feeding in choanoflagellates," *Eur. J. Protist.*, vol. 38, pp. 313–332, 2002.

[19] E. M. Purcell, "Life at low Reynolds number," *Am. J. Phys.*, vol. 45, no. 1, pp. 3–11, 1977.

[20] J. Shimeta and M. A. R. Koehl, "Mechanisms of particle selection by tentaculate suspension feeders during encounter, retention, and handling," *J. Exp. Mar. Biol. Ecol.*, vol. 209, no. 1-2, pp. 47–73, 1997.

[21] N. Weissenfels, "The filtration apparatus for food collection in freshwater sponges (Porifera, Spongillidae)," *Zoomorph.*, vol. 112, no. 1, pp. 51–55, 1992.

Part II

Articles

Article A

Hydrodynamics of microbial filter-feeding

Lasse Tor Nielsen[1], **Seyed Saeed Asadzadeh**[2], Julia Dölger[3], Jens Honoré Walther[2,4], Thomas Kiørboe[1], Anders Andersen[3]

[1]National Institute of Aquatic Resources and Centre for Ocean Life, Technical University of Denmark, DK-2800 Kgs. Lyngby, Denmark
[2]Section for Fluid Mechanics, Coastal and Maritime Engineering, Department of Mechanical Engineering, Technical University of Denmark, Nils Koppels Allé, 2800 Kgs. Lyngby, Denmark.
[3]Department of Physics and Centre for Ocean Life, Technical University of Denmark, DK-2800 Kgs. Lyngby, Denmark
[4]Computational Science and Engineering Laboratory, ETH Zürich, Clausiusstrasse 33 ETH-Zentrum, CH-8092 Zürich, Switzerland

This is a revised layout of the article published in *Proc. Natl. Acad. Sci. USA* Vol. 114, pp. 9373–9378, 2017.

Contributions

Major contributions to the work:

- Carrying out presented CFD simulations.

Minor contributions to the work:

- Internal review of the manuscript.

Abstract

Microbial filter-feeders are an important group of grazers, significant to the microbial loop, aquatic food webs, and biogeochemical cycling. Our understanding of microbial filter-feeding is poor, and importantly, it is unknown what force microbial filter-feeders must generate to process adequate amounts of water. Also, the trade-off in the filter spacing remains unexplored, despite its simple formulation: A filter too coarse will allow suitably-sized prey to pass unintercepted, whereas a filter too fine will cause strong flow resistance. We quantify the feeding flow of the filter-feeding choanoflagellate Diaphanoeca grandis using particle tracking, and demonstrate that the current understanding of microbial filter-feeding is inconsistent with computational fluid dynamics (CFD) and analytical estimates. Both approaches underestimate observed filtration rates by more than an order of magnitude: The beating flagellum is simply unable to draw enough water through the fine filter. We find similar discrepancies for other choanoflagellate species, highlighting an apparent paradox. Our observations motivate us to suggest a radically different filtration mechanism that requires a flagellar vane (a sheet), something notoriously difficult to visualize but sporadically observed in the related choanocytes (sponges). A CFD model with a flagellar vane correctly predicts the filtration rate of D. grandis, and using a simple model we can account for the filtration rates of other microbial filter-feeders. We finally predict how optimum filter mesh size increases with cell size in microbial filter-feeders, a prediction that accords very well with observations. We expect our results to be of significance for small scale biophysics and trait-based ecological modeling.

1 Introduction

Heterotrophic microorganisms in the oceans inhabit a dilute environment and they need efficient feeding mechanisms in order to acquire enough food to sustain growth [1]. At the microscale the Reynolds number is low and viscous forces govern hydrodynamical interactions. This implies extensive, long-range flow disturbances around moving particles and microswimmers, impeding cell-cell contact and prey capture [2, 3]. However, to encounter enough food, purely heterotrophic plankton that rely solely on prey capture typically need to clear a volume of water for prey corresponding to one million times their own body volume per day [3]. Thus, heterotrophic microbes face a difficult challenge, and the prevailing viscous forces must strongly influence prey capture, and shape the various feeding modes through evolution.

Many unicellular flagellates as well as colonial sponges and metazoans, e.g., tunicates, use filter-feeding to catch bacteria-sized prey [1, 4–6]. They establish a feeding current, from which prey particles are sieved using filter structures. Such filter-feeders benefit from having filters with small mesh size

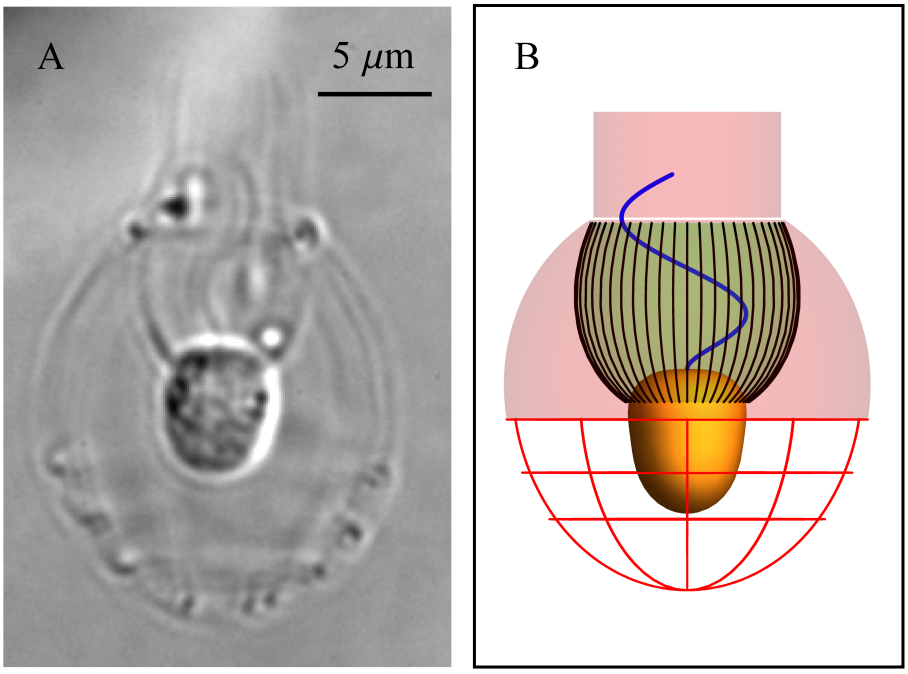

Fig. A.1: Morphology of *Diaphanoeca grandis*. (A) Microscope image of freely swimming choanoflagellate. (B) Model morphology with cell (orange), collar filter (green surface and black lines), flagellum (blue), and lorica (red). The ribs (costae) in the lower (posterior) part of the lorica are indicated, whereas for clarity the ribs in the finely netted, upper (anterior) part of the lorica are not shown.

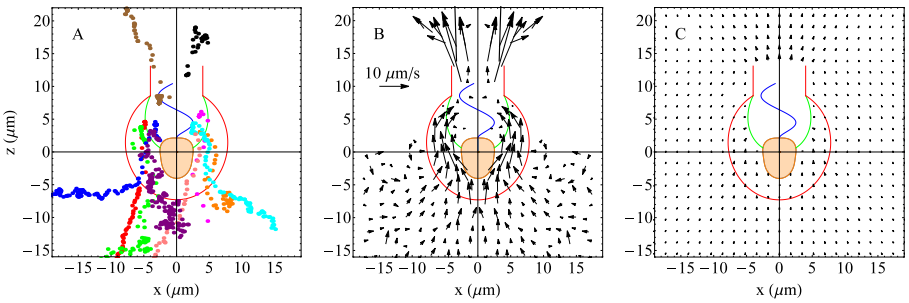

Fig. A.2: Observed feeding flow generated by *Diaphanoeca grandis* and velocity field from CFD model based on the standard description of morphology and flagellum. The model morphology shows the cell (orange), the collar filter (green), the flagellum (blue), and the lorica (red). (A) Representative particle tracks. The ten different colors correspond to ten discrete tracks and the dots show particle positions with 0.1 s time intervals. The particles below the choanoflagellate move randomly due to Brownian motion and display a slow net flow towards the lorica openings. (B) Average velocity field based on particle tracking. The flow velocities increase dramatically as the particles enter the lorica and approach the collar filter where the particles are eventually caught. The filtered water is expelled in a concentrated jet flow upwards and out of the "chimney" of the lorica opposite to and clearly separated from the intake region. (C) The CFD velocity field in the xz-plane is time-averaged over the flagellar beat cycle, and the velocity vectors "inside" filter and chimney are omitted for clarity. The CFD model based on the standard description of morphology and flagellum predicts a feeding flow that is more than an order of magnitude weaker than the experimentally observed flow, and it can not account for the observed clearance rate.

that allow the organisms to capture small prey [4, 7]. However, filter spacing involves a trade-off: The finer the mesh size, the higher the availability of food but the lower the clearance rate due to a dramatic decrease in filter permeability [8]. An optimum mesh size must therefore exist. While microbial filter-feeding has been studied regarding the pressure drop across the filter and the observed clearance rates [4], clearance rates have never been related to the force production of the flagellum that drives the feeding current. Can a beating flagellum even produce sufficient force to account for the observed clearance rates through such fine filters?

Choanoflagellates are the prime example of unicellular filter-feeders [1, 9, 10]. They are equipped with a single flagellum that is surrounded by a funnel-shaped collar filter made up of microvilli extending from the cell. Some species are sessile and attach with a stalk to solid surfaces whereas others are freely swimming and have a basket-like structure (lorica) that surrounds cell, flagellum, and filter (Fig. B.1). The beating flagellum creates a feeding current that transports bacteria-sized prey to the outside of the collar filter from where the prey are transported to the cell surface and phagocytosed [9, 11–15]. Far field flows created by choanoflagellates have recently been measured and modeled for the sessile choanoflagellate *Salpingoeca rosetta* [13]. However, the essential near cell feeding flow in choanoflagellates is poorly understood and has not been resolved quantitatively in experiments [9, 10].

As a model organism of microbial filter feeders, we focus on the choanoflagellate *Diaphanoeca grandis* that swims freely and carries a lorica (Fig. B.1). The lower part of the lorica has large openings, whereas the upper part is covered by a fine web with small pore sizes [12]. The collar filter therefore supposedly functions as an internal filter, and prey particles should not circumvent the filter once inside the lorica.

Using *D. grandis*, we here ask: What are the mechanisms of particle capture in choanoflagellates, and what is the optimum filter spacing? We use high-speed videography and particle tracking to quantify the feeding flow. For comparison, we use computational fluid dynamic (CFD) simulations and simple estimates of the filter resistance and the force production due to the beating flagellum. Our analysis shows that modeling the beating flagellum as a simple, slender structure produces a force that is an order of magnitude too small to account for the observed clearance rate. This demonstrates the strong trade-off in small-scale filter-feeding, and leads us to suggest an alternative flagellar pumping mechanism.

Table A.1: Characteristic morphological and kinematic parameters for selected choanoflagellate and choanocyte species.

Species	ESR (μm)	L (μm)	f (Hz)	A (μm)	λ (μm)	a (μm)	l (μm)	W (μm)	Q_T (μm^3 s^{-1})	Q_V (μm^3 s^{-1})	Q (μm^3 s^{-1})	References
Codosiga botrytis[1]	3.75	29.0	30.0	$^{\oplus}$6.4	17.5	0.088	0.25	$^{\oplus}$10.3	64	34,600	*2,600	[16, 17]
Codosiga gracilis[1]	1.84	8.3	10.0	‡1.5	10.3	0.075	0.54	‡5.5	42	850	1,000	[9, 18]
Diaphanoeca grandis[2]	2.50	11.0	10.0	4.0	10.0	0.075	0.40	8.0	65	3,200	4,400	[12]
Diaphanoeca grandis[2]	2.80	11.7	7.3	2.8	8.6	0.075	0.54	8.0	75	1,410	1,220	This study
Monosiga brevicollis[1]	†2.00	†13.8	50.0	2.4	12.2	0.055	0.45	6.6	476	9660	*400	[19]
Monosiga ovata[1]	1.26	6.0	14.4	$^{\perp}$2.0	$^{\perp}$15.8	0.100	0.28	$^{\perp}$4.4	3	2,340	1,800	[20, 21]
Monosiga sp.[1]	1.63	5.5	32.5	1.0	6.0	0.100	0.50	2.5	35	490	600	[1]
Salpingoeca amphoridium[1]	2.30	20.7	17.0	‡3.0	17.9	0.050	0.70	‡3.8	716	3,470	*600	[9]
Stephanoeca diplocostata[2]	1.80	8.3	10.0	‡2.0	8.6	0.075	0.47	‡5.4	40	930	4,400	[9, 18]
Spongilla lacustris[3]	$^{\perp}$2.00	10.4	11.0	$^{\perp}$1.5	12.2	0.060	0.18	3.1	2	620	*400	[19]

ESR=equivalent spherical radius of cell, L=flagellum length, f=flagellum beat frequency, A=amplitude of flagellar beat, λ=flagellar wavelength, a=microvillum radius, l=distance between centers of neighboring microvilli, W=chimney diameter, Q_T=theoretical estimate of clearance rate based on eq. A.4, Q_V= clearance rate estimate based on the presence of a vane according to eq. A.5 and Q=observed clearance rate from incubation experiments or similar. [1]Sessile. [2]Loricate, freely swimming. [3]Choanocyte. †Measured using original videos kindly provided by Mah et al. [19]. ‡Estimated from [9]. $^{\oplus}$Estimated from [17]. $^{\perp}$Estimated from [20]. *Data on Q was unavailable, and instead Q was estimated as one million cell volumes per day [3]. In species with different morphotypes, data are for single, sessile cells

Results

Observed Feeding Flow and Clearance Rate

We developed a generic model morphology of *D. grandis* in order to collate particle track observations from individual cells (Supporting Information and Fig. B.1). The feeding flow is driven by the beating flagellum. The flow transports particles from the region below the choanoflagellate, in through the large openings in the lower part of the lorica and up toward the collar filter on which the particles are caught (Fig. A.2 and Movie S1). The detailed visualization reveals a true filtration flow that undoubtedly passes through the filter, confirming the current understanding of filter-feeding in choanoflagellates [10]. However, our results are for a loricate species, and it is uncertain if, and to what extent, non-loricate species can filter the same way, since flow could pass along the filter on the outside and circumvent the filter. From the flow field, one important function of the lorica seems to be the separation of in- and exhalent flow, reducing re-filtration. The clearance rate Q can be expressed as the volume flow rate through the filter

$$Q = \int_{A_F} v \, \mathrm{d}A \,, \tag{A.1}$$

where A_F is the surface area of the filter and v is the normal component of the flow velocity. The observed velocity field shows that the water that passes the filter first passes the equator ($z = 0$) in the annular region between the cell and the finely netted part of the lorica. We determine the clearance rate as the volume flow rate upwards across the annular region in the equator plane. This procedure is more precise than directly using the flow through the filter. No-slip boundary conditions would suggest reduced flow velocities near the cell and lorica. At the spatial resolution of our experiment, however, the z-

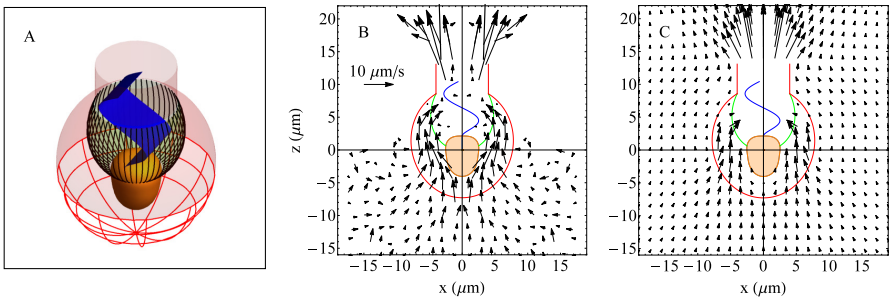

Fig. A.3: Model morphology with a flagellar vane, observed average velocity field for *Diaphanoeca grandis*, and velocity field from CFD model including a 5 μm wide flagellar vane. (A) The model morphology shows the cell (orange), the collar filter (green), the flagellum with a 5 μm wide flagellar vane (blue), and the lorica (red). (B) Observed average velocity field. The velocity field is identical to the velocity field in Fig. A.2B, and it is shown repeatedly to facilitate comparison with the CFD result. (C) The CFD velocity field in the xz-plane is time-averaged over the flagellar beat cycle, and the velocity vectors inside filter and chimney are omitted for clarity. The CFD model with a flagellar vane predicts a feeding flow and a clearance rate in good agreement with the experimental observations for *D. grandis*.

components of the flow velocities in the annular region do not depend on the distance from the longitudinal axis (Fig. S1A). To determine the clearance rate we therefore use the average value $v_z = 7.3 \pm 4.4\,\mu\mathrm{m\,s^{-1}}$ (mean $\pm$ SD) times the area of the annular region. We find $Q = (1.22 \pm 0.72) \cdot 10^3\,\mu\mathrm{m^3\,s^{-1}}$, or 1.20 million cell volumes per day, where the cell volume $V_C = 88\,\mu\mathrm{m}^3$. The corresponding flagellar beat frequency is $f = 7.3 \pm 2.6\,\mathrm{Hz}$ (Fig. S1B).

Computational Fluid Dynamics and Theoretical Clearance

To explore the feeding flow theoretically we numerically solve the Navier-Stokes equation and the equation of continuity for the incompressible Newtonian flow due to the beating flagellum with the known morphology (Supporting Information). The collar filter consists of approximately 50 evenly distributed microvilli [12], with a fairly uniform filter spacing and permeability along most of their length (Fig. B.1). The finely netted upper part of the lorica has pore sizes in the range $0.05 - 0.5\,\mu$m [12], and for simplicity we treat it as an impermeable, rigid surface and neglect the ribs in the lower part of the lorica. *Diaphanoeca grandis* carries a standard eukaryotic flagellum with diameter $b = 0.3\,\mu$m [22], and high-speed videography showed that the flagellum beats, like most other eukaryotic flagella, in a single plane (Movie S2). For computational simplicity we model the flagellum as a thin sheet of width b that is oriented perpendicular to the plane of beating and moving with simple traveling wave motion in the positive z-direction. Based on our validation of the CFD simulations, we estimate that this approach underestimates the

flagellar forces by approximately 20% (Table S4). The time-averaged CFD flow is an order of magnitude weaker than the flow observed experimentally for *D. grandis* (Fig. A.2). The model leads to the time-averaged flagellum force in the z-direction $F_{0.3} = 1.1\,\mathrm{pN}$, the time-averaged power $P_{0.3} = 0.31\,\mathrm{fW}$, and the clearance rate $Q_{0.3} = 95\,\mu\mathrm{m}^3\,\mathrm{s}^{-1}$, which is approximately 13 times lower than the clearance rate based on the observed flow field.

In order to generalize our CFD results and roughly estimate the clearance rates of other species of choanoflagellates, we model filter resistance and flagellum force. We describe the filter locally as a row of parallel and equidistantly spaced solid cylinders, and we model the flow far from the filter as uniform and perpendicular to the filter plane. For such simple filters we can express the flow speed through the filter

$$v = \kappa \frac{a}{\mu} \Delta p \,, \tag{A.2}$$

where Δp is the pressure drop across the filter, κ the dimensionless permeability of the filter, and μ the dynamic viscosity. The dimensionless permeability κ is a function only of the dimensionless filter spacing l/a. We model κ by combining previous theoretical work on closely and distantly spaced filter structures, respectively [23, 24]. The dimensionless permeability κ increases strongly with l/a and contributes to the filter spacing trade-off as discussed above (Fig. S8). For the model morphology we find the average dimensionless permeability $\langle\kappa\rangle = 0.41$. With a flagellum of length L and diameter b we can estimate the flagellum force

$$F_T \;=\; C_F\,\mu\,L\,U \;=\; 4\,C_F\,\mu\,L\,A\,f \,, \tag{A.3}$$

where C_F is the drag coefficient, $\mu = 1.0 \cdot 10^{-3}\,\mathrm{Pa\,s}$ the viscosity, and A the amplitude of the flagellar beat. The average speed of the flagellum is estimated as $U = 4\,A\,f$. For simplicity we take C_F to be the drag coefficient of a slender spheroid that is moving sideways $C_F = 4\,\pi/(\ln(2\,L/b) + 1/2)$ [25]. The estimate neglects the presence of filter and lorica structures surrounding the flagellum and assumes that all (primarily transversal) drag on the flagellum is converted into longitudinal flow. The corresponding power estimate is $P_T = F_T\,U = 16\,C_F\,\mu\,L\,A^2\,f^2$. To estimate the theoretical clearance rate we assume that the pressure drop is $\Delta p = F/A_F$ and we obtain

$$Q_T \;=\; \langle\kappa\rangle\,\frac{a}{\mu}\,F_T \;=\; 4\,\langle\kappa\rangle\,C_F\,a\,L\,A\,f \,. \tag{A.4}$$

For *D. grandis* the estimate predicts the flagellum force $F_T = 2.5 \pm 0.9\,\mathrm{pN}$, the power $P_T = 0.20 \pm 0.14\,\mathrm{fW}$, and the clearance rate $Q_T = 75 \pm 26\,\mu\mathrm{m}^3\,\mathrm{s}^{-1}$ in rough agreement with the CFD results.

For other choanoflagellate species we calculate the clearance rate from the analytical estimate (equation A.4) and compare it with observations (Table A.1). In most species, the theoretical clearance rate grossly underestimates the realized, and only two species seem able to filter significant volumes of water. Of the species listed, only *D. grandis* and *Stephanoeca diplocostata* carry a lorica. The rest are non-loricate and potentially subject to filter circumvention, which we did not account for. Filter circumvention would increase the flow rate, but potentially reduce the clearance rate, since water would not actually be filtered.

Discussion

The Filter-Feeder Paradox

Our results reveal a paradox: The CFD model and the simple estimates underestimate the clearance rate based on the observed flow field by more than an order of magnitude. The flow field derived clearance rate seems robust, as it is similar to an earlier observation [12], and at the same time consistent with the general notion that heterotrophic plankton need to daily clear a volume of approximately one million times their own body volume [3]. Instead, the theory can of course be questioned, most obviously perhaps through the notion that various types of flagellar hairs often line eukaryotic flagella and could increase the force output of the flagellum [22]. However, the force estimate is only weakly influenced by the flagellum diameter (equation A.3), so long as we neglect interaction between flagellum and filter, and simple flagellar hairs would have little influence on the clearance rate. It is thus difficult to see how the flagellum would be able to deliver the force required to account for the experimentally observed clearance rate; unless some major aspect of its morphology or function has been overlooked.

Pumping Mechanism Conjecture

A few choanoflagellate species have been shown to have a so-called flagellar vane comprising a sheet-like structure along the length of the flagellum [16, 19, 26]. Although a flagellar vane has been observed in a few choanoflagellate species, the structure remains elusive. Leadbeater went so far as to call it a "mystery" because the structure is notoriously difficult to visualize using electron microscopy [26]. While a vane cannot account for the clearance rate due to increased flagellum drag so long as interactions between flagellum and filter are neglected, this structure could still offer a satisfactory solution to the apparent paradox: With a vane, the distance between flagellum and the inside of the collar would be reduced, reducing transversal flow past

the beating flagellum inside the collar. Instead, more fluid would be forced upwards, and the resulting low pressure would have to be equalized by a flux through the filter. With a flagellar vane nearly as wide as the collar, or even physically attached to the inside of the collar, the pumping mechanism would be radically different. The highly similar choanocytes of aquatic sponges have been shown to have flagellar vanes that indeed are attached to the filter or span its width [19, 27, 28]. The flagellum together with its vane would function as a waving wall forming two adjacent peristaltic pumps [29], one on each side of the vane, that draw in water through the filter and expel it out of the chimney of the lorica. To explore such a pumping mechanism we replace the flagellum in the CFD model with a $b = 5\,\mu$m wide sheet that spans almost the entire width of the filter (Movies S3, S4, and S5). The time-averaged CFD flow agrees well with the flow observed for *D. grandis* (Fig. A.3). The model leads to the time-averaged flagellum force in the z-direction $F_5 = 12.1\,$pN, the time-averaged power $P_5 = 2.20\,$fW, and the clearance rate $Q_5 = 898\,\mu\text{m}^3\,\text{s}^{-1}$; slightly lower than the experimentally observed clearance rate.

To explore the vane-based pumping mechanism conjecture for other choanoflagellates, we make a rough estimate of the clearance rate as the volume flow rate given by the simple model

$$Q_V = A\,W\,\lambda\,f\,, \tag{A.5}$$

where W is the diameter of the chimney of the lorica and λ the flagellar wavelength. We assume that the flagellum is moving in the central beat plane with amplitude A, and that the flagellar vane is attached to filter and chimney. The average peak-to-peak amplitude of the flagellar vane must therefore be A, and we assume that a water volume $A\,W\,\lambda$ is forced through the filter and out of the chimney per flagellar beat period. For *D. grandis* we find the estimate $Q_V = (1.41 \pm 0.50) \cdot 10^3\,\mu\text{m}^3\,\text{s}^{-1}$ in good agreement with the clearance rate based on the observed flow field (Table A.1).

In fact, Q_V provides a solid prediction of the observed clearance rate Q in six out of the seven species for which the naked flagellum clearance rate estimate Q_T cannot account for Q (Table A.1). Thus, two species seem to use a simple flagellum to drive the feeding current, whereas six choanoflagellate species and the choanocyte rely on a flagellar vane. A narrow vane has been observed in *M. brevicollis*, but a vane this small would only have limited influence on the clearance rate (Fig. S7), and the apparent discrepancy is certainly within estimate uncertainties. Only for *Codosiga botrytis* does neither of the two models adequately predict Q. This species has a long and rapidly beating flagellum that extends far beyond the collar, and also the finest of the choanoflagellate filters. Combined, this suggests that this species may not perform actual filter-feeding, but instead relies on cross flow filtration in which the flow passes along and not through the filter. The suggested

pumping mechanism would also provide a mean to avoid unwanted filter circumvention in loricate as well as non-loricate species. If the vane spans most of the collar width, a flagellum wavelength "traps" a package of water that has to be expelled with the flagellar beat. Furthermore, typical flagellar beat frequencies of eukaryotic organisms are in the range 30-70 Hz [1, 17], and the low beat frequencies found in *D. grandis* and a number of other choanoflagellate species stand out (Table A.1). We speculate that the low beat frequencies are the result of extensive flagellar vanes and their high force requirements. While the dynein motor proteins themselves would easily provide the needed force [30], the shear due to the flagellar beat motion could be too much for delicate vane structures. The presence of a $5\,\mu$m wide vane increases the energetic costs of beating the flagellum by an order of magnitude, making the energetic costs a significant fraction of the total energy budget of the cell, contrary to common belief [31, 32]. This is in agreement with results from the similar choanocytes [33], and demonstrates a strong trade-off for microbial filter-feeders between acquiring new energy and investing energy to do so.

The Filter-Feeder Trade-Off and the Optimum Filter

The main purpose of the filter is to intercept as much food as possible. The above mentioned filter trade-off suggests that there is an optimum filter spacing that will maximize the prey encounter rate E in terms of prey biomass per unit time. The encounter rate can be expressed as the integral

$$E \;=\; Q \int_0^\infty \beta(s)\, C(s)\, \mathrm{d}s \;, \tag{A.6}$$

where β is the collection efficiency, C the size-specific mass concentration of prey particles, and s the particle diameter. It is generally accepted that logarithmic particle size bins contain approximately equal amounts of biomass [34]:

$$C(s) \;=\; \frac{C_0 / \ln 10}{s} \;, \tag{A.7}$$

where C_0 is the particle mass concentration within each decade in particle diameter. Now, if the particles are captured by sieving, we can assume 100% collection efficiency, $\beta = 1$, for particles with diameter greater than the filter gap $l - 2\,a$ and smaller than the maximum prey size d. In this case we can write the encounter rate as

$$E = Q \int_{l-2a}^{d} C(s)\mathrm{d}s = E_0 \langle \kappa \rangle \log \frac{d/a}{l/a - 2}, \tag{A.8}$$

where $E_0 = (a/\mu) F C_0$ is independent of l and d. Independent of the flagellum force F and method of pumping, it is thus possible to predict the optimum filter spacing of aquatic microbial filter-feeders. With the maximum prey size $d = (1/3)\,\mathrm{ESR} = 0.93\,\mu\mathrm{m}$ for *D. grandis* (approximately the openings of the coarse outer filter), we obtain the optimum dimensionless filter spacing $l/a = 8.4$ in close agreement with the observed average value (Fig. A.4A). The optimum filter spacing increases approximately linearly with the maximum prey size in the range relevant for choanoflagellates, and it is consistent with observations (Fig. A.4B). One species, *Codosiga botrytis*, deviates from this pattern, consistent with our suggestion that this species may not be a true filter feeder. We can approximate the encounter rate when $l/a \gg 1$ as

$$E \approx E_0 \frac{l/a}{8\,\pi} \left(1 - 2 \ln \frac{2\,\pi}{l/a}\right) \log \frac{d/a}{l/a}, \tag{A.9}$$

which allows analytical determination of the optimum filter spacing

$$\frac{l}{a} \approx \exp\left[-1 + \frac{1}{\ln(d/a)} + \frac{\ln(2\,\pi) - 1}{[\ln(d/a)]^2}\right] \frac{d}{a}. \tag{A.10}$$

The expression shows that the optimum filter spacing is approximately proportional to the maximum prey size when the filter spacing is large, leading to a relatively small prey size range. Particles smaller than the filter spacing can be collected by direct interception or diffusional deposition, but these effects are estimated to be small compared to sieving for the measured filter spacing of *D. grandis* [35].

Conclusion

We have shown that a simple, naked flagellum can not account for the clearance rates observed in many choanoflagellate species. Instead, we suggest a widespread presence of the sporadically observed flagellar vane. The proposed pumping mechanism is radically different and can explain how choanoflagellates can perform efficient small-scale filter-feeding. The explored problems and our model estimates are relevant to the understanding of small-scale filtering in general, and the mechanistic insights allow quantification of the trade-offs involved in various microbial feeding modes. We have, for instance, demonstrated that microbial filter-feeding is an energetically costly

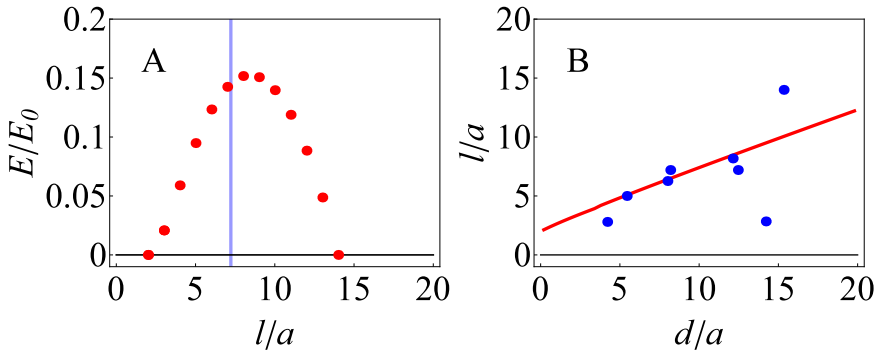

Fig. A.4: Optimum choanoflagellate filters. (A) Encounter rate as function of dimensionless filter spacing (equation A.8). The vertical line (blue) indicates the observed average of the dimensionless filter spacing. (B) The theoretical prediction for the optimum dimensionless filter spacing (solid line, red) and the observed dimensionless filter spacing for the choanoflagellates in Table A.1 (filled circles, blue) as functions of the maximum dimensionless prey diameter. We have assumed that the maximum prey diameter is equal to (1/3) ESR. The outlier below the predicted line is *Codosiga botrytis*, speculated to rely on cross flow filtration rather than true filtration.

process, that takes up much more than a few percent of the total energy budget of the cell as otherwise typically believed.

Experimental Organisms

The choanoflagellate *Diaphanoeca grandis* (ACCT no. 50111) was grown non-axenically in the dark in B1 medium (salinity 32) at 10°C. The culture was diluted once every 2-3 week, and a few organically grown, autoclaved, rice grains were added per 65 mL flask to serve as bacterial substrate.

Videography of Flagellum Motion and Feeding Flow

To explore the near-cell flow field and the motion of the beating flagellum, cells were observed at high magnification using high-speed digital video. An Olympus IX-71 inverted microscope equipped with a UPLSAPO60XO/1.35 oil-immersion objective and a U-ECA magnifying lens provided a total of 1920 $\times$ magnification. Video sequences were obtained using a Phantom v210 high-speed digital video system. Videos were recorded at a frame rate of 100 fps and a resolution of 1024 pixels $\times$ 800 pixels. This provided 10 pixels per μm. Observations were done in a $\approx$ 1 mL chamber, constructed as a 5 mm high polycarbonate ring (diameter 2 cm) mounted with silicone between an objective slide and a cover glass. Cells were either free-swimming or settled onto the slide. Flagellum length and average amplitude of the flagellar beat were estimated on five individuals that were oriented with the flagellum beat

plane aligned with the focal plane of the microscope. For each frame in a single beat cycle, the flagellum position was digitized manually using ImageJ by identifying approximately 15 points along the flagellum. Neutrally buoyant, 300 nm polystyrene beads were added to a concentration of approximately $1 \cdot 10^6\,\mathrm{mL}^{-1}$ in order to visualize the water flow. The particles were pretreated with bovine serum albumin and sonicated before use to avoid clumping.

Flow Field Analysis

Based on cell alignment, a total of 19 video sequences, each fielding a unique individual, were selected for use in the flow field analysis. The frequency of the flagellar beat was noted at one second intervals, by manual, visual inspection of the slowed down 100 fps video sequences. Two-dimensional particle tracks were resolved on reduced frame rate video sequences (10 fps) using the Manual tracking plugin for ImageJ. A total of 73 tracks were used to construct the velocity field. Each particle track was associated with the frequency of the flagellar beat at the corresponding time. All particle tracks were collated using the average model morphology, and the velocity field in the xz-plane was constructed using a square grid with $2\,\mu\mathrm{m} \times 2\,\mu\mathrm{m}$ spatial resolution. The velocity field was assumed to have rotational symmetry about the longitudinal axis of the cell, and the observed velocity field in the xz-plane was therefore correspondingly assumed to have left-right reflection symmetry with respect to the longitudinal axis. Within each grid window the manually detected particle positions were selected and for each particle track the average particle position and velocity were determined. Position and velocity associated with a given grid window were subsequently determined as the equally weighted average over all particle tracks within the window.

Acknowledgment

We thank Jasmine Mah for providing videos of *Monosiga brevicollis*, and Øjvind Moestrup and Helge Abildhauge Thomsen for helpful discussions. The Centre for Ocean Life is a VKR Centre of Excellence supported by the Villum Foundation, and S.S.A. and J.H.W. were supported by a research grant (9278) from the Villum Foundation.

2 Numerical Models Appendix

Summary

The supporting information is mainly devoted to our computational fluid dynamics (CFD) simulations, including verification, validation, results, and movies with flow animations. Additionally, we present movies of observed particle tracks and flagellar beats, details of the model morphology, and details of the analytical modeling of the filter resistance.

Model Morphology and Observed Flow

In order to collate particle tracks from the different individuals and to set up the CFD simulation geometry, we construct a generic morphology model to which all observations are scaled. We focus on six individuals that are viewed from the side with the longitudinal axis of the cell in the focal plane. To good approximation the cell surface and the outline of the lorica have rotational symmetry about the longitudinal axis, and we therefore describe them as surfaces of revolution. In spherical polar coordinates we write

$$R(\theta) \;=\; R_0\,(1 \,+\, \alpha_1 \cos\theta \,+\, \alpha_2 \cos 2\,\theta \,+\, \alpha_3 \cos 3\,\theta)\;, \qquad \text{(A.11)}$$

where R_0, α_1, α_2, and α_3 are morphology parameters. The polar angle θ is defined relative to the longitudinal axis of the cell, and the location of the flagellum, i.e., the flagellar basal body, is used to define the north (anterior) pole of the cell. For both the cell surface and the outline of the lorica we list the morphology parameters (Table A.2).

	$R_0\,(\mu\mathrm{m})$	α_1	α_2	α_3
cell	2.8 ± 0.3	-0.24	0.10	-0.10
lorica	8.1 ± 0.4	0.15	0.05	0.00

Table A.2: Average morphology parameters that describe both size R_0 and shape α_1, α_2, and α_3 of the cell and the outline of the lorica.

To model the outline of the filter we use the interpolation

$$R_F(\theta) \;=\; R_C(\theta_C) \,+\, [R_L(\theta_L) \,-\, R_C(\theta_C)]\;\frac{\theta \,-\, \theta_C}{\theta_L \,-\, \theta_C}\;, \qquad \text{(A.12)}$$

where $\theta_C \;=\; 76\,\mathrm{deg}$ and $\theta_L \;=\; 25\,\mathrm{deg}$ are the polar angles where the filter connects to cell R_C and lorica R_L, respectively. The average dimensionless filter spacing is $\langle l/a \rangle \;=\; 7.2$, where l denotes the distance between the centers of neighboring microvilli and $a \;=\; 0.075\,\mu\mathrm{m}$ the radius of an individual

microvillum. The flagellum length and the average amplitude of the flagellar beat are $L = 11.7 \pm 1.5\,\mu$m and $A = 2.8 \pm 0.2\,\mu$m, respectively.

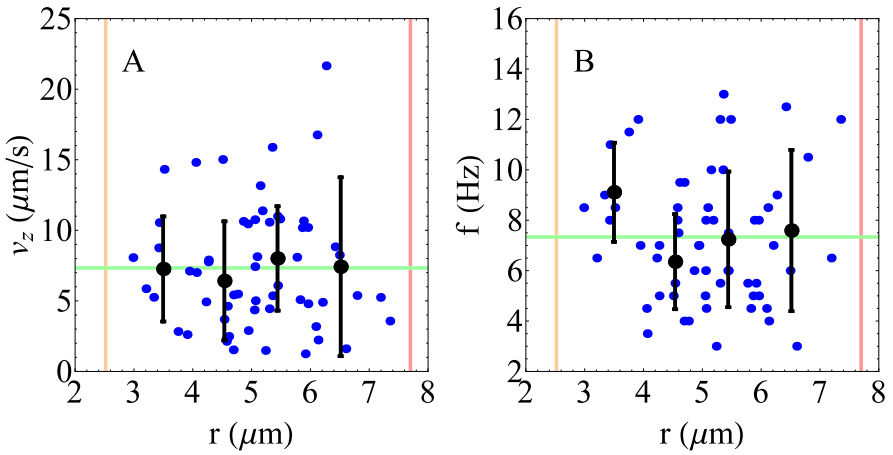

Fig. A.5: Flow velocities as function of the distance r from the longitudinal axis (A) and corresponding flagellar beat frequencies used for the clearance rate calculation (B). The cell surface (orange) and the lorica (red) at the equator are indicated by the vertical lines. The average values are shown as the horizontal lines (green). (A) The z-components of the particle velocities in the equatorial region between $z = \pm 1\,\mu$m (dots, blue), and the z-components of the flow velocities obtained by binning (dots and errorbars, black). (B) The corresponding flagellar beat frequencies.

Computational Fluid Dynamics Simulations

Simulation Setup

We apply the commercial computational fluid dynamics (CFD) program STAR-CCM+ (12.02.010-R8) to numerically solve the Navier-Stokes equation and the equation of continuity for incompressible Newtonian flow using the finite volume approach. Both the frequency parameter and the Reynolds number are much smaller than unity, and the flow is therefore a quasi-steady Stokes flow [36]. We use the model morphology and a spherical computational domain with the model cell held stationary at the center (Fig. A.6). The no-slip boundary condition is applied at the surfaces of the cell and the microvilli. The upper part of the lorica and the chimney of height $5\,\mu$m are treated as impermeable surfaces with no-slip boundary condition, and the lower part of the lorica is disregarded (Fig. A.6A).

We treat the beating flagellum as a thin sheet of width b that is moved in the xz-plane with prescribed kinematics and on which the no-slip boundary

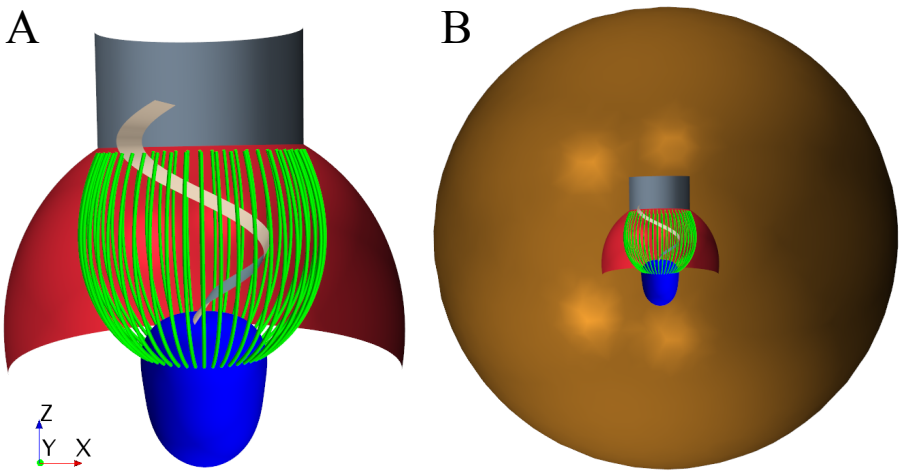

Fig. A.6: Model geometry and computational domain. (A) The model organism consisting of cell (blue), flagellum (light gray), filter (green), upper part of lorica (red), and chimney (dark gray). The coordinate system is defined so that the flagellum is beating in the xz-plane. (B) The model organism at the center of the spherical computational domain (brown).

condition is satisfied. We model the displacement of the flagellum in the x-direction as the simple traveling wave

$$h(z,t) \;=\; A\left[1 \;-\; e^{-(z-z_B)/\delta}\right] \sin[k\,(z-z_B) - \omega\,t]\,, \tag{A.13}$$

where z_B is the z-coordinate of the flagellar basal body at the cell surface, $\delta \;=\; 1.0\,\mu$m the characteristic length scale of the amplitude modulation, $k \;=\; 2\,\pi/\lambda$ the wave number, and $\omega \;=\; 2\,\pi f$ the angular frequency. At the exterior boundary of the computational domain we apply a constant pressure boundary condition (Fig. A.6B).

We take advantage of mesh morphing to avoid reconstructing the mesh geometry at the different flagellum positions during the flagellar beat. The morphing motion redistributes mesh vertices in response to the movement of the flagellum at each time step. Therefore, between two time steps, the mesh is morphed in response to the flagellar movement and at each time step, the discretized form of the governing equations are solved inside the entire computational domain. We employ polyhedral cells for the discretization since they allow mesh morphing and flexibility when representing the complex geometry of the model organism (Fig. A.7).

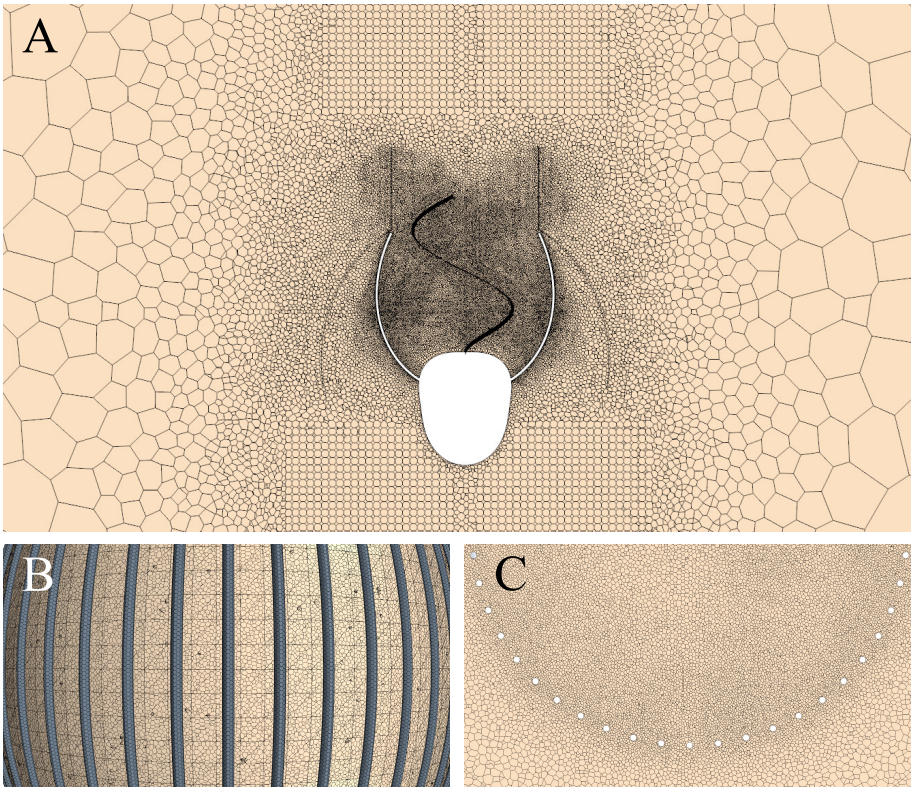

Fig. A.7: The computational cells in the discretized computational domain with 4.8 million computational cells for a flagellum of width 5 μm. (A) The mesh is chosen very fine around the flagellum and in between the microvilli to resolve the flow structures, whereas a coarse mesh is sufficient to resolve the flow in the far field. (B) and (C) Details of the mesh between the microvilli seen from the side and in the z-direction.

Verification

The residuals of the four governing equations as functions of the computational iteration step show that the governing equations are satisfied with negligible error (Fig. A.8). We find that the flagellum force converges for each time step during the computational iteration process, i.e., between consecutive spikes (Fig. A.9). To verify that the solutions for the time-averaged flagellum force and the time-averaged clearance rate do not depend on the mesh size, we discretize the computational domain with different mesh sizes. For meshes with more than four million computational cells we find approximately 1% variation, and in the result simulations we use 4.8 million computational cells (Fig. A.10). We use two different time steps to check the time step independence, and we conclude that 24 time steps per flagellar beat period are sufficient (Table A.3). To make sure that the solution is in-

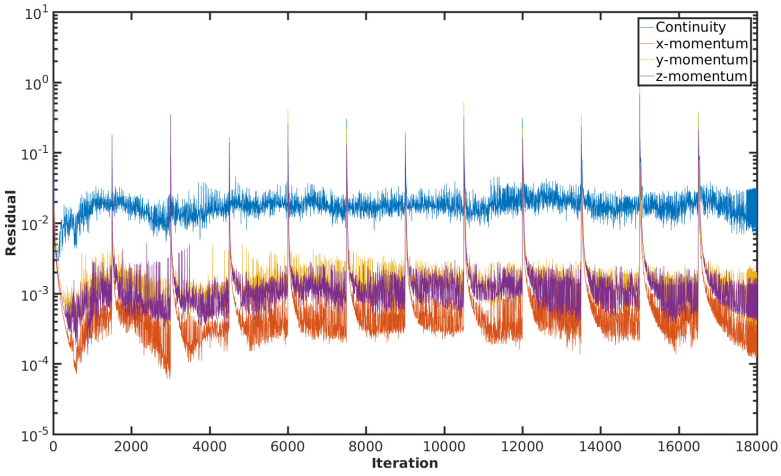

Fig. A.8: Residual convergence in simulation with flagellum of width 5 μm.

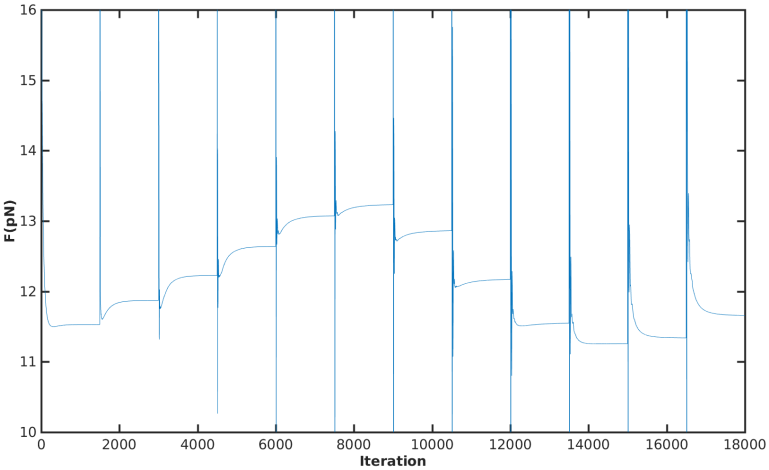

Fig. A.9: Force convergence in simulation with flagellum of width 5 μm.

dependent of the size of the computational domain, we solve the governing equations inside domains with different sizes. We find minute differences between domains with radius 30 μm and 40 μm, respectively, and in the result simulations we therefore use domains with radius 30 μm (Table A.4).

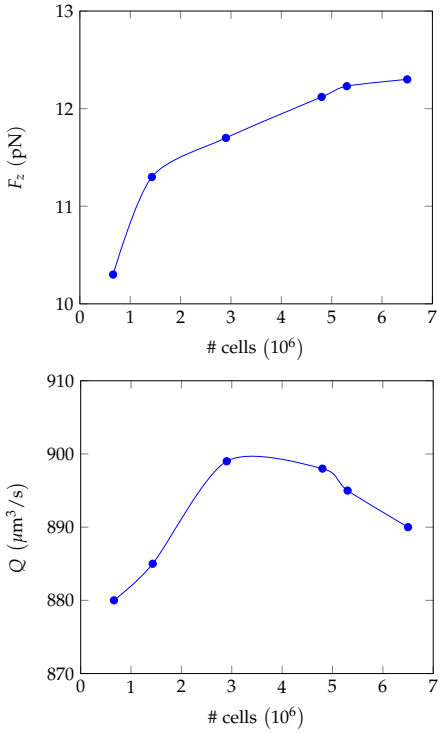

Fig. A.10: Mesh size independence of the time-averaged force F_z and the time-averaged clearance rate Q with a flagellum of width 5 μm.

# time steps per beat cycle	F_z (pN)	Q (μm^3/s)
24	12.1	898
48	12.2	895

Table A.3: Independence of the time-averaged force F_z and the time-averaged clearance rate Q of the number of time steps per beat cycle.

Domain radius (μm)	F_z (pN)	Q (μm^3/s)
30	12.1	898
40	12.2	909

Table A.4: Independence of the time-averaged force F_z and the time-averaged clearance rate Q of the size of the computational domain.

Validation

To validate the computational approach we use it to numerically calculate the drag forces on a slender cylinder and a slender thin sheet in steady flow at Reynolds numbers comparable to the low Reynolds number for the flagellar motion. Our goal is both to validate the results for the slender cylinder against known analytical theory, and to validate the approximation of a beating cylindrical flagellum using a thin sheet. We consider the drag force components F_s and F_n in the lengthwise and the sidewise directions

$$F_s = C_s \mu L U , \tag{A.14}$$

$$F_n = C_n \mu L U , \tag{A.15}$$

where we define the drag coefficients C_s and C_n in the lengthwise and the sidewise directions, respectively, and where L denotes the length of the slender object and U the speed of the steady far-field flow relative to the object. For the slender cylinder we use the analytical approximations

$$C_s \approx \frac{2\pi}{\ln(2L/b) - 0.72} , \tag{A.16}$$

$$C_n \approx \frac{4\pi}{\ln(2L/b) + 0.50} , \tag{A.17}$$

that were derived by Burgers [37, equations (5-11.52) and (5-11.54)]. In the numerical simulations we apply a cylindrical computational domain that in extension is an order of magnitude larger than the length of the cylinder or plate. The object is held stationary at the center of the domain, and the no-slip boundary condition is applied at the surface of the object. A flow inlet boundary condition is applied on one end face of the computational domain,

and a pressure boundary condition is used on the other external boundaries. The CFD results and the approximate theoretical results agree within the expected accuracy, and the CFD results for the thin plate are roughly 20% smaller that the CFD results for the cylinder (Table B.2). We therefore expect the CFD simulation using the thin plate model to underestimate the force due to the cylindrical flagellum by roughly 20%.

Case	C_s	C_n	Δ_s (%)	Δ_n (%)
Cylinder, theory	1.81	2.67	0.0	-5.0
Cylinder, CFD	1.81	2.81	-	-
Plate, CFD	1.35	2.35	-25.4	-16.4

Table A.5: Drag coefficients C_s and C_n for steady flow past a cylinder and a thin plate, and the differences relative to the CFD results for the cylinder. All objects are slender with $b/L = 0.03$, where b denotes the cylinder diameter and the plate width, respectively, and L the object length.

Results

The main simulation results are the time-averaged flagellum forces in the z-direction F_z and the time-averaged clearance rates Q for different widths of the flagellum b. In addition to the simulation data for the narrow flagellum with $b = 0.3\,\mu$m and the wide flagellum with $b = 5.0\,\mu$m that we discuss in the main text, we show results for intermediate b values (Fig. A.11). Both F_z and Q increase with b, and they are roughly proportional.

Filter Resistance

For the drag force per unit length D on a single cylinder in the filter we introduce a dimensionless drag coefficient C_D. We write it in the form $D = C_D\,\mu\,v$, since we consider low Reynolds number flows. The relationship between the dimensionless permeability and the drag coefficient becomes $\kappa = (l/a)/C_D$. Simple filter flows with closely spaced cylinders were modeled by Keller using lubrication theory [23]. In this approximation:

$$C_D = \frac{9\,\pi}{2^{3/2}} \left(1 - \frac{2}{l/a}\right)^{-5/2} . \tag{A.18}$$

The flow can also be analyzed for a filter with widely spaced cylinders, and this was done using the Oseen equation by Tamada and Fujikawa [24]. In this case it is convenient to introduce the parameter $\tau = 2\,\pi/(l/a)$, and to write the drag coefficient $C_D = 8\,\pi/\Lambda$, where Λ has the form

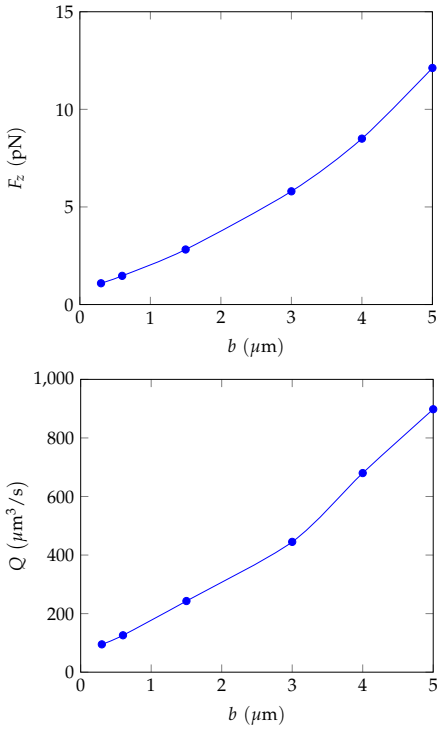

Fig. A.11: Time-averaged flagellum force in the z-direction F_z and time-averaged clearance rate Q for different widths of the flagellum b.

$$\Lambda = 1 - 2\ln\tau + \frac{1}{6}\tau^2 - \frac{1}{144}\tau^4 + \frac{1}{1080}\tau^6 - \frac{53}{345600}\tau^8 + \frac{139}{5443200}\tau^{10} + \mathcal{O}(\tau^{12}) \,. \tag{A.19}$$

It is not clear a priori how well the two models work for intermediate filter spacing, and we therefore follow Ayaz and Pedley and compare the two models with numerical results [8]. Keller's model is qualitatively correct for both closely and widely spaced cylinders, but it is only quantitatively correct when $l/a < 4$ (Fig. A.12A). In contrast, the model by Tamada and Fujikawa works well when $l/a > 4$, and it breaks down for closely spaced cylinders. Thus, we estimate κ following Keller's model when $l/a < 4$ and using Tamada and Fujikawa's work when $l/a \geq 4$ (Fig. A.12B).

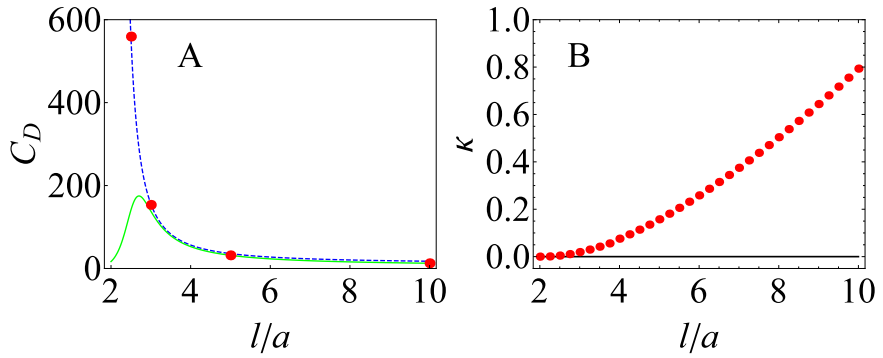

Fig. A.12: Filter characteristics. (A) The drag coefficient C_D as function of l/a in Keller's model (dashed line, blue), in the model by Tamada and Fujikawa (solid line, green), and in the simulations by Ayaz and Pedley (filled circles, red). (B) The dimensionless filter permeability κ using Keller's model when $l/a < 4$ and the model by Tamada and Fujikawa when $l/a \geq 4$.

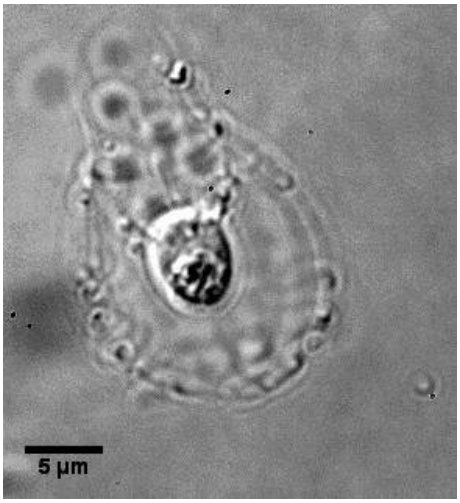

Fig. A.13: *Diaphanoeca grandis* capturing several 300 nm polystyrene tracer particles. Videos like this were used to construct the flow field (Fig. 2) by manually tracking the tracer particles over time. Real time.

References

[1] T. Fenchel, "Ecology of Heterotrophic Microflagellates. I. Some Important Forms and Their Functional Morphology," *Mar. Ecol. Prog. Ser.*, vol. 8, pp. 211–223, 1982.

[2] T. Kiørboe, H. Plough, and U. H. Thygesen, "Fluid motion and solute distribution around sinking aggregates. i. small-scale fluxes and heterogeneity of nutrients in the pelagic environment," *Mar. Ecol. Prog. Ser.*, vol. 211, pp. 1–13, 2001.

[3] T. Kiørboe, "How zooplankton feed: mechanisms, traits and trade-offs," *Biol. Rev.*, vol. 86, pp. 311–339, 2011.

[4] T. Fenchel, "Protozoan filter feeding," *Prog. in Protistology*, vol. 1, pp. 65–113, 1986.

[5] P. S. Larsen and H. U. Riisgård, "The sponge pump," *J. Theor. Biol.*, vol. 168, pp. 53–63, 1994.

[6] H. U. Riisgård and P. S. Larsen, "Particle capture mechanisms in suspension-feeding invertebrates," *Mar. Ecol. Prog. Ser.*, vol. 418, pp. 255–293, 2010.

[7] T. Fenchel, "Relation between particle size selection and clearance in suspension-feeding ciliates," *Limnol. Oceanogr.*, vol. 25, no. 4, pp. 733–738, 1980.

[8] F. Ayaz and T. J. Pedley, "Flow through and particle interception by an array of closely-spaced circular cylinders," *Eur. J. Mech. B/Fluids*, vol. 18, pp. 173–196, 1999.

[9] M. E. Pettitt, B. A. A. Orme, J. R. Blake, and B. S. C. Leadbeater, "The hydrodynamics of filter feeding in choanoflagellates," *European Journal of Protistology*, vol. 38, pp. 313–332, 2002.

[10] B. S. C. Leadbeater, *The Choanoflagellates: Evolution, Biology and Ecology*. Cambridge, UK: Cambridge University Press, 2015.

[11] G. Lapage, "Notes on the choanoflagellate, *Codosiga botrytis*, ehrbg." *Quarterly Journal of Microscopical Science*, vol. 69, pp. 471–508, 1925.

[12] P. Andersen, "Functional biology of the choanoflagellate *Diaphanoeca grandis* Ellis," *Marine Microbial Food Webs*, vol. 3, pp. 35–50, 1988/1989.

[13] M. Roper, M. J. Dayel, R. E. Pepper, and M. A. R. Koehl, "Cooperatively generated stresslet flows supply fresh fluid to multicellular choanoflagellate colonies," *Phys. Rev. Lett.*, vol. 110, p. 228104, 2013.

[14] M. J. Dayel and N. King, "Prey capture and phagocytosis in the choanoflagellate *Salpingoeca rosetta*," *PLOS ONE*, vol. 9, p. e95577, 2014.

[15] J. B. Kirkegaard and R. E. Goldstein, "Filter-feeding, near-field flows, and the morphologies of colonial choanoflagellates," *PRE*, vol. 94, p. 052401, 2016.

[16] D. J. Hibbert, "Observations on the ultrastructure of the choanoflagellate *Codosiga botrytis* (ehr.) saville-kent with special reference to the flagellar apparatus," *J Cell Sci*, vol. 17, pp. 191–219, 1975.

[17] M. A. Sleigh, "Flagellar movement of the sessile flagellates *Actinomonas*, *Codonosiga*, *Monas*, and *Poteriodendron*," *Quarterly Journal of Microscopical Science*, vol. 105, pp. 405–414, 1964.

[18] P. J. D. Eccleston and B. S. C. Leadbeater, "A comparison of the growth kinetics of 6 marine heterotrophic nanoflagellates fed with one bacterial species," *Mar. Ecol. Prog. Ser.*, vol. 105, pp. 167–178, 1994.

[19] J. L. Mah, K. K. Christensen-Dalsgaard, and S. P. Leys, "Choanoflagellate and choanocyte collar-flagellar systems and the assumption of homology," *Evolution and Development*, vol. 16, no. 1, pp. 25–37, 2014.

[20] J. Boenigk and H. Arndt, "Comparative studies on the feeding behavior of two heterotrophic nanoflagellates: The filter-feeding choanoflagellate *Monosiga ovata* and the raptorial-feeding kinetoplastid *Rhynchomonas nasuta*," *Aquatic Microbial Ecology*, vol. 22, no. 3, pp. 243–249, 2000.

[21] B. S. C. Leadbeater, "Fine-structural observations on some marine choanoflagellates from the coast of norway," *Journal of the Marine Biological Association of the United Kingdom*, vol. 52, no. 1, pp. 67–79, 1972.

[22] Ø. Moestrup, "Flagellar structure in algae - a review, with new observations particularly on the chrysophyceae, phaeophyceae (fucophyceae), euglenophyceae, and reckertia," *Phycologia*, vol. 21, pp. 427–528, 1982.

[23] J. B. Keller, "Viscous flow through a grating or lattice of circular cylinders," *J. Fluid Mech.*, vol. 18, pp. 94–96, 1964.

[24] K. Tamada and H. Fujikawa, "The steady two-dimensional flow of viscous fluid at low Reynolds numbers passing through an infinite row of equal parallel circular cylinders," *Q. J. Mech. Appl. Math.*, vol. 10, pp. 423–431, 1957.

[25] H. C. Berg, *Random Walks in Biology*. Princeton University Press, 1993.

[26] B. S. C. Leadbeater, "The 'mystery' of the flagellar vane in choanoflagellates," *Beiheft zur Nova Hedwigia 130*, pp. 213–223, 2006.

[27] D. Mehl and H. M. Reiswig, "The presence of flagellar vanes in choanomeres of porifera and their possible phylogenetic implications," *J Zool Syst Evol Res*, vol. 29, pp. 312–319, 1991.

[28] N. Weissenfels, "The filtration apparatus for food collection in freshwater sponges (porifera, spongillidae)," *Zoomorphology*, vol. 112, pp. 51–55, 1992.

[29] M. Y. Jaffrin and A. H. Shapiro, "Peristaltic pumping," *Ann. Rev. Fluid Mech.*, vol. 3, pp. 13–37, 1971.

[30] C. B. Lindemann, "Structural-functional relationships of the dynein, spokes, and central-pair projections predicted from an analysis of the forces acting within a flagellum," *Biophysical Journal*, vol. 84, no. 6, pp. 4115–4126, 2003.

[31] E. M. Purcell, "Life at low Reynolds number," *Am. J. Phys.*, vol. 45, pp. 3–11, 1977.

[32] J. S. Guasto, R. Rusconi, and R. Stocker, "Fluid mechanics of planktonic microorganisms," *Annu. Rev. Fluid Mech.*, vol. 44, no. 1, pp. 373–400, 2012.

[33] S. P. Leys, G. Yahel, M. A. Reidenbach, V. Tunnicliffe, U. Shavit, and H. M. Reiswig, "The sponge pump: The role of current induced flow in the design of the sponge body plan," *PLoS ONE*, vol. 6, no. 12, p. e27787, 2011.

[34] R. W. Sheldon, A. Prakash, and W. H. Sutcliffe Jr., "The size distribution of particles in the ocean," *Limnology and Oceanography*, vol. 17, no. 3, pp. 327–340, 1972.

[35] L. A. Spielman, "Particle capture from low-speed laminar flows," *Ann. Rev. Fluid Mech.*, vol. 9, pp. 297–319, 1977.

[36] C. Pozrikidis, *Introduction to Theoretical and Computational Fluid Dynamics*, 2nd ed. Oxford University Press, 2011.

[37] J. Happel and H. Brenner, *Low Reynolds number hydrodynamics: with special applications to particulate media*. Martinus Nijhoff Publishers, 1983.

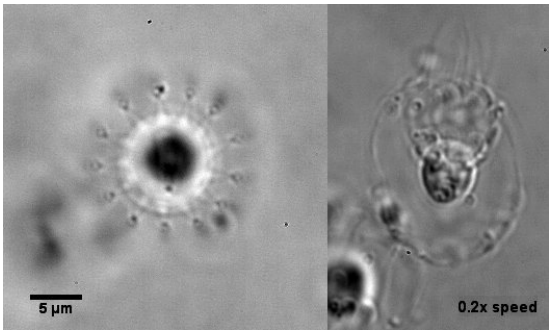

Fig. A.14: Flagellar beat pattern of *Diaphanoeca grandis*. Left: Cell viewed from the top (apex). The symmetrical pattern surrounding the dark cell is the costae that make up the lorica. Right: Cell seen from the side with the outline of cell, flagellum, lorica, collar, and chimney all visible. Movies demonstrate the planar beat pattern of *D. grandis*.

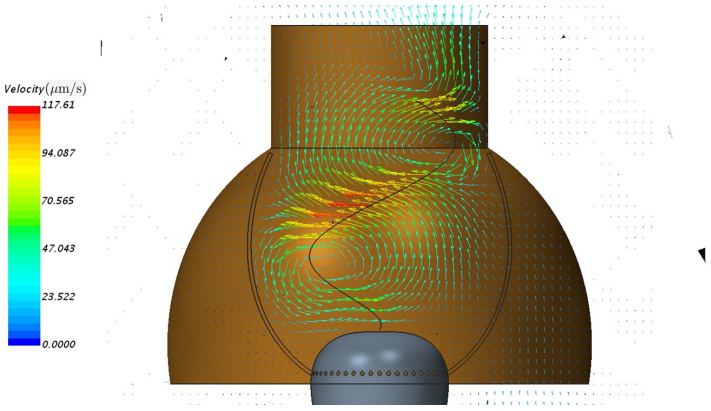

Fig. A.15: *Diaphanoeca grandis* CFD simulation with a 5 μm wide vane and 1.5 million computational cells. Lateral view as observed perpendicular to the xz-plane of the flagellar beat. Notice how the flux through the filter is highly time-dependent. Figure 3C of the manuscript presents the time-averaged data from this video.

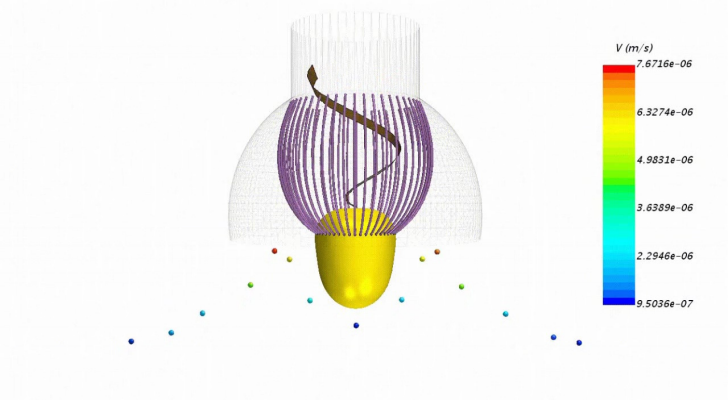

Fig. A.16: *Diaphanoeca grandis* CFD simulation with a 5 μm wide vane (brown) and 1.1 million computational cells. Passive tracer particle trajectories in the xz-plane of the flagellar beat. The vane extends toward and away from the observer. Notice how particle velocities are highly time-dependent in this plane.

Fig. A.17: *Diaphanoeca grandis* CFD simulation with a 5 μm wide vane (brown) and 1.1 million computational cells. Passive tracer particle trajectories in the yz-plane perpendicular to the flagellar plane of beat. Particle velocities are much less time-dependent in this plane compared to the plane parallel to this (Movie A.16).

Article B

Hydrodynamic functionality of the lorica in choanoflagellates

Seyed Saeed Asadzadeh[1], Lasse Tor Nielsen[2], Anders Andersen[3], Julia Dölger[3], Thomas Kiørboe[2], Poul S. Larsen[1], Jens Honoré Walther[1,4]

[1]Section for Fluid Mechanics, Coastal and Maritime Engineering, Department of Mechanical Engineering, Technical University of Denmark, Nils Koppels Allé, 2800 Kgs. Lyngby, Denmark.
[2]National Institute of Aquatic Resources and Centre for Ocean Life, Technical University of Denmark, DK-2800 Kgs. Lyngby, Denmark
[3]Department of Physics and Centre for Ocean Life, Technical University of Denmark, DK-2800 Kgs. Lyngby, Denmark
[4]Computational Science and Engineering Laboratory, ETH Zürich, Clausiusstrasse 33 ETH-Zentrum, CH-8092 Zürich, Switzerland

This is a revised layout of the article published in *Journal of Royal Society Interface* Vol. 16, pp. 20180478, 2019.

Contributions

Major contributions to the work:

- Designing the research together with all co-authors.
- Developing a new method and mathematical framework to simulate the force and torque free organism.
- Carrying out presented CFD simulations and analyzing the results.
- Preparing all figures and writing all text, including corrections from the co-authors.

Abstract

Choanoflagellates are unicellular eukaryotes that are ubiquitous in aquatic habitats. They have a single flagellum that creates a flow toward a collar filter composed of filter strands that extend from the cell. In one common group, the loricate choanoflagellates, the cell is suspended in an elaborate basket-like structure, the lorica, the function of which remains unknown. Here, we use Computational Fluid Dynamics to explore the possible hydrodynamic function of the lorica. We use the choanoflagellate Diaphaoneca grandis as a model organism. It has been hypothesized that the function of the lorica is to prevent refiltration (flow recirculation) and to increase the drag and, hence, increase the feeding rate and reduce the swimming speed. We find no support for these hypotheses. On the contrary, motile prey are encountered at a much lower rate by the loricate organism. The presence of the lorica does not affect the average swimming speed, but it suppresses the lateral motion and rotation of the cell. Without the lorica, the cell jiggles from side to side while swimming. The unsteady flow generated by the beating flagellum causes reversed flow through the collar filter that may wash away captured prey while it is being transported to the cell body for engulfment. The lorica substantially decreases such flow, hence it potentially increases the capture efficiency. This may be the main adaptive value of the lorica.

1 Introduction

Choanoflagellates are filter feeders and an important component of microbial foodwebs [1, 2]. They share ancestry with animals and have remarkably common characteristics with the choanocytes of sponges [3]. During the past century, choanoflagellates have been subject to numerous studies with the goal of understanding the evolution of multicellularity in animals [4, 5]. Like other microswimmers, choanoflagellates live in a low Reynolds number world that is dominated by friction and very different from the inertia-dominated world of macroswimmers [6, 7]. This is important to these purely heterotrophic organisms that rely exclusively on prey captured from a very dilute suspension, requiring them to daily clear a volume of water corresponding to one million times their own body volume [8].

Choanoflagellates are equipped with a single flagellum that creates a flow toward the collar filter where bacteria-sized prey are retained on the microvilli tentacles. Some choanoflagellates (over 150 species) construct a very ornate extra-cellular basket-like structure, known as lorica [2] (Figure B.1). We shall focus on the loricate choanoflagellate *Diaphanoeca grandis* that has a flagellum beating in a plane and a collar filter consisting of approximately 50 microvilli. The lorica of *D. grandis* contains 12 longitudinal and 4 transverse costae (ribs) [2] (Figure 1B). The upper part of the lorica is covered by an organic investment composed of numerous filaments (veil) woven tightly.

As the flagellum beats, water enters the lorica chamber from the large spacings between the ribs in the lower part. The water is transported toward the equator and then passes through the collar filter and finally exits from the chimney. Nielsen et al. [5] demonstrated that the observed high flow rate through the collar filter of *D. grandis* can be explained by the inclusion of a flagellar vane, a structure that has been reported in closely related organisms [3, 9–12], but has not so far been observed in *D. grandis*. In the choanocytes of the leucon sponge, Asadzadeh et al. [13] demonstrated that the presence of the vane together with its interaction with the fine-meshed collar are indispensable for providing sufficiently high pressure to drive the flow through the sponge canal system [14–16].

The presence of the lorica has puzzled scientists for almost a century, and despite extensive research on the morphology, construction, and assembly of the lorica, there are only few and limited studies on its functionality [2]. Proposed functionalities are based on pure conjecture by analyzing morphological and ecological information [2]. Thus far three functions of the lorica have been proposed: First, the lorica functions as a drag-anchor that counteracts propulsion such that the force generated by the flagellum is rather spend on forcing water through the collar filter [17]. Second, the presence of the fine-meshed veil on the lorica acts in a hydrodynamic sense by funneling the inflow through the lorica and increases the water flow [17]. Third, the silicified lorica likely reduces the sinking velocity, especially in those species that possess spines [2], analogous to the function of spines in many diatom species [18].

Although the above suggestions seem plausible, they lack evidence and remain speculative. To examine the actual effect of the lorica, one direct approach is to study a loricate species with and without its lorica. However, as pointed out by Pettitt et al. [19] this is not a feasible experiment. Here we choose an alternative approach and use computational fluid dynamics (CFD) to study the flow around a single but representative model organism (*D. grandis*) with and without its lorica to elucidate the hydrodynamic functions of the lorica and test the validity of the proposed functionalities. Additionally, we experimentally measured the forward swimming speed of freely swimming individuals of *D. grandis*, and we used the results to validate our CFD simulations.

We first investigate the permeability of the veil on the lorica in a tethered *D. grandis*, and we find that it is practically impermeable to the flow. Modeling the lorica as an impermeable structure in the upper part, we then study the effect of the lorica on the cell motion and power consumption by the flagellum. We further study the flow rate, the flow recirculation, and the resulting clearance rate for the capture of motile and non-motile prey in the freely swimming choanoflagellate. In most cases the lorica has no beneficial role except in stabilizing the cell motion. However, the stabilized cell motion

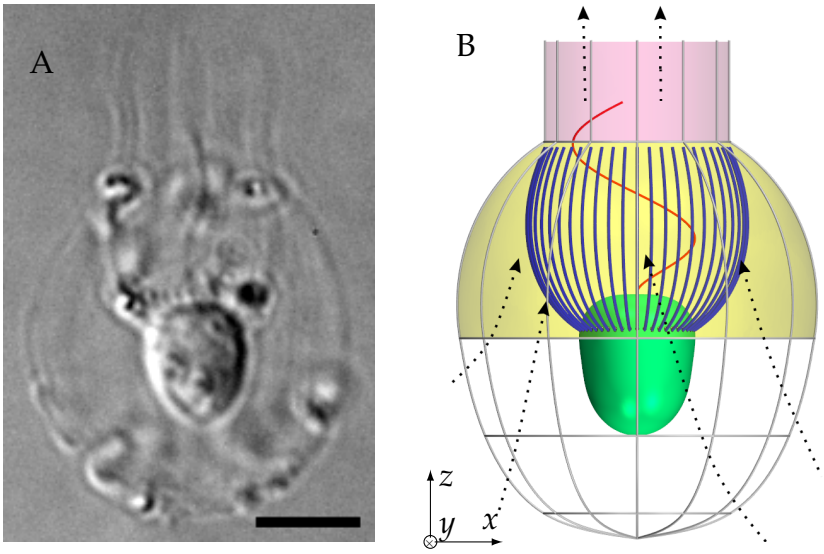

Fig. B.1: Morphology of *Diaphanoeca grandis*. A) Microscopic image (scale bar: 5 μm). B) Model morphology with collar filter composed of 50 microvilli (blue), cell (green), flagellum (red), and lorica containing 12 longitudinal and 4 transvesre ribs (grey) with a fine network of filaments (the veil) on the lorica dome (yellow) and chimney (pink). The arrows indicate the direction of the flow.

reduces the 'back-flow' through the filter and thus may increase the efficiency of prey retention on the collar filter.

2 Material and Methods

In this section we explain the numerical approach and the method employed for simulating a permeable lorica. We further explain the technique developed to simulate the freely swimming organism as well as our procedure to simulate advective and diffusive prey capture. Finally, we describe the experimental measurements of the swimming speed of *D. grandis*.

2.1 Computational Fluid Dynamics

We use Computational Fluid Dynamics (CFD) simulations to study the flow around *D. grandis*. The domain is discretized by polyhedral cells and a finite volume method is used to discretize and solve the governing equations on each cell by applying the commercial CFD program STAR-CCM+ (12.02.010-R8).

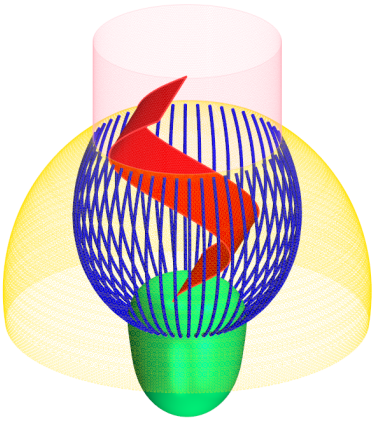

Fig. B.2: CFD model morphology of *Diaphanoeca grandis* with a 5-μm wide flagellar vane (red), the microvilli (blue), and the cell (green) which are all subject to no-slip boundary conditions, and the lorica dome (yellow) and the chimney (pink) treated as porous baffle with an adjustable porosity. The ribs in the lower part of the lorica are neglected in the CFD model.

$A\,(\mu\mathrm{m})$	$L\,(\mu\mathrm{m})$	$f\,(\mathrm{Hz})$	$\lambda\,(\mu\mathrm{m})$	$W\,(\mu\mathrm{m})$
2.8	8.3	7.3	8.6	5

Table B.1: Characteristic parameters of the flagellum in *D. grandis* [5]. A is the amplitude, L the length on the central z-axis, f the frequency, λ the wavelength, and W the width of the flagellar vane.

2.1.1 Governing equations and power expenditure

The governing equations of an incompressible Newtonian fluid with density ρ and viscosity μ are the continuity and Navier-Stokes equations:

$$\nabla \cdot \mathbf{u} = 0 \tag{B.1}$$

$$\rho\left(\frac{\partial \mathbf{u}}{\partial t} + (\mathbf{u}\cdot\nabla)\mathbf{u}\right) = -\nabla p + \mu\nabla^2\mathbf{u} \tag{B.2}$$

where $\mathbf{u}$ and p denote flow velocity and pressure, respectively.

Figure B.2 shows the CFD model of *D. grandis* with applied boundary conditions. Since the observed flow is only obtained by inclusion of a vane on the flagellum and not by a naked flagellum, we model this structure by a 5 μm-wide sheet which beats in a plane [5]. We model the lateral displacement of the flagellum during its beat with the following traveling wave form:

$$d(z,t) = A[1 - e^{-(z-z_B)/\delta}]\sin\left(k(z-z_B) - \omega t\right) \tag{B.3}$$

for $z \geq z_B$ where z_B is the z-coordinate of the flagellum at its base where it is connected to the cell, $\delta = 1.0\,\mu$m the characteristic length scale of the amplitude modulation, $k = 2\pi/\lambda$ the wave number, and $\omega = 2\pi f$ the angular frequency. The exponential term ensures that the velocity of the flagellum is zero at its base. Table B.1 lists the characteristic parameters of the flagellum [5]. The details of the CFD model morphology for cell, filter and lorica are provided in the Supplementary Information (section 5). The Reynolds number is the ratio of inertial to viscous forces, and in small scale flows around flagellate cells it is much smaller than unity, ranging from 10^{-2} to 10^{-4} [20, 21]. Employing $\rho = 997\,\mathrm{kg/m^3}$ and $\mu = 0.001\,\mathrm{Pa \cdot s}$, here $\mathrm{Re} = \rho L^2 f/\mu \sim 5 \times 10^{-4}$. Therefore the inertial terms on the left hand side of Eq. (D.3) are negligible and the governing equations reduce to the Stokes equations that are time independent [7]. Hence, it suffices to solve the flow around the choanoflagellate at only some discrete positions of the periodically beating flagellum during a half period. However, here we solve the full Navier-Stokes equations including the unsteady and the nonlinear inertial terms that are both embedded in the STAR-CCM+ software. By retaining the unsteady term and using mesh morphing, which redistributes mesh vertices in response to the movement of the flagellum, the new position of the flagellum is updated during each time step. This method dramatically reduces the extra work of otherwise constructing the new geometry and repeated generation of the finite volume mesh.

The flagellar vane, the microvilli and the cell are subject to the no-slip boundary condition. The lorica in the upper part is treated as a permeable surface with an adjustable porosity to study the effect of the lorica pore size on the flow, but as an impermeable surface in the remainder of this study. The ribs in the lower part are neglected in the CFD simulations. The whole organism is inserted inside a spherical domain, and a pressure boundary condition is applied on the external boundary. The computational domain is discretized with 4.8 and 2.3 million computational cells for loricate and non-loricate cases, respectively. In both cases the force and the flow rate are independent of the number of cells ($\sim$ 2% variations). For the advection and diffusion problem, the mesh is further refined on and in between the microvilli and downstream of the collar, where the concentration gradients are high, resulting in 12 and 13 million computational cells for loricate and non-loricate cases, respectively. Finally, to ensure independence of the size of the domain, we solve the governing equations on three different domain sizes with diameters of 60 μm, 80 μm and 120 μm, and we find less than 1% variations in the results. Therefore we use a domain with a diameter of 60 μm.

Once the velocity field has been determined, the power (P) expended by the beating flagellum is calculated as the surface integral over the flagellum area (S_{fl}) of its local velocity (Eq. (D.1)) times the resultant stress vector ($\sigma \cdot \mathbf{n}$). We verify that the total power expenditure equals the volume integral over

the fluid domain (V) of the viscous dissipation:

$$P = \iint_{S_{fl}} \mathbf{u} \cdot (\sigma \cdot \mathbf{n}) \, \mathrm{d}S = 2\mu \iiint_{V} \mathbf{E} : \mathbf{E} \, \mathrm{d}V \tag{B.4}$$

where $\mathbf{n}$ denotes the unit normal vector on the surface S_{fl} pointing into the fluid and $\mathbf{E} = (\nabla\mathbf{u} + (\nabla\mathbf{u})^{\mathrm{T}})/2$ the fluid strain rate tensor [22]. Equation (C.4) is valid for both tethered and freely swimming organism.

2.1.2 Model of the lorica as a permeable structure

The veil in the upper part of the lorica is composed of $\sim 0.01\,\mu$m thick filaments with radius $a = 0.005\,\mu$m, and it has a pore size $h = 0.05$-$0.5\,\mu$m [17]. To study the effect of the porosity of the lorica on the flow around the cell, we consider the lorica as a porous baffle that the flow can pass through subject to a pressure drop. We model this structure as a square network of cylinders of spacing h. The pressure drop (Δp_p) due to fluid flow through such a network can be related to the velocity normal to the network surface (v_n) as:

$$\Delta p_p = \frac{16\pi\mu}{h\Lambda_e} v_n \tag{B.5}$$

where $\Lambda_e = 1 - 2\ln\tau + \tau^2/6 - \tau^4/144 + \tau^6/1080 + ...$ and $\tau = 2\sqrt{2}\pi a/h$ [23]. Equations (D.2) and (D.3) subject to Eq. (B.5) are solved to obtain the velocity and pressure fields.

2.1.3 Solution procedure to model free swimming

For swimming at low Reynolds numbers, the change in the momentum is negligible compared to the pressure and viscous forces. Therefore, at any instant of time, the forces ($\mathbf{F}$) and torques ($\mathbf{L}$) of the fluid (as given by viscous and pressure forces in the stress tensor) are balanced by any external forces and torques acting on the swimmer [7]:

$$\begin{pmatrix} \mathbf{F} \\ \mathbf{L} \end{pmatrix}_{\text{ext}} + \begin{pmatrix} \mathbf{F} \\ \mathbf{L} \end{pmatrix}_{\text{fluid}} = \mathbf{0} \tag{B.6}$$

The fluid forces and torques are calculated by integrating the stress tensor over the swimmer surface:

$$\mathbf{F} = \iint_{S} \sigma \cdot \mathbf{n} \, \mathrm{d}S, \quad \mathbf{L} = \iint_{S} \mathbf{r} \times (\sigma \cdot \mathbf{n}) \, \mathrm{d}S \tag{B.7}$$

where $\mathbf{r}$ denotes the position on the surface S.

The motion of a microswimmer is a superposition of a deformation and a rigid body motion. The rigid body forces and torques are related to the

translation velocity and rotation rate through the resistive matrix $\mathbf{R}$ of the body [7]. In our case the flagellum beats in xz-plane and because of the mirror-symmetry with respect to this plane, only translation and rotation in the xz-plane are allowed. Therefore

$$\mathbf{F}_{\text{ext}} + \mathbf{F}_{\text{def}} + \mathbf{R}\mathbf{U} = \mathbf{0} \tag{B.8}$$

where

$$\mathbf{F}_{\text{ext}} = \begin{bmatrix} F_x \\ F_z \\ L_y \end{bmatrix}_{\text{ext}}, \quad \mathbf{F}_{\text{def}} = \begin{bmatrix} F_x \\ F_z \\ L_y \end{bmatrix}_{\text{def}}, \quad \mathbf{U} = \begin{bmatrix} U_x \\ U_z \\ \Omega_y \end{bmatrix}$$

Here F_x and F_z denote x and z-component of the force, and U_x, U_z are the x and z-component of the velocity, respectively. L_y and Ω_y are the torque and rotation rate with respect to an arbitrary point. Here, we choose the base of the flagellum $(0, 0, z_B)$ as the point about which the organism rotates. The resistive matrix $\mathbf{R}$ is a square 3×3 matrix:

$$\mathbf{R} = \begin{bmatrix} r_{11} & r_{12} & r_{13} \\ r_{21} & r_{22} & r_{23} \\ r_{31} & r_{32} & r_{33} \end{bmatrix}$$

The unknown matrix elements depend on the shape of the organism and since the flagellum is constantly changing its shape, the matrix is also time-dependent. It can be shown that $\mathbf{R}$ is always symmetric, resulting in 6 unknowns in the matrix [24]. In the absence of any external forces and torque, the organism is freely swimming and Eq. (B.8) reduces to:

$$\mathbf{F}_{\text{def}} + \mathbf{R}\hat{\mathbf{U}} = 0 \tag{B.9}$$

where

$$\hat{\mathbf{U}} = \begin{bmatrix} \hat{U}_x \\ \hat{U}_z \\ \hat{\Omega}_y \end{bmatrix}$$

represents the swimming vector. Equation (B.9) represents 3 equations with 12 unknowns. However, $\mathbf{U}$ in Eq. (B.8) is arbitrary, and 4 appropriate choices of $\mathbf{U}$ yield 9 independent equations to solve for all elements of the matrix $\mathbf{R}$ and vector $\mathbf{F}_{\text{def}}$. This is equivalent to the problem of towing the organism with some arbitrary velocity $\mathbf{U}$ and imposing the external forces and torque that equal the fluid forces and torque calculated by Eq. (B.7). Once these quantities are found, the swimming vector $\hat{\mathbf{U}}$ is determined by Eq. (B.9).

The arbitrary choices of the vector $\mathbf{U}$ in Eq. (B.8) are as follow:

1. $\mathbf{U} = \begin{bmatrix} 0 \\ 0 \\ 0 \end{bmatrix}$ gives $\mathbf{F}_{\text{def}}$

2. $\mathbf{U} = \begin{bmatrix} 1 \\ 0 \\ 0 \end{bmatrix}$ gives r_{11}, $r_{21} = r_{12}$ and $r_{31} = r_{31}$

3. $\mathbf{U} = \begin{bmatrix} 0 \\ 1 \\ 0 \end{bmatrix}$ gives r_{22} and $r_{32} = r_{23}$

4. $\mathbf{U} = \begin{bmatrix} 0 \\ 0 \\ 1 \end{bmatrix}$ gives r_{33}

Finally, once the swimming vector $\hat{\mathbf{U}}$ is determined, one more simulation is conducted to obtain the pressure and velocity fields, and to extract the forces on the different body parts of the choanoflagellate in the freely swimming form. The above calculations have been performed independently for 12 different positions of the flagellum during the first half of its beat period.

2.1.4 Advection and diffusion of prey

In loricate choanoflagellates the structure of the lorica is such as to guide the flow through the lorica chamber [2]. In *D. grandis* specifically, the beating flagellum sucks in the water from the lower part of the lorica through the equator and expels it out from the chimney resembling a jet [5]. This arrangement may suggest that the cell is directing the water far away from itself in order to prevent refiltration of once filtered water, a phenomenon which the volume flow rate *per se* does not account for. To test this hypothesis, we assume that prey concentration (C) satisfies the advection-diffusion equation [25, 26]:

$$\frac{\partial c}{\partial t} + \mathbf{u} \cdot \nabla c = D \nabla^2 c \tag{B.10}$$

where $c = C/C_\infty$ is the dimensionless concentration field, C_∞ the concentration of the prey in the far field, and D the diffusivity of the prey due to Brownian motion and motility. The collar filter acts as a sink and consumes the prey once it reaches it, essentially leading to a vanishing value of c. To model this behaviour, we set $c = 0$ in a thin volume inside the collar filter, in close proximity of the microvilli using a source term that is active in this region [27]. We set $c = 1$ on the outer boundary where the flow enters the domain. Initially the concentration inside the collar filter volume is zero and elsewhere $c = 1$. Both the advective and the diffusive transport through the filter contribute to the clearance rate:

$$Q_{net} = -\int_{S_{filter}} (c\mathbf{u} - D\nabla c) \cdot \mathbf{n} \, \mathrm{d}S \tag{B.11}$$

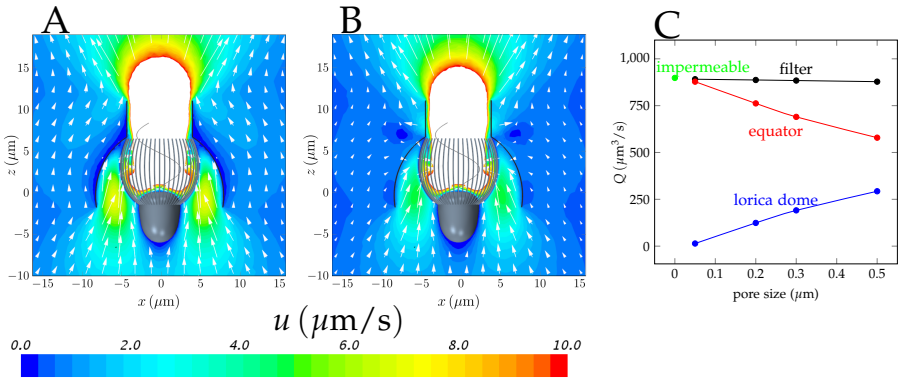

Fig. B.3: Dependence of flow velocities and flow rates on the permeability of the lorica. Velocity field in the xz-plane for the lorica pore sizes of 0.05 μm (A) and 0.5 μm (B) time-averaged over the flagellum beat cycle. For clarity, the velocity magnitudes higher than 10 μm/s are omitted. (C) Mean flow rate through the filter, equator plane and lorica dome for different pore sizes of the lorica. As the pore size increases, the volume flow rate through the equator plane decreases while more flow permeates through the lorica dome which intercepts the prey particles larger than its pore size. The flow through the collar filter is independent of the lorica pore size and very close to the case of an impermeable lorica.

The simulations are performed for 40 beat cycles at which time the flow is sufficiently developed and periodicity in the net clearance rate has been obtained.

2.2 Observed swimming speed

Diaphanoeca grandis (American Type Culture Collection no. 50111) was cultured non-axenically in the dark at 10^{o}C, using B1 medium with a salinity of 32. Organically grown, autoclaved rice grains were added as bacterial substrate [5]. To determine the swimming speed, freely swimming *D. grandis* cells were observed using an Olympus IX-71 inverted microscope equipped with a UPLSAPO60XO/1.35 oil-immersion objective and a U-ECA magnifying lens. Image sequences were recorded at 100 frames per second and a resolution of 1024 $\times$ 800 pixels using a Phantom v210 high-speed camera. Observations were done in a chamber constructed from a 5 mm high polycarbonate ring (diameter $\sim$1 cm) mounted with non-hardening silicone between an objective slide and a coverslip.

3 Results and Discussion

3.1 Permeability of the lorica

In this section we simulate a tethered *D. grandis* and model the lorica as a porous structure with a range of pore sizes between 0.05 and 0.5 μm. Figure B.3 depicts the velocity field in the xz-plane for the two different pore sizes of 0.05 and 0.5 μm averaged over the flagellum beat cycle. A pore size of 0.05 μm practically acts as an impermeable structure (Figure B.3A). However, as the porosity increases from 0.05 to 0.5 μm, the lorica becomes permeable to the flow (Figure B.3B), in response to the negative pressure created below the lorica dome (Eq. (B.5)). Consequently, a portion of the flow reaching the collar filter passes through the lorica dome which results in less flow entering the collar filter through the equator plane. Figure B.3C shows the time-averaged flow rate through the equator plane, the collar filter, and the lorica dome for a complete beat cycle. The flow through the filter is almost independent of the lorica porosity, and for all cases it is very close to the volume flow rate approximated by the pumping mechanism value of $Q_V = AW\lambda f = 879\,\mu\text{m}^3/\text{s}$ proposed by Nielsen et al. [5] (Eq. 5 therein). This is because the flagellum acts nearly as a positive displacement pump in a system of small overall resistance as flow shifts between paths for changing lorica porosity.

Since only the collar filter captures prey, the lorica blocks prey larger than its pore size (i.e. typical bacteria-sized prey) from reaching the filter. Thus, only flow passing the equator plane provides nutrition for the cell, and this decreases as the porosity of the veil increases. This suggests that the lorica costae either should be covered with a fine mesh, virtually impermeable to the flow, or with a very coarse mesh not to intervene in the prey capture process. An intermediate pore size allows water to pass through while intercepting bacteria-sized prey, consequently impairing the feeding process. In fact, the lorica either contains a fine veil, as compared to the filter spacing, or in some species it appears as an open structure [2]. Nevertheless, even with a medium pore size, more than 80% of the flow goes through the equator plane. Therefore, modeling the lorica as an impermeable structure in the CFD study is an acceptable approximation to the actual structure, and henceforth, employing the previously used CFD model [5], we consider the lorica as an impermeable baffle subject to the no-slip boundary condition.

3.2 Swimming motion and power expenditure

Loricate choanoflagellates are generally slow swimmers compared to non-loricate species [2, 17]. Figure B.4 shows the velocity components and the rotation rate of our modeled freely swimming *D. grandis* with and without its lorica. The forward swimming velocity ($\hat{U}_z$) of *D. grandis* varies slightly

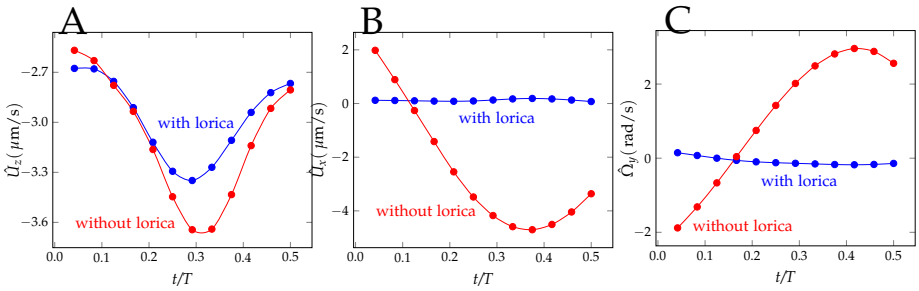

Fig. B.4: Velocity components and rotation rate during one half cycle for *Diaphanoeca grandis* with and without its lorica. The presence of the lorica does not significantly alter the swimming velocity (A), but it dampens significantly the lateral velocity (B) and the rotation rate (C).

during the half cycle with a mean value of $3.0\,\mu$m/s (Figure B.4A). This is in agreement with experiments where the forward swimming velocity $U_{exp} = 2.2 \pm 1.1\,\mu$m/s was obtained as the average of 6 different individuals of *D. grandis*. The forward swimming is the dominant motion of the choanoflagellate and the lateral velocity and rotation are relatively small (Figures B.4B and B.4C). As a result, *D. grandis* swims smoothly forward along a rather straight line without additional motion (Movies S1 and S2). When the lorica is removed, the choanoflagellate appears to remain a slow swimmer with a mean forward swimming velocity of $3.1\,\mu$m/s very close to that of the loricate one. However, in this case, the lateral velocity components and rotation rate are significant and the cell wiggles from side to side as it swims forward (Movie S3). Hence, the lorica appears to stabilize the movement of the cell. It is striking that the forward swimming velocity of *D. grandis* is almost independent of the presence of a lorica since previously it has been suggested that the lorica slows down the forward motion by imposing a significant drag that counteracts the locomotory flagellum force [17]. Table B.2 lists the force in the swimming direction on different parts of *D. grandis* with and without its lorica in the freely swimming form, as well as in the case of externally towed, rigid body with a mean swimming velocity of $3\,\mu$m/s. In the freely swimming *D. grandis* the flagellum force nearly balances the drag on the body and filter, while the drag on the lorica is insignificant.

The reason that the large lorica does not create significant drag is that the flow is driven "internally" by the beating flagellum. The resulting flow differs markedly from the flow around the towed cell (Figure B.5). In the latter, the drag force is owing to positive contributions of both the pressure and shear forces [24]. However, in an internal flow, the pressure contribution can counteract the viscous forces depending on the shape of the object and its interaction with other body parts, resulting in a smaller net drag force. This is the case for the lorica, for which the flow is internal. The time-averaged pres-

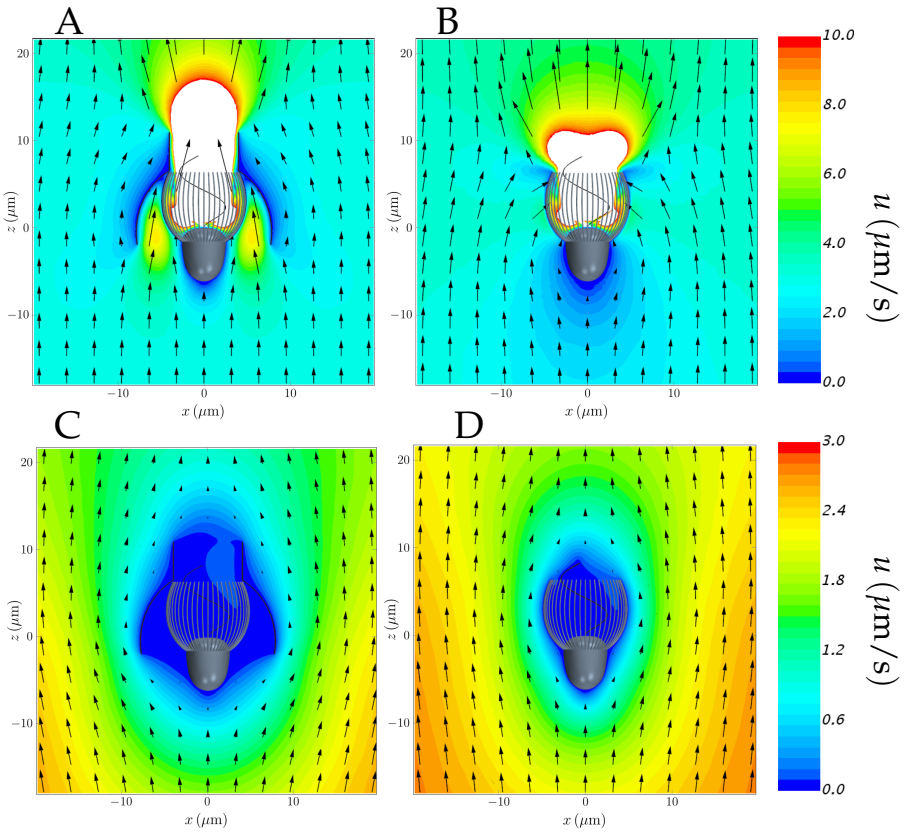

Fig. B.5: Flow fields in the freely swimming and towed choanoflagellates in the frame of reference moving with the cell. A and B) Velocity field around freely swimming *Diaphanoeca grandis* with and without its lorica averaged over the flagellum beat cycle. C and D) Velocity field around the towed *D. grandis* with and without its lorica with a velocity of $3\,\mu m/s$. The flow near and through the lorica and the filter is dominated by the beating flagellum. Moreover, when towed, the presence of the lorica reduces the flow velocity over the cell and hence reducing the force on the cell and the collar filter.

Case		Force (pN)				
		Flagellum	Cell	Filter	Lorica	Total
Freely swimming	With lorica	- 12.091	4.343	7.169	0.580	0.001
	Without lorica	- 8.522	3.344	5.173	-	0.004
Towed	With lorica	0.027	0.008	0.027	0.382	0.444
	Without lorica	0.027	0.057	0.208	-	0.292

Table B.2: The z-component of the force on different parts of *Diaphanoeca grandis* with and without its lorica in the freely swimming and towed choanoflagellate with velocity of $3\,\mu\mathrm{m/s}$ in the swimming direction.

sure field in the xz-plane reveals a low pressure region right below the lorica dome which creates a suction region pulling the lorica down (Figure B.6). As a result, the pressure force acts in the opposite direction of the flow and counteracts the shear drag such that the net drag on the lorica is comparably small.

When *D. grandis* is towed (or is exposed to an external flow), the drag on the lorica plays a significant role, contributing 86 % to the total drag (Table B.2). However, the force on the lorica is very small in comparison with the force due to the beating flagellum of the freely swimming organism. In addition, the presence of the lorica significantly decreases the drag force on the filter and the cell by factors of 7.7 and 7.1, respectively. The lorica increases the total external drag force on the choanoflagellate by 52% (Table B.2).

Finally, Figure B.7 shows the mechanical power consumption by the flagellum over a half cycle for *D. grandis* with and without its lorica; the average power consumption is 2.20 and 1.75 fW, respectively. To compare these values to the metabolic budget of the choanoflagellate, we use the size dependent mass-specific metabolic rate for the flagellate, $\mathrm{RR} = 173\,\mathrm{M}^{0.17}$ [28], where RR is the specific respiration rate in $^{-}\mathrm{l\,O_2\,mg\,C^{-1}\,h^{-1}}$ and M the body mass of the organism in mgC. As an estimate of the carbon content, we take 10% of the organism mass, resulting in 9.2×10^{-9}mgC. To relate the respiration rate to metabolic rate, we use a standard oxycalorific value of 13.8 $\mathrm{J\,mg\,O_2^{-1}}$ [29, p. 592] which gives a value of 375 fW, two orders of magnitudes bigger than the power expenditure by the flagellum. Even though the efficiency of conversion is not 100%, the relative cost of beating the flagellum is low, and therefore the additional power consumption with the lorica

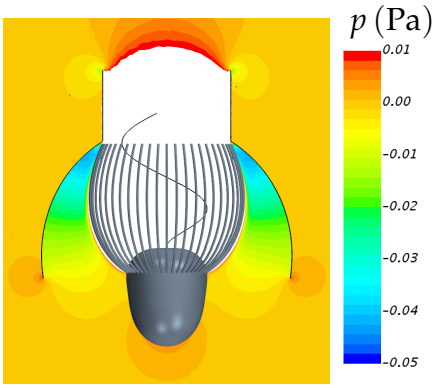

Fig. B.6: The time-averaged pressure field in the xz-plane around the freely swimming *D. grandis* reveals a low pressure region right below the lorica dome which results in a pressure force in the swimming direction. For clarity, the pressure inside the filter and chimney is not shown.

is insignificant.

3.3 Clearance rate

This section presents the effect of the lorica on the clearance rate in the freely swimming choanoflagellate. First we discuss the flow rate through the collar filter, i.e. neglecting the diffusion and depletion of the prey, and then on the net clearance rate where advection and diffusion of the prey are considered.

3.3.1 Flow rate through the collar filter

In the absence of prey diffusion, Eq. (B.11) gives the volume flow rate Q by setting $c = 1$ (the case $D = 0.0$ marked with asterisk in Table B.3). The lorica has a slight effect on the volume flow rate increasing it only by $\sim$5 %. This is consistent with the result of section 3.1 where the flow passing through the filter is shown to be unaffected by the lorica porosity.

Another important aspect is that the slow swimming motion of *D. grandis* does not significantly increase the volume flow rate as compared to the tethered value of $Q = 898\,\mu\text{m}^3/\text{s}$ in the previous study [5]. This is because of a significant resistance by the cell, the filter and the lorica to the swimming, and most of the flow bypasses the collar filter (Figure B.5, C and D).

3.3.2 Advection and diffusion effect

The volume flow rate does not reveal possible effects of flow recirculation and prey diffusivity on feeding. Flow recirculation, i.e. backflow from downstream of the chimney toward the upstream of the lorica, can potentially im-

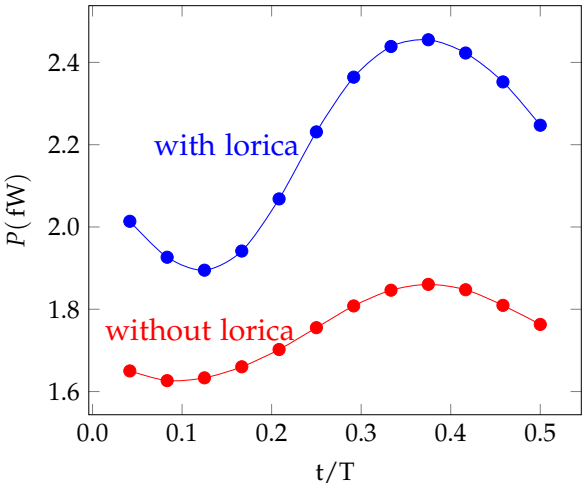

Fig. B.7: Power consumption by the flagellum for *Diaphanoeca grandis* with and without its lorica. The presence of the lorica increases the average required power by $\sim$ 25%, however the power magnitudes are insignificant when compared to the metabolic rate.

$D\,(\mu\mathrm{m}^2/\mathrm{s})$	$Q_{net}\,(\mu\mathrm{m}^3/\mathrm{s})$		$\Delta\,(\%)$
	with lorica	without lorica	
0.0*	902	867	-3.9
0.0	900	853	-5.2
0.4	904	860	-4.9
4.0	920	950	3.3
30.0	1290	2150	66.7

Table B.3: Mean clearance rate Q_{net} for different values of diffusivity D. Δ is percentage difference in Q_{net} with and without lorica. *corresponds to the volume flow rate Q which is obtained by setting $c = 1$ in Eq. (B.11).

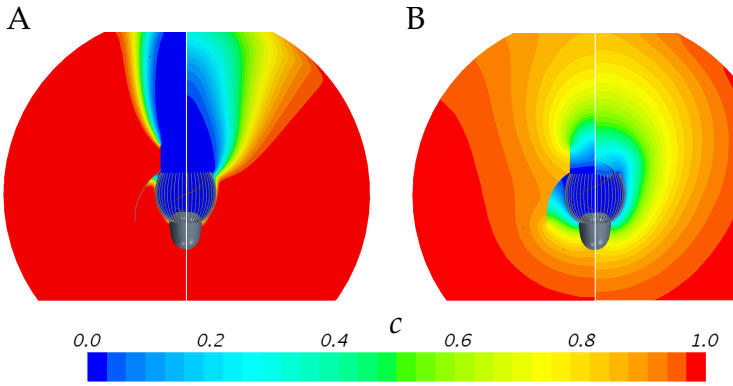

Fig. B.8: Prey concentration (c) in the xz-plane around the freely swimming *Diaphanoeca grandis*. A) $D = 0.4\,\mu\text{m}^2/\text{s}$ which corresponds to the effective diffusivity of typical passive prey due to Brownian motion. B) $D = 30\,\mu\text{m}^2/\text{s}$ which corresponds to the effective diffusivity of typical motile prey. For each case, the left and right half of the plot shows the result with and without its lorica, respectively. At small diffusivity (high Pe), the advection is the dominating transport factor while at higher diffusivity (low Pe), the diffusion becomes dominant. In this case the lorica would act as an insulation to prey diffusion towards the filter, thus reducing the net clearance rate as compared to that of the non-loricate case.

ply refiltration of already filtered water. To determine a more correct volume cleared for prey, we study the net clearance rate Q_{net} of Eq. (B.11) including advection and diffusion of the prey. Table B.3 lists the net clearance rate for different values of prey diffusivity. First we consider only advection of a passive prey ($D = 0.0$), i.e. in the limit of infinite Péclet number. This case is suitable to study the possible recirculation of the flow. Here there is only a minor difference (-5.2%) in the net clearance rate of *D. grandis* with and without its lorica. The function of the lorica is thus not to prevent recirculation.

The case $D = 0.4\,\mu\text{m}^2/\text{s}$ in Table B.3 corresponds to the effective diffusivity due to the Brownian motion of a typical spherical prey of $0.5\,\mu\text{m}$ in diameter at 16^o. In this regime the advective transport is dominant, and the difference in the clearance rate is still small. Although the chimney in *D. grandis* directs the flow far from the choanoflagellate resembling a jet, there is still no sign of recirculation even after the lorica is removed (Figure B.8A). However, as we increase the diffusivity D, i.e. smaller Péclet number, the clearance rate becomes dominated by the diffusion mechanism. At $D = 30\,\mu\text{m}^2/\text{s}$, which is the effective diffusivity of a typical motile prey with swimming speed $44\,\mu\text{m}/\text{s}$ and run time $0.04\,\text{s}$ [30], the net clearance rate of the non-loricate choanoflagellate surpasses the loricate one by 67% (Table B.3). In a pure diffusive transport regime, the flux through a spherical sink in an infinite domain is $Q_{diff} = 4\pi D R_{sink}$ where R_{sink} is the radius of the sink [31]. Employing a mean filter radius of $R_f = 4.3\,\mu\text{m}$ and a diffusivity of $D = 30\,\mu\text{m}^2/\text{s}$, for the case without the lorica we find $Q_{diff} = 1620\,\mu\text{m}^3/\text{s}$

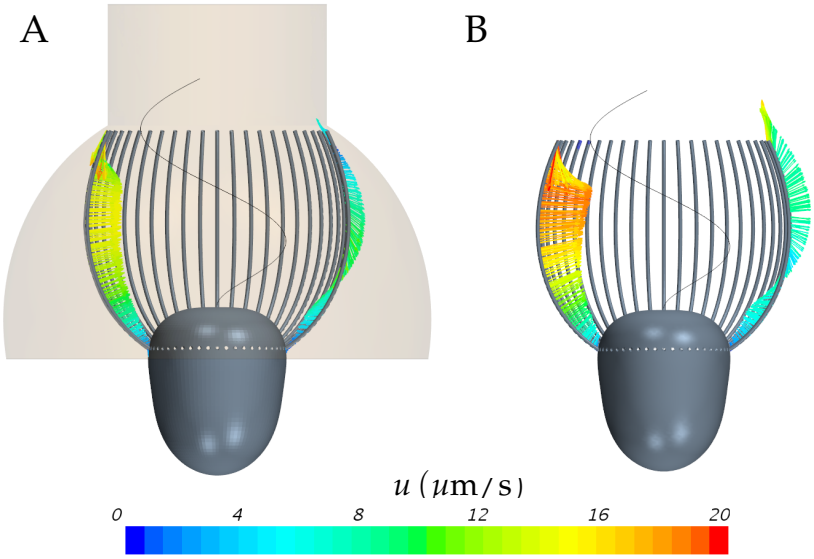

Fig. B.9: Snapshot of the velocity field between the microvilli in the flagellar beat plane (xz-plane) of *Diaphanoeca grandis* with (A) and without (B) its lorica. The lorica mitigates the outward flow from the distal part of the microvilli, potentially increasing the chance of retaining the prey on the collar.

comparable with the total clearance rate indicating the complete dominance of diffusive transport when prey motility is considered. In such a diffusion dominated regime, the lorica suppresses the prey transfer toward the filter (Figure B.8B). This suggests that loricate choanoflagellates are inefficient feeders on motile bacteria.

3.4 Prey retention

Thus far, our results on clearance rates for different scenarios and energy expenditure reveal no significant advantage of the lorica, but rather the opposite for motile prey. However, the clearance rate estimated above assumes that all encountered prey are captured. One should also consider the efficiency of prey capture, that is the ratio of the number of prey particles captured to those encountered. Filter feeding consists of three successive steps: prey encounter, retention and handling [32]. Once the prey is in contact with the microvilli during the encounter process, the cell must retain and transfer it down to the base of the collar toward the cell where it is phagocytosed. This process may take several seconds [19], and in the choanoflagellate *Salpingoeca rosetta*, Dayel et al. [33] report that the movement of bacteria prey to the base and engulfing takes on average 12.5 s and 20 s, respectively. Given that the

flagellum beat period in choanoflagellates is a fraction of a second, the prey experiences hundreds of beat cycles as it is being moved along the collar, with a potential to be lost before being engulfed. We speculate that the lorica increases the efficiency of prey capture by three mechanisms.

Firstly, without lorica, the cell and specifically the microvilli exhibit intense movements from side to side, which possibly hinders prey retention and transportation down to the base of the collar. However in the loricate cells, the lorica stabilizes the cell motion by reducing the lateral motion of the cell and microvilli which could reduce the risk of prey escape. Being thecate or part of a colony could have a similar effect where the cells attach to a substrate or stick together via filopodia and intercellular bridges [34–36]. Attachment or colony formation stabilizes the individual cell and the collar motion, potentially increasing the retention efficiency. This could also be the reason why the flagella beat is not synchronized in colonies [37, 38], as the lateral force and torque from neighbouring cells would stack rather than cancel out.

Secondly, while the flagellum is beating, in some areas at the distal part of the microvilli, the flow direction is outward from the collar. This phenomenon is observed in both loricate and non-loricate cells, but it is much more intense in the latter. Figure B.9 depicts snapshots of the velocity field between the microvilli in the xz plane. Without lorica, the velocity in the upper part of the collar is outward and bigger in magnitude than for the loricate one. Including the lorica mitigates this effect not only by lowering the velocity magnitude, but also by slight downward deflection of the flow. This may increase the likelihood of prey retention on the collar. For the cell to retain a passive prey that encounters the outer surface of the microvilli, the adhesive force by the collar must equal or exceed the local fluid forces resisting the adhesion [32]. For a given adhesive force, the smaller the local fluid forces on the particle, the bigger the likelihood of the bacteria retention on the collar. The lorica reduces velocities on the distal part of the filter, and thus could improve prey retention. Poor particle retention and loss of bacteria from the distal part of the collar has been observed in some species of non-loricate choanoflagellates such as *Salpingoeca amphoridium* [**?**] and *S. rosetta* single cells and colonies [33]. Another remedy to this problem would be to have the prey capture zone mostly on the lower part of the microvilli where there is no outflow; the veil in the loricate choanoflagellate *Didymoeca costata* guides the inflow directly toward the collar base [2] where the prey is immediately captured and ingested.

Thirdly, the lorica chamber, especially in species with a veil on the inner surface of the lorica such as *D. grandis, D. costata* and *Crinolina aperta*, is similar to a trap; even if the prey escapes from the collar, the lorica veil does not allow it to go beyond reach and it is more likely for the choanoflagellate to recapture its prey.

4 Conclusion

In this study, using detailed CFD simulations, we explore the hydrodynamic function of the lorica in the standard tectiform loricate choanoflagellate *Diaphanoeca grandis*. Our results provide no support for the several previous hypotheses regarding the effects of the choanoflagellate lorica. Rather, our simulations suggest that the main function of the lorica is to enhance the capture efficiency, but this happens at the cost of lower encounter rate with motile prey. We note that our study concerns mainly hydrodynamic effects of the lorica. There could well be other effects of the lorica, including e.g. protection against predators.

5 Appendix

Model morphology of *Diaphanoeca grandis*

To prepare the geometry of *D. grandis* for CFD simulations, we use data collated from six individuals that are viewed from the side [5]. We assume that the cell surface and the outline of the lorica have rotational symmetry about the longitudinal axis. In polar spherical coordinates, the cell and the outline of the lorica are described as:

$$R(\theta) = R_0(1 + \alpha_1 \cos\theta + \alpha_2 \cos 2\theta + \alpha_3 \cos 3\theta) \tag{B.12}$$

where θ is the polar angle, and R_0, α_1, α_2 and α_3 are shape parameters. Table B.4 describes the shape parameters used for the cell and the lorica dome. The centerline of a single microvillus with circular cross-section of radius 0.075 ¯m is described as:

$$R_F(\theta) = R_C(\theta_C) + [R_L(\theta_L) - R_C(\theta_C)]\frac{\theta - \theta_C}{\theta_L - \theta_C} \tag{B.13}$$

where $\theta_L = 25$ deg and $\theta_C = 76$ deg are angles where the microvillus connects to the cell and the lorica, respectively. This microvillus is then copied in a circular pattern to obtain 50 evenly distributed microvilli to construct the collar filter.

case	R_0 (¯m)	α_1	α_2	α_3
Cell	2.8	-0.24	0.10	-0.10
Lorica	8.1	0.15	0.05	0.00

Table B.4: Average morphology parameters used to describe the cell and outline of the lorica

References

[1] T. Fenchel, "Suspended marine bacteria as a food source," in *Flows of energy and materials in marine ecosystems*. Springer, 1984, pp. 301–315.

[2] B. S. Leadbeater, *The Choanoflagellates: Evolution, Biology and Ecology*, 1st ed. Cambridge: Cambridge University Press, 2015.

[3] J. L. Mah, K. K. Christensen-Dalsgaard, and S. P. Leys, "Choanoflagellate and choanocyte collar-flagellar systems and the assumption of homology," *Evol. & Develop.*, vol. 16, no. 1, pp. 25–37, 2014.

[4] M. Maldonado, "Choanoflagellates, choanocytes, and animal multicellularity," *Invert. Biol.*, vol. 123, no. 1, pp. 1–22, 2004.

[5] L. T. Nielsen, S. S. Asadzadeh, J. Dölger, J. H. Walther, T. Kiørboe, and A. Andersen, "Hydrodynamics of microbial filter feeding," *Proc. Natl. Acad. Sci. USA*, vol. 114, no. 35, pp. 9373–9378, 2017.

[6] E. M. Purcell, "Life at low Reynolds number," *Am. J. Phys.*, vol. 45, no. 1, pp. 3–11, 1977.

[7] E. Lauga and T. R. Powers, "The hydrodynamics of swimming microorganisms," *Rep. Prog. Phys.*, vol. 72, no. 9, p. 096601, 2009.

[8] T. Kiørboe, "How zooplankton feed: mechanisms, traits and trade-offs," *Biol. Rev.*, vol. 86, no. 2, pp. 311–339, 2011.

[9] E. J. Fjerdingstad, "The ultrastructure of choanocyte collars in *Spongilla lacustris* (l.)," *Z. Zellforsch.*, vol. 53, no. 5, pp. 645–657, 1961.

[10] D. Mehl and H. M. Reiswig, "The presence of flagellar vanes in choanomeres of Porifera and their possible phylogenetic implications," *J. Zoo. Sys. Evol. Res.*, vol. 29, no. 4, pp. 312–319, 1991.

[11] N. Weissenfels, "The filtration apparatus for food collection in freshwater sponges (Porifera, Spongillidae)," *Zoomorph.*, vol. 112, no. 1, pp. 51–55, 1992.

[12] B. S. C. Leadbeater, "The mystery of the flagellar vane in choanoflagellates," *Nova Hedwigia Beiheft*, vol. 130, p. 213, 2006.

[13] S. S. Asadzadeh, P. S. Larsen, H. U. Riisgård, and J. H. Walther, "Hydrodynamics of the leucon sponge pump," *J. Roy. Soc. Inter*, vol. 16, no. 150, p. 20180630, 2019.

[14] P. S. Larsen and H. U. Riisgård, "The sponge pump," *J. Theor. Biol.*, vol. 168, pp. 53–63, 1994.

[15] S. P. Leys, G. Yahel, A. Reidenbach, V. Tunnicliffe, U. Shavit, and H. Reiswig, "The sponge pump: the role of current induced flow in the design of the sponge body plan," *PLoS One*, vol. 6, no. 12, p. e27787, 2011.

[16] D. A. Ludeman, M. A. Reidenbach, and S. P. Leys, "The energetic cost of filtration by demosponges and their behavioural response to ambient currents," *J. Exp. Biol.*, vol. 220, no. 6, pp. 995–1007, 2017.

[17] P. Andersen, "Functional biology of the choanoflagellate *Diaphanoeca grandis Ellis*," *Marine Microbial Food Webs*, vol. 3, no. 2, pp. 35–50, 1988.

[18] A. E. Walsby and A. Xypolyta, "The form resistance of chitan fibres attached to the cells of Thalassiosira fluviatilis Hustedt," *British Phycological Journal*, vol. 12, no. 3, pp. 215–223, 1977.

[19] M. E. Pettitt, B. A. A. Orme, J. R. Blake, and B. S. C. Leadbeater, "The hydrodynamics of filter feeding in choanoflagellates," *Eur. J. Protist.*, vol. 38, pp. 313–332, 2002.

[20] J. J. L. Higdon, "A hydrodynamic analysis of flagellar propulsion," *J. Fluid Mech.*, vol. 90, no. 4, pp. 685–711, 1979.

[21] M. A. Sleigh, "Mechanisms of flagellar propulsion," *Protoplasma*, vol. 164, no. 1-3, pp. 45–53, 1991.

[22] G. K. Batchelor, *An Introduction To Fluid Dynamics*, 1st ed. Cambridge University Press, 1967.

[23] N. R. Silvester, "Some hydrodynamic aspects of filter feeding with rectangular-mesh nets," *J. Theor. Biol.*, vol. 103, no. 2, pp. 265–286, 1983.

[24] J. Happel and H. Brenner, *Low Reynolds number hydrodynamics*, 2nd ed. Kluwer Academic Publishers, 1983.

[25] S. Michelin and E. Lauga, "Optimal feeding is optimal swimming for all Péclet numbers," *Phys. Fluids*, vol. 23, no. 10, p. 101901, 2011.

[26] J. B. Kirkegaard and R. E. Goldstein, "Filter-feeding, near-field flows, and the morphologies of colonial choanoflagellates," *Phys. Rev. E*, vol. 94, no. 5, p. 052401, 2016.

[27] S. V. Patankar, *Numerical Heat Transfer and Fluid Flow*. Hemisphere, 1980.

[28] T. Kiørboe and A. G. Hirst, "Shifts in mass scaling of respiration, feeding, and growth rates across life-form transitions in marine pelagic organisms," *The American Naturalist*, vol. 183, no. 4, pp. E118–E130, 2014.

[29] S. G. Gordon, *Animal Physiology: Principles and adaptations*, 2nd ed. New York: Macmillan Publishing Co, 1972.

[30] J. Dölger, L. T. Nielsen, T. Kiørboe, and A. Andersen, "Swimming and feeding of mixotrophic biflagellates," *Scientific Reports*, vol. 7, p. 39892, 2017.

[31] H. C. Berg, *Random walks in biology*. Princeton University Press, 1993.

[32] J. Shimeta and M. A. R. Koehl, "Mechanisms of particle selection by tentaculate suspension feeders during encounter, retention, and handling," *J. Exp. Mar. Biol. Ecol.*, vol. 209, no. 1-2, pp. 47–73, 1997.

[33] M. Dayel and N. King, "Prey capture and phagocytosis in the choanoflagellate *Salpingoeca rosetta*," *PLoS One*, vol. 9, no. 5, p. e95577, 2014.

[34] M. Dayel, R. Alegado, S. Fairclough, T. Levin, S. Nichols, K. McDonald, and N. King, "Cell differentiation and morphogenesis in the colony-forming choanoflagellate *Salpingoeca rosetta*," *Develop. Biol.*, vol. 357, no. 1, pp. 73–82, 2011.

[35] A. Sebé-Pedrós, P. Burkhardt, N. Sánchez-Pons, S. R. Fairclough, B. F. Lang, N. King, and I. Ruiz-Trillo, "Insights into the origin of metazoan filopodia and microvilli," *Mol. Bio. Evol.*, vol. 30, no. 9, pp. 2013–2023, 2013.

[36] T. T. Hoffmeyer and P. Burkhardt, "Choanoflagellate models-*Monosiga brevicollis* and *Salpingoeca rosetta*," *Curr. Opin. Struct. Biol.*, vol. 39, pp. 42–47, 2016.

[37] J. B. Kirkegaard, A. O. Marron, and R. E. Goldstein, "Motility of colonial choanoflagellates and the statistics of aggregate random walkers," *Phys. Rev. Lett.*, vol. 116, no. 3, p. 038102, 2016.

[38] M. Roper, M. J. Dayel, R. E. Pepper, and M. A. R. Koehl, "Cooperatively generated stresslet flows supply fresh fluid to multicellular chanoflagellate colonies," *Phys. Rev. Lett.*, vol. 110, p. 228104, 2013.

Article C

Hydrodynamics of the leucon sponge pump

Seyed Saeed Asadzadeh[1], Poul S. Larsen[1], Hans Ulrik Riisgård[2], Jens Honoré Walther[1,3]

[1]Section for Fluid Mechanics, Coastal and Maritime Engineering, Department of Mechanical Engineering, Technical University of Denmark, Nils Koppels Allé, 2800 Kgs. Lyngby, Denmark.
[2]Marine Biological Research Centre, University of Southern Denmark, Hindsholmvej 11, DK-5300, Kerteminde, Denmark
[3]Computational Science and Engineering Laboratory, ETH Zürich, Clausiusstrasse 33 ETH-Zentrum, CH-8092 Zürich, Switzerland

This is a revised layout of the article published in *Journal of Royal Society Interface* Vol. 16, pp. 20180630, 2019.

Contributions

Major contributions to the work:

- Designing the research together with all co-authors.
- Developing and deriving a theoretical model for the choanocyte pump model.
- Carrying out presented CFD simulations and analyzing the results.
- Preparing all figures and writing the paper, including corrections from the co-authors.

Abstract

Leuconoid sponges are filter-feeders with a complex system of branching inhalant and exhalant canals leading to and from the close-packed choanocyte chambers. Each of these choanocyte chambers hold many choanocytes that act as pumping units delivering the relatively high pressure rise needed to overcome the system pressure losses in canals and constrictions. Here, we test the hypothesis that in order to deliver the high pressures observed, each choanocyte operates as a leaky, positive displacement-type pump due to interaction between its beating flagellar vane and the collar, open at the base for inflow but sealed above. The leaking backflow is caused by small gaps between the vaned flagellum and the collar. The choanocyte pumps act in parallel, each delivering the same high pressure, because low pressure and high pressure zones in the choanocyte chamber are separated by a seal (secondary reticulum). A simple analytical model is derived for the pump characteristic and by imposing an estimated system characteristic we obtain the back-pressure characteristic that shows good agreement with available experimental data. Computational fluid mechanics is used to verify a simple model for the dependence of leak flow through gaps in a conceptual collar-vane-flagellum system and then applied to models of a choanocyte tailored to the parameters of the freshwater demosponge Spongilla lacustis to study its flows in detail. It is found that both the impermeable glycocalyx-mesh covering the upper part of the collar, and the secondary reticulum are indispensable features for the choanocyte pump to deliver the observed high pressures. Finally, the mechanical pump power expended by the beating flagellum is compared to the useful (reversible) pumping power received by the water flow to arrive at a typical mechanical pump efficiency of about 70%.

1 Introduction

Grazing on phytoplankton and free-living bacteria in marine filter-feeding invertebrates implies feeding on highly dilute suspensions of food particles, and therefore, they must process large volumes of water in highly efficient filters in order to cover their food requirements [1]. Thus, filter-feeding sponges filter a water volume 6 times [2], or higher [3] their volume body per minute. A basic understanding of the pumping and filter mechanisms, and the energy cost therefore continue to attract attention [1, 3–8].

To understand the overall pump function in a filter-feeding organism it is common practice to consider the pump and system characteristics expressed by pressure change P versus water flow rate Q [1]. Thus, as a pump faces an increase in pressure head, the flow generally decreases as given by the pump characteristic $P_{\mathrm{p}}(Q)$. On the other hand, the system pressure drop due to friction through canals and restrictions increases with increasing flow as given by the system characteristic $P_{\mathrm{s}}(Q)$. The intersection between the two relations

defines the operating point, and the pressure head at this point is termed the normal operating pump pressure (cf. e.g. [6, Fig. 14.6 therein]; [1, Fig. 1 therein]). None of these characteristics have so far been measured directly in an organism but they can be estimated from models. However, the so-called back-pressure characteristic $P_b(Q)$ may be determined experimentally by measuring the flow Q for increasing values of back-pressure P_b imposed at the exhalant flow from the organism. Adding an estimated system characteristic to a measured back-pressure characteristic gives the pump characteristic, which was done by [5] for the marine demosponge *Haliclona urceolus*. Despite the linearity of the governing equations of the flow in the low Reynolds number regime inside the the canal system, the measured back-pressure characteristic was found to be non-linear. These authors suggested that changes in diameter of the elastic inhalant and exhalant canals with changes in local hydrostatic pressure might explain the curved back-pressure characteristic. However, the leaky positive displacement pump model presented here also leads to a curved model-pump characteristic due to increased leakage in the pump in response to increasing pressure.

Further, noting the high back-pressure at zero flow (about 2.7 mm H_2O) and high inferred normal operating pump pressure (0.673 mm H_2O) [5] suggested that the choanocyte chamber in demosponges was the basic pump unit, acting as a leaky positive displacement pump due to a constructive interaction between the long flagella of the many choanocytes in the chamber, but this may be erroneous for several reasons. Video recordings [8] have shown that the flagella beat asynchronously and at different frequencies hence excluding coordinated interaction. Also, the structure of the choanocyte chamber with a low and a high pressure zone [7–9] suggests that all choanocytes at the distal part of collars are exposed to the same pressure. In the present study, the positive displacement mechanism is suggested to be at play in the collar of each choanocyte which is therefore suggested to be the basic pump unit, and these units act independently in parallel, each delivering the full pressure required to drive the flow.

In asconoid and syconoid body type sponges [10] where choanocytes line walls, they appear to work in parallel, and are therefore the basic pump units. They deliver the moderate pressure rise required to draw water through the inhalant openings (ostia) and to maintain flow through the rather short and open canals and the exhalant openings (oscula) of these species. In leuconoid type sponges, choanocytes may still be the basic pump units now lining the walls of choanocyte chambers. But because of the much higher pressure required to drive flow through longer and more complex system of canals, the choanocyte chambers are designed with sealed zones of low pressure and high pressure [7–9]. The pressure rise between these zones are maintained by the action of vaned flagella essentially functioning as leaky positive displacement pumps in the collars with well-spaced microvilli near the cell but

essentially sealed microvilli by a mesh of glycocalyx in the upper part of the collar [7–9].

As noted by [8] the collar-flagellum system should be seen as a functionally integrated unit and an integrated collar-vane-flagellum system would require more complex modeling than e.g. slender body theory traditionally used in describing choanoflagellate propulsion or pumping by a beating flagellum. We support this view in the present modeling of the leucon sponge pump.

We first derive a simple analytical gap model which is verified by results from Computational Fluid Mechanics (CFD) applied to a conceptual model of the collar-vane-flagellum system. This model is subsequently used to derive the pump characteristic by imposing an estimated system characteristic to finally obtain the back-pressure characteristic that is compared to available experimental data. The CFD model is then extended to a choanocyte model representing a unit-section of the choanocyte chamber holding one choanocyte to study the effects of different elements of the choanocyte pump on its functionality.

2 Material and Methods

In this section we first describe the numerical approach for studying the flow in choanocyte models. Next we explain the theory for the gap and the pump model.

2.1 Computational Fluid Dynamics

We use Computational Fluid Dynamics (CFD) to numerically solve the governing Navier-Stokes equations of the fluid dynamics in both the conceptual collar-vane-flagellum model and in a choanocyte model. A finite volume method is used to discretize and solve the equations on a discrete representation of the computational domain consisting of polyhedral cells (Figure C.8) by applying the commercial CFD code STAR-CCM+(13.02.011-R8).

2.1.1 Governing equations

The governing equations of an incompressible Newtonian fluid with density ρ and viscosity μ are the continuity and Navier-Stokes equations:

$$\nabla \cdot \mathbf{u} = 0 \tag{C.1}$$

$$\rho \left(\frac{\partial \mathbf{u}}{\partial t} + (\mathbf{u} \cdot \nabla)\mathbf{u} \right) = -\nabla p + \mu \nabla^2 \mathbf{u} \tag{C.2}$$

where $\mathbf{u}$ and p denote the velocity and pressure, respectively. In the small scale world of choanocytes the Reynolds number, the ratio of inertia to viscous forces, is small, here $\mathrm{Re} = \rho V L/\mu = 5.7 \times 10^{-4}$, employing $\rho = 997\,\mathrm{kg/m^3}$, $\mu = 0.001\,\mathrm{Pa \cdot s}$, and $L = 10.4\,\mu\mathrm{m}$ the flagellar central length and $V = \lambda f$ the wave speed, in which $f = 11.0\,\mathrm{Hz}$ is the frequency and $\lambda = 5\,\mu\mathrm{m}$ the wavelength [8]. Therefore the left hand side of Eq. D.3 is negligible, and the flow can be considered as quasi-steady.

We model the displacement of the flagellum in the x direction as a simple traveling wave:

$$d(z,t) = a(1 - e^{-z}) \sin\left(\frac{2\pi}{\lambda}(z - Vt)\right) \tag{C.3}$$

where d is the lateral displacement of the flagellum, a the amplitude, z the centerline axis of the collar, and t time. With this model, the flagellar length varies slightly in time during the beat cycle (a maximum of 1.6%). And since the flow is quasi-steady, the variation in length depends only on two successive positions of the flagellum which is significantly smaller ($\sim 0.02\%$ with a time step $\delta t = 0.0001\,\mathrm{s}$ between two successive positions of the flagellum).

The power expenditure by the vaned flagellum is calculated as:

$$\mathcal{P} = \iint_{S_{\mathrm{fl}}} \mathbf{u} \cdot (\sigma \cdot \mathbf{n})\,\mathrm{d}S \tag{C.4}$$

where $\sigma = -p\mathbf{I} + \mu(\nabla\mathbf{u} + (\nabla\mathbf{u})^T)$ denotes the stress tensor, $\mathbf{n}$ the unit normal vector on the surface S pointing into the fluid, and S_{fl} the flagellar vane area.

2.1.2 Collar-vane-flagellum model

The key to delivering a relatively high pressure (in order to drive flow through the narrow canals in sponges) lies in the collar-vane-flagellum system that effectively functions as a leaky pump. For the conceptual study of the effect of gap size on the maximum pressure delivered by the flagellum pump we replace the cylindrical collar of circular cross section ($3.1\,\mu$m diameter) by one of square cross section ($3.1\,\mu$m width). This model provides well-defined gaps s_1 and s_2 between the beating flagellar vane edges and the collar (Figure C.1). The flagellar vane is modeled as a plate beating in a plane subject to a no-slip boundary condition relative to the motion of the flagellum. The sides (collar) of the computational domain are subject to the no-slip condition, and the inlet and the outlet to pressure boundary conditions representing the imposed system pressure losses associated with flow through restrictions and canals in the sponge.

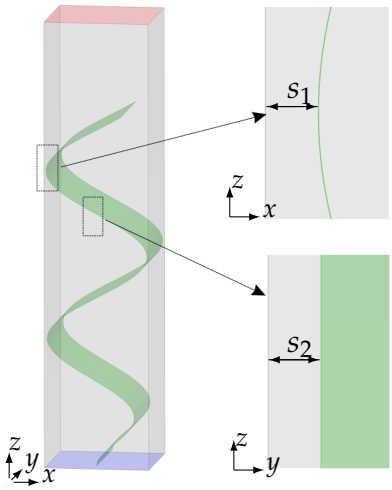

Fig. C.1: Conceptual collar-vane-flagellum model. Flagellar vane (green) inside a sealed collar of 3.1 μm square cross section and height 13.2 μm (grey) with inlet (blue), outlet (red), and defined gaps s_1 and s_2 for flow leaks between the beating flagellum edges and the collar.

2.1.3 Choanocyte model

The choanocyte chamber holds a large number of choanocytes (Figure C.2A) in a close-packed array on its nearly spherical inner wall (primary reticulum) [3, 9]. Our simplified choanocyte model for CFD studies (Figure C.2C) is based on the description by [9]. Here, Figure C.2A shows the choanocyte chamber in the freshwater demosponge *Spongilla lacustris* and Figure C.2B a schematic of a unit-section of the choanocyte chamber holding one choanocyte. In *S. lacustris*, the average collar length is $\sim 8.2\,\mu$m and the collar has 24–36 microvilli of diameter $\sim 0.12\,\mu$m and spacing $\sim 0.06\,\mu$m at their base [8, 11]. The microvilli over the two-third distal part of the collar are tightly held together with a glycocalyx mesh [7, 8]. Despite variations in the collar length and the number of choanocytes, the microvilli and the glycocalyx mesh are believed to be similar among many species of sponges [3, 7–9, 12].

Inflow through a sponge body is driven by suction through numerous small openings (ostia) in its outer surface and further through incurrent canals to enter the choanocyte chambers through several prosopyles before it reaches the choanocyte collars [3, 7]. The choanocyte pumps provide the suction for inflow and further the pressure for the subsequent outflow from the choanocyte chambers through the apopyle and excurrent canals to the exit at the osculum. Inside the flagellated collar chamber, the water is sucked through the relatively large openings between the microvilli at the base of the collar (marked 'oc' in Figure C.2B) and its pressure then increases in the mesh-sealed part of the collar (marked 'sc' in Figure C.2B) by the beat-

ing flagellum on its way into the the inner region of the chamber. This is possible because a low pressure zone is established between primary and secondary reticula (R1 and R2, respectively, Figure C.2B) and a high pressure zone between secondary reticulum and a cone cell ring (near the apopyle, not shown). The secondary reticulum consists of a rather dense, mucus-like material [9, 13]. This arrangement implies that all choanocytes within a chamber experience and hence deliver the same pressure head. Therefore, it is sufficient to simulate a unit-section of the choanocyte chamber holding one choanocyte and subsequently account for possible interactions with neighboring unit-sections by applying various appropriate boundary conditions on the surface of such a unit-section.

In the choanocyte model used for the CFD simulations (Figure C.2C), the flagellum (green) beats with an amplitude of 1.5 μm, has a 3 μm vane only along the sealed part of the collar while it is unvaned and of width 0.3 μm over the rest of its length as observed by [14] and [8]. But we also model the flagellum as vaned over its full length to study its effect on the pump performance. The cross section of the collar is the same as given in Figure C.1. The proximal 2.1 μm length of the collar with opening (oc) is modeled as a porous surface with an assigned porosity corresponding to that of a network of parallel and equidistantly spaced cylinders [15]. The distal fine-meshed part of the collar (sc) is treated as an impermeable surface, but cases of an semipermeable surface [16, 17] is also considered to study the effect of the mesh pore size on the pump performance. Primary and secondary reticula (R1 and R2) are modeled as impermeable surfaces subject to the no-slip condition. A pressure boundary is imposed on the outer surfaces representing the high pressure zone (red). The other four sides of the outer domain (light grey) are exposed to different boundary conditions, i.e. pressure, periodic, symmetry, to model different scenarios of interaction between unit-sections. The last two cases, for example, represent a colony of choanocytes with flagella beats in phase or completely out of phase, respectively. The prosopyle is a semi-circle with a diameter of 5 μm subject to either a pressure boundary, to represent choanocytes sitting near the prosopyle, or to a no-slip boundary (i.e. closed), to represent those sitting far from the prosopyle.

2.2 Theory

2.2.1 Leak flow through gaps

To relate the leak flow to pressure rise and widths of the gaps we consider the collar-vane-flagellum system presented in Figure C.1. The net volume flow Q of the leaky pump is the difference between the positive displacement flow Q_{pos} and the negative leak flows through the gaps:

$$Q = Q_{\text{pos}} - (Q_{\text{s}_1} + Q_{\text{s}_2} - Q_{\text{s}_1,\text{s}_2}) \tag{C.5}$$

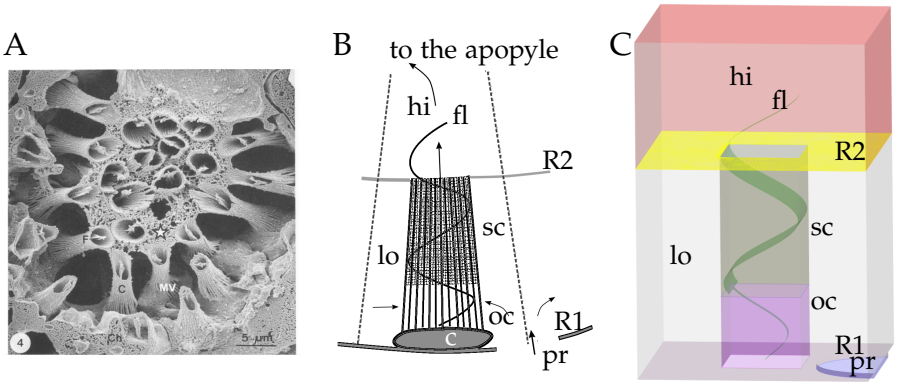

Fig. C.2: Choanocyte chamber and model. A) Scanning electron microscope (SEM) image of choanocyte chamber of the freshwater sponge *Spongilla lacustris*. Choanocyte (Ch), microvilli (MV) of collars, flagellum with vane (F), ends of collars (C) connected to the secondary reticulum (*). From [9] (used by permission: License Number 4464811172505). B) Schematic of a unit-section of the choanocyte chamber holding one choanocyte. Cell (c); flagellum (fl); collar, open near cell (oc), sealed by glycocalyx mesh above (sc), and connected to other collars at distal ends by a sealed secondary reticulum (R2) bounding the high pressure zone (hi). Arrows show inflow from incurrent canal system through prosopyle (pr) to low pressure zone (lo) bounded by the primary reticulum (R1) and through opening at the collar base (oc). Stippled lines represent surface between adjacent similar domains, each with one choanocyte. The flow from the many (50-80) choanocytes in the chamber leaves the high pressure zone through a single outlet, the apopyle (not shown), leading to the excurrent canal system. C) Choanocyte model used in the CFD study where different boundary conditions (Table C.2) are imposed on surfaces between adjacent choanocytes to simulate possible interactions between neighboring choanocytes. The computational domain consists of a 3.1 μm square by 8.2 μm high collar centered in a 9 μm square by 13.2 μm high outer domain with a semi-circular prosopyle inlet of diameter 5 μm at lower right.

where $Q_{pos} = \lambda f(W - 2s_1)(W - 2s_2)$ and W is the square collar width, Q_{s_1} and Q_{s_2} the leak flow through the gaps of width s_1 and s_2, respectively, and Q_{s_1,s_2} the leak flow through overlapping areas where the two gaps meet in the corners of the collar.

The leak flow depends on the excess pressure P generated by the positive displacement effect and the width of gaps between the flagellum and the collar. For an estimate of the leak flow through the gap width s_i (Q_{s_i}, i = 1, 2), consider the leak to be fully developed laminar flow between two parallel plates of spacing s, length l, and width w ($s \ll w$) for which the frictional pressure drop is $P = 12\mu Ul/s^2$ [1, 18]. Here, U denotes the mean velocity that is related to leakage by $Q_s = swU$, yielding the relation:

$$Q_s = Pws^3/12\mu l \simeq cs^2P \tag{C.6}$$

where we have assumed a geometric scaling in which $s/l \simeq const.$ which along with other constant parameters are lumped into the constant c. For an estimate of Q_{s_1,s_2} we use the pressure drop expression for an orifice of diameter r ($Q_r = 24\mu Pr^3$) [19] and assume the same order of magnitude gap widths ($s_1 \sim s_2$):

$$Q_{s_1,s_2} \simeq c_3 s_2^3 P \tag{C.7}$$

where c_3 is a constant. Using Eq. C.6 for the leak flow through the gap width s_i (Q_{s_i}) and combining it with Eqs. C.5 and C.7, in the shut-off condition of no net flow ($Q = 0$), gives:

$$P_{max} = \frac{\lambda f(W - 2s_1)(W - 2s_2)}{c_1 {s_1}^2 + c_2 {s_2}^2 - c_3 s_2^3} \tag{C.8}$$

where c_1 and c_2 are constants corresponding to the gap widths s_1 and s_2, respectively.

2.2.2 Leaky positive displacement pump model

To derive a simple model for the pump characteristic, we assume one and the same small gap size in both directions (Figure C.1 with $s_1 = s_2 = s \ll W$) or, as a special case, contact between the flagellum and the collar in one direction at all times ($s_1 = 0$, $s_2 \neq 0$). Using Eqs. C.5 and C.6 (neglecting the third order term of Eq. C.7), the leaky positive displacement choanocyte pump, consisting of a vaned flagellum beating in the sealed part of the collar, delivers a net volume flow rate of

$$Q = Q_{pos} - Q_{leak} \simeq \lambda f A - \alpha_s s^2 P \tag{C.9}$$

where A is the cross sectional area of the collar and α_s a constant. Note that in case of a cylindrical collar, the gap shape within the collar is more

complex and the gap width might vary inside the collar. Assume a gap shape $s(h)$ as a function of arc length h along the flagellum edges. Now $\mathrm{d}Q_{\mathrm{s(h)}} = c_s \mathrm{d}h\,[s(h)]^2 P$ defines the leak for a segment length $\mathrm{d}h$. For the total leak flow we have:

$$Q_{\mathrm{cyl,leak}} = \int_0^H \mathrm{d}Q_{\mathrm{s}(h)} = \alpha(\frac{1}{H}\int_0^H [s(h)]^2 \mathrm{d}h)P \tag{C.10}$$

where H is the total arc length along the flagellum edges, and $\alpha = c_s H$ a constant. Hence, for a cylindrical collar Eq. C.9 is still valid but the gap width s should be replaced by the root mean square of the varying gap $s(h)$.

It is furthermore expected that the gap width s will increase with increasing pressure due to linear elastic deformation of the flagellar vane and/or the collar according to

$$s - s_o = P/k \tag{C.11}$$

where k is an elastic modulus and s_o denotes the minimum gap width at zero pressure. Inserting Eq. C.11 into Eq. C.9 gives the equation for the model-pump characteristic

$$Q = Q_{\mathrm{pos}} - \alpha_s P(s_o + P/k)^2 \tag{C.12}$$

or in normalized form in terms of pump pressure head $P = P_{\mathrm{pump}}$, satisfying the conditions of $Q(P_{\mathrm{pump}} = 0) = Q_o$ and $P_{\mathrm{pump}}(Q = 0) = P_o$,

$$Q = Q_o \left\{ 1 - \frac{P_{\mathrm{pump}}}{P_o} \left(C_1 + (1 - C_1)\frac{P_{\mathrm{pump}}}{P_o} \right)^2 \right\} \tag{C.13}$$

where $C_1 = s_o/(s_o + P_o/k)$ is a constant.

3 Results and Discussion

In this section we first present the results for the conceptual flagellum-vane-collar system. Next we compare the derived pump model to experiment data, and finally examine detailed CFD results obtained with the choanocyte pump model in regard to the functionality of the pump.

3.1 Effect of gap sizes on pressure rise

To study the gap size effect, we perform CFD simulations of the collar-vane-flagellum system (Figure C.1) for the 'shut-off' condition (closed inlet and outlet) to obtain the maximum pump pressure versus changes in gap widths s_1 and s_2. As shown in Figure C.3 the 16 points obtained from the CFD simulations show very good agreement with the analytical model (Eq. C.8). The three constants c_1, c_2 and c_3 in Eq. C.8 are found by using three arbitrary

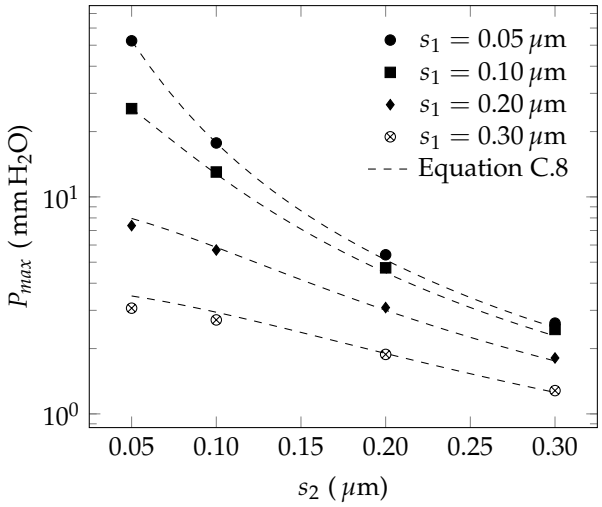

Fig. C.3: Effect of gap widths s_1 and s_2 on the maximum pressure delivered by the flagellum-vane-collar system (Figure C.1) under the 'shut-off' condition of closed inlet and outlet. Equation C.8 (dashed curves) fits well the CFD results (symbols). The pressure rise highly depends on the gap sizes and thus on the flagellum collar interaction.

points from the CFD results. The pressure depends strongly on gap sizes and it decreases dramatically as gaps become larger. This also indicates that an unvaned flagellum would be unable to generate the required pressure due to the huge gap between the flagellum and the collar.

Note that Eq. C.8 gives the maximum pressure delivered by the leaky pump for a rigid flagellum and a rigid collar with an asymptotic infinite pressure as the gap widths decrease to zero (Figure C.3). Although the vane in choanoflagellates is a delicate structure, the vane in choanocytes appears "dense and massive" [14], but nevertheless the flagellar vane and/or the collar are still deformable and likely to bend or expand, resulting in gaps of increasing widths if the pressure load increases sufficiently. Therefore, the actual maximum pressure that a flexible flagellum-vane-collar system is able to deliver will remain finite.

3.2 Sponge pump

To test the leaky pump model (Eq. C.13) against experimental data we consider the measured back-pressure data of the marine demosponge *Haliclona urceolus* [5, Fig. 1c and Table 1 therein]. To obtain the model back-pressure characteristic we subtract the system characteristic from the model pump characteristic (Eq. C.13). The system characteristic is obtained from the esti-

mated system pressure losses given in Table 1 of [5] for the 'standard sponge' of [4], with a modified value for the pressure drop in the collar slits. Since the collar is sealed over the distal two-thirds of its length [8], and the flow only passes through the collar slits at the proximal part, the velocity and hence the table value of pressure drop through the slits is increased by a factor three to give a total of $0.7596 + 0.1576 = 0.9172\,\mathrm{mm\,H_2O}$ at the operating point of the 'standard sponge' in Table 1 of [5]. Noting that the contribution from kinetic energy of exhalant jet from the osculum is quadratic in velocity (or volume flow) while other contributions are linear, and that values correspond to an operating point (zero back-pressure) of $Q_{\mathrm{op}} = 6\ \mathrm{ml\,min^{-1}}$, we scale to the present case of $Q_{\mathrm{op}} = 4.96\ \mathrm{ml\,min^{-1}}$ (read from measured zero back-pressure) by the expression [5]

$$P_{\mathrm{s}} = 0.628Q/Q_{\mathrm{op}} + 0.108(Q/Q_{\mathrm{op}})^2 \tag{C.14}$$

To plot the modeled pump characteristic of Eq. C.13, the parameter $P_o = 2.69\,\mathrm{mm\,H_2O}$ is taken from the measured shut-off pressure head at $Q = 0$, and the parameter $Q_o \simeq 5.07\,\mathrm{ml\,min^{-1}}$ is obtained employing the operating condition $(P_{\mathrm{s,op}}, Q_{\mathrm{op}})$ in Eq. C.13. Figure C.4 shows the back-pressure experimental data, the system characteristic (P_{s}) from Eq. C.14, the model pump characteristic (P_{pump} with $C_1 = 0$ in Eq. C.13 corresponding to zero gap at zero pressure) and the resulting back-pressure characteristic (P_{b}). The modeled back-pressure characteristic captures the general trend of the experimental data.

It can be seen from Figure C.4 that flow rate Q_{op} at the operating point lies very close to the maximum flow rate (Q_o) indicating a minimal leakage from the pump units of about 2%, as reflected by the steepness of the pump characteristic. Thus, the pump continues to operate almost at its full potential (at a given frequency) with minimal leakage for an increase to system pressure losses in the range from zero to $0.736\,\mathrm{mm\,H_2O}$.

As an estimate of the maximum flow rate per individual choanocyte, i.e. the positive displacement flow ($Q_{\mathrm{pos}} \simeq \lambda f A$), we use the dimensions for *S. lacustris* choanocytes [8, Table 1 therein]. Employing the mean value of collar width at the collar base (3.1 μm) and the collar angle (-5 deg), the collar width at its tip is $\sim 1.67\,\mu\mathrm{m}$ resulting in a flow rate of $Q_{\mathrm{pos}} \sim 0.43 \times 10^{-6}\,\mathrm{ml\,h^{-1}}$. This value is similar to the mean flow rate per choanocyte for different species of both glass sponges and demosponges (Table C.1), obtained from measured volume flow rate (per ml sponge) divided by the number of choanocytes per mm^3 [3]. This suggests that choanocytes as the basic pumping units are functionally similar among different species and the positive displacement pumping rate appears to be a realistic approximation of the mean flow rate of a choanocyte. Nonetheless, the exact pumping rate per individual choanocyte might still vary even among those inside the same chamber as a result of

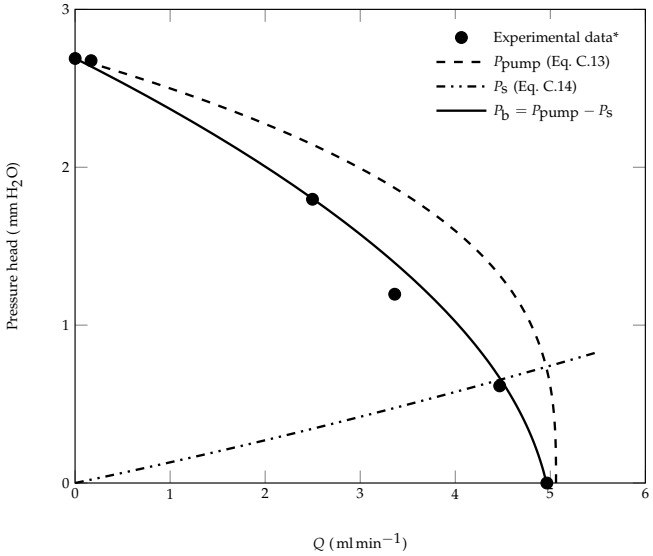

Fig. C.4: Modeled pump characteristic (P_{pump}, obtained from Eq. C.13 with $C_1 = 0$, dashed) minus estimated system characteristic (P_{s}, Eq. C.14, dash-dot) gives resulting back-pressure characteristic (P_{b}, solid) in good agreement with experimantal data (symbols). * [5, Fig. 1c therein].

observed variations in both beat frequency (ranging from 3.2 to 20.9 Hz for *Spongilla lacustris*) and dimensions of the collar [8].

3.3 Choanocytes in chamber

In this section, using the choanocyte model of Figure C.2C, we present results of CFD simulations of the flow in and around the choanocyte of *Spongilla lacustris* as a model organism, discuss the possible interaction among adjacent choanocytes, and study the influence on pump performance of the glycocalyx mesh and of the secondary reticulum (R2).

3.3.1 Choanocytes interactions

To examine the possible hydrodynamic interaction between adjacent choanocytes exposed to the same pressure load, we measure the flow rate and the power required for the pumping under different scenarios obtained by applying different boundary conditions on the outer boundary of the solution domain in Figure C.2C.

Table C.2 lists the results for 4 different boundary conditions (BC) for two cases, i.e. the normal one where the vane of the flagellum exists over the length of the distal part of the collar (partial), and the hypothetical one where

Species	$Q_{ch}(\mathrm{ml\,h^{-1}}) \times 10^6$
Cliona delitrix	0.22 ± 0.01
Callyspongia vaginalis	0.85 ± 0.13
Tethya californiana	0.06 ± 0.01
Haliclona mollis	0.35 ± 0.03
Neopetrosia problematica	0.36 ± 0.06
*Aphrocallistes vastus**	0.51 ± 0.34
*Haliclona urceolus***	$0.20 \pm -$

Table C.1: Mean volume flow rate (Q_{ch}) per choanocyte for different species of demosponges and one species of glass sponge (*Aphrocallistes vastus*). Data obtained from measured volume flow rate divided by the number of choanocytes, both per unit volume of sponge [3, Table 1 and 2 therein], * [7, Table 3 therein], and ** [5, Table 1 therein]. For comparison, for demosponge *Spongilla lacustris*, the mean volume flow per choanocyte is calculated to $Q_{\mathrm{pos}} \simeq 0.43 \times 10^{-6}\,\mathrm{ml\,h^{-1}}$.

the vane exists along the full length of the flagellum (full). The results are for an imposed pressure difference of $1\,\mathrm{mm\,H_2O}$ between the inlet and the outlet of the domain. For both cases of partial and full flagellar vane, there is no change in either flow rate or power, regardless of the in phase (BC 2) or completely out of phase (BC 3) flagella beat, as compared to the reference case (BC 1), indicating negligible hydrodynamic interactions between adjacent choanocytes. The results are also unaltered for those choanocytes sitting far from the flow inlet through a prosopyle in which case we let water enter through the lower sides into the domain (BC 4). The interaction is expected to be weak since the part of the flagellum responsible for the pressure rise lies within the distal part of the collar that is tightly held together and sealed with the glycocalyx mesh, hence to a large extend isolating this pumping region from the neighboring ones. The lack of hydrodynamic interaction might be one reason why the beat of the flagella within a given chamber is not synchronized [8].

Additionally, a full flagellar vane does not significantly change the volume flow rate as compared to the partial flagellar vane. This is not surprising since the free part of the flagellum cannot produce any pressure rise when not beating in a sealed collar, instead it dissipates the energy by stirring the flow in a very viscous environment. Thus, in view of the non-negligible increase in power expenditure (by about 13%) and no gain in pumping rate it makes functional sense that the vane does not extend beyond the collar filter [14] while (as another benefit) 'it appeared to narrow or be absent' toward the base of the flagellum [8]. Likewise, since the vaned flagellum and collar interaction takes place only in the distal sealed part of the collar, the first contact (or small gap) between flagellum and collar is expected to be where the glycocalyx mesh begins. This feature has been reported by [8] for

BC	partial flagellar vane		full flagellar vane	
	Q ($\mu m^3 s^{-1}$)	$\mathcal{P}$ (fW)	Q ($\mu m^3 s^{-1}$)	$\mathcal{P}$ (fW)
1	454	12.6	456	14.2
2	453	12.6	456	14.3
3	453	12.6	456	14.3
4	454	12.6	456	14.2

Table C.2: Flow rate (Q) and power expenditure ($\mathcal{P}$) by a partial and full flagellar vane for 4 different boundary conditions (BC) on the choanocyte model (Figure C.2C), subject to an imposed pressure head of 1 mm H_2O. (1) specified inlet pressure on sides, (2) periodicity on sides, (3) symmetry on sides, (4) specified inlet pressure on sides with no prosopyle. The hydrodynamic interaction between adjacent choanocytes is negligible, and the full flagellar vane does not increase flow rate significantly, as compared to the partial flagellar vane, but is energetically more demanding.

choanocytes of *Spongilla lacustris*.

3.3.2 Effect of glycocalyx mesh

Thus far, we have treated the fine-meshed part of the collar as impermeable to flow. But how vital is the presence of the glycocalyx mesh and how dense should it be?

To answer these questions, we first simulate the choanocyte model (Figure C.2) subject to an imposed canal system pressure loss of $P_{ch} = 1$ mm H_2O (i.e. total pressure loss excluding contributions from within choanocyte chambers), modeling the distal part of the collar with the same permeability as that of the microvilli array in the proximal part of the collar. Figure C.5 shows the velocity fields for cases with and without the presence of the glycocalyx mesh. With the mesh, water enters through the base of the collar, then its pressure increases in the fine-meshed part of the collar, and it enters the inner high pressure zone above the secondary reticulum (R2 in Figure C.2C). Without the mesh, a portion of water entering the collar from the base leaks out from the distal part rather than flowing into the high-pressure zone above the reticulum, thus reducing the net pumping rate (see Figure C.6). Therefore, the primary hydrodynamic function of the glycocalyx mesh is to seal the distal part of the collar to prevent a leakage while allowing the water to be pressurized in order to ultimately flow through the canal systems of the sponge. In the low Reynolds number regime of flow in flagellated chambers, this sealing is of paramount importance since with the lack of inertia, the flow is pressure driven only. Besides the hydrodynamic function, the mesh also provides support against the pressure forces from within the collar to prevent a possible deformation or spreading of the microvilli.

Next, to account for possible leaks through the glycocalyx mesh, we model the fine-meshed distal part of the collar as a permeable structure composed

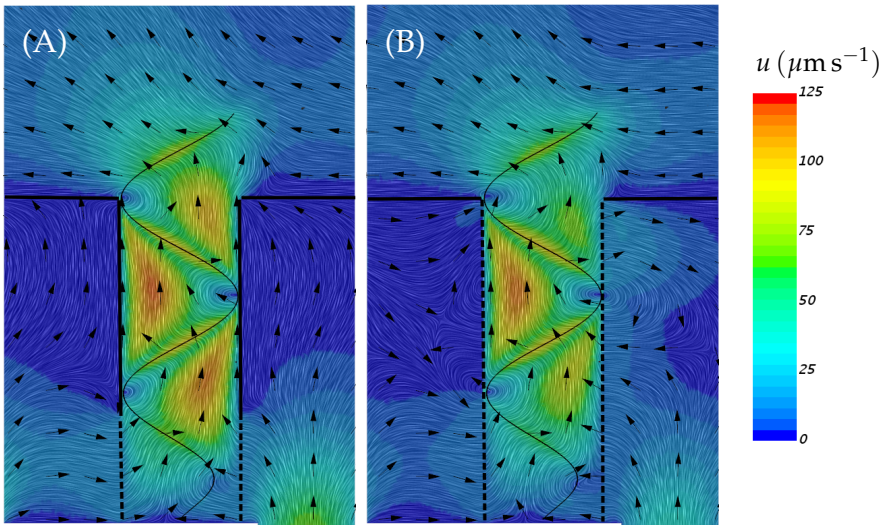

Fig. C.5: Velocity fields in the choanocyte model (Figure C.2C) with (A) and without (B) presence of the glycocalyx mesh on the distal 2/3 length of the collar, for the case of an imposed canal system pressure loss of $P_{\mathrm{ch}} = 1\,\mathrm{mm\,H_2O}$. With the mesh, flow enters the collar at its base, and after its pressure increases inside the sealed part of the collar, it leaves the collar toward the apopyle. Without the mesh, some flow leaks out through the distal part of the collar, reducing the net pumping rate as seen from the reduced inflow through the prosopyle at the lower right (see also Figure C.6). The color bar and arrows (constant length) show the magnitude and direction of the velocity field, respectively.

Species	$P_{ch}(\mathrm{mm\,H_2O})$
Cliona delitrix	5.803
Callyspongia vaginalis	2.676
Tethya californiana	0.233
Haliclona mollis	0.583
Neopetrosia problematica	0.867
*Aphrocallistes vastus**	0.855
*Haliclona urceolus***	0.436

Table C.3: Pressure loss from the canal system (P_{ch}) (i.e. total pressure loss excluding contributions from within choanocyte chambers) for different species of demosponges and one species of glass sponge (*Aphrocallistes vastus*). The relatively high pressure loss in canals requires a high yield pump. Data extracted from [3], * [7], ** [5].

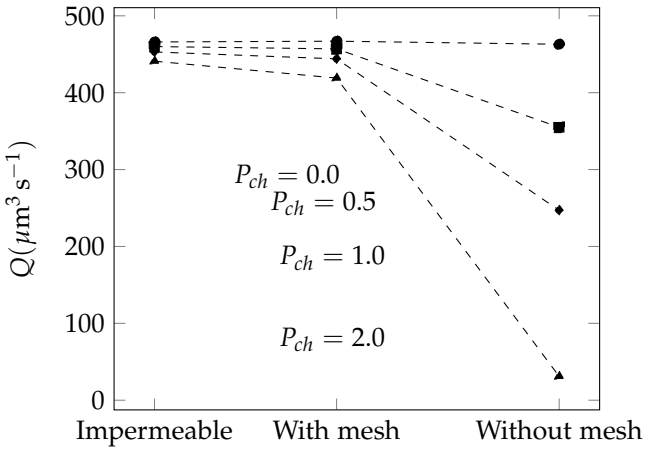

Fig. C.6: Volume flow rate (Q) versus permeability of the collar for different values of imposed canal system pressure loss P_{ch} ($\text{mm}\,\text{H}_2\text{O}$). For $P_{\text{ch}} = 0$, the volume flow rate is constant. For increasing values of imposed system pressure loss, the fine glycocalyx mesh is essential for the pump to deliver the required flow rate.

of two layers of $\sim 0.024\,\mu$m filaments with a pore size of $\sim 0.045\,\mu$m [7, 8]. This may be a conservative estimate of the density because of the very small spacing between the microvilli in this region [8, 9].

Figure C.6 presents the volume flow rate for different levels of imposed pressure and for three cases of permeability of the distal part of the collar, i.e. impermeable, with the glycocalyx mesh, and microwilli without a mesh. When the pressure load is negligible, flow rate is independent of the permeability. But as the pressure resistance increases, the beneficial effect of the glycocalyx mesh becomes evident; here the pump can handle any pressure load with little change in delivered flow rate. System pressure losses from canals vary among sponges (Table C.3) and may also vary within a given sponge body because of different locations of choanocyte chambers and various sizes of incurrent and excurrent canals [20]. Despite the conservative estimate of the permeability of the glycocalyx mesh it is seen to nearly act as an impermeable surface. It may also be noted that a zero pressure condition is essentially similar to the environment of choanoflagellates because they face no imposed pressure load from a canal system, and their flagella are able to create relatively high volume flow rates in free space (or near surfaces) [17, 21]. This may be one reason why the collar in choanoflagellates lack a dense mesh and instead, in some cases, have a fine ring of glycocalyx mesh encircling the microvilli [8]. But of course, the main purpose of the collar is to act as a filter which is not impaired by a narrow ring that might serve a structural purpose.

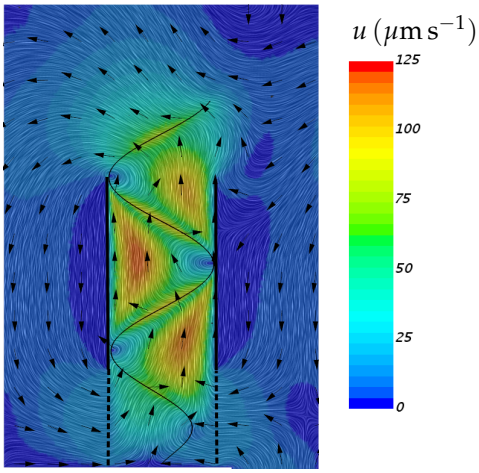

Fig. C.7: Velocity field in the choanocyte model of *S. lacustris* without the secondary reticulum (R2 of Figure C.2C) for no imposed system pressure loss ($P_{\mathrm{ch}} = 0$). While the flow through the collar exit is nearly the same as with the reticulum ($Q \sim 453\,\mu\mathrm{m^3\,s^{-1}}$) the net flow rate leaving the choanocyte model is very low ($Q = 60\,\mu\mathrm{m^3\,s^{-1}}$) because the pressure provided by the flagellum drives a strong backflow from the exit of the collar to its base as there is no reticulum to stop this. The color bar and arrows (constant length) show the magnitude and direction of the velocity field, respectively.

3.3.3 Effect of the secondary reticulum

The secondary reticulum (R2) separates the high pressure zone from the low pressure zone as shown in Figure C.2B [9]. We therefore examine the hydrodynamic importance of R2 by removing this structure from the model (Figure C.2C) for an ideal case of zero imposed canal system pressure loss. Figure C.7 shows the resulting velocity field in and around the choanocyte without the presence of R2. The flow rate through the collar is still similar to that without R2 ($453\,\mu\mathrm{m^3\,s^{-1}}$), but only $\sim$ 13% of this flow is found to enter the domain from the prosopyle. The rest is a recirculating backflow from the inner part of the chamber around the collar. Consequently, the net pumping rate drops dramatically although without becoming zero. But in the real case with the presence of pressure resistance from the canals, the choanocyte pump would fail completely leading to reversed flow driven by the imposed pressure load.

Hydrodynamically, the three design elements, i.e. the R2, the glycocalyx mesh on the collar, and the minimal gap between flagellar vane and collar, are crucial to the functionality of the choanocyte pump. As the glycocalyx mesh and the minimal gap are crucial to prevent leakage within individual choanocytes, the R2 reticulum is crucial for the assembly of choanocytes in the chamber to function in parallel, each being exposed to and able to deliver the required high pressure.

It remains to explain why the many choanocytes sit in a chamber with multiple prosopyles for inflow but a single apopyle for outflow. It is apparently not because of a favorable interaction because we have already shown that the hydrodynamic interaction between the choanocytes is negligible (Table C.2). Besides protection and being part of a larger organism, thanks to high choanocyte density and structural rigidity, it also brings variety to their diet [9, 12, 20]. The reduced filter area for capturing bacteria has directed choanocytes to primarily become strong pumps with a relatively low filtration rate, which is compensated by the ability of leucon sponges to generate a strong inflow to the sponge, drawing phytoplankton into long inhalant canals for capture which contributes about 80% to their diet [22] But the most compelling reason for near spherical choanocyte chambers is probably that they are a structurally practical and an optimal design that can feature a two-pressure zone essential for parallel-coupled pumps that must yield high pressure. Here it is noted that in both asconoid and sycoid sponges, choanocytes with cylindrical collars sit in close arrays on open surfaces, and there are no signs of reticula [10] which seems to agree with the fact that imposed flow resistance from the rather open canal structure is minimal.

3.4 Pump power and mechanical efficiency

The mechanical power expended by the beating motion of the flagellum in the choanocyte model (Figure C.2C), calculated from Eq. C.4 for the normal case of BC #1 (in Table C.2), is $\mathcal{P}_{\mathrm{P,mech}} = 12.6\,\mathrm{fW}$. For comparison the (reversible) useful pumping power received by the water flow at $Q = 454\,\mu\mathrm{m}^3\,\mathrm{s}^{-1}$ and an imposed system pressure loss of $1.0\,\mathrm{mm\,H_2O}$ plus the inner pressure drop of $0.95\,\mathrm{mm\,H_2O}$ through inlet to the collar, a total of $P_{\mathrm{T}} = 1.95\,\mathrm{mm\,H_2O}$, amounts to $\mathcal{P}_{\mathrm{P,rev}} = P_{\mathrm{T}}Q = 8.68\,\mathrm{fW}$. The ratio of these powers represents the mechanical efficiency of the choanocyte pump model, $\eta_{\mathrm{mech}} = \mathcal{P}_{\mathrm{P,mech}}/\mathcal{P}_{\mathrm{P,rev}} \approx 70\,\%$ which seems reasonable for a positive displacement pump. Our simulations also show η_{mech} to increase with decreasing gap width at higher values of pressure and flow rate, i.e. approaching an ideal displacement pump.

4 Appendix

4.1 Mesh study

Figure C.8 shows the discretized domain using a polyhedral mesh with a fine resolution in the gaps between the flagellum and the square-cross section collar. Figure C.9 shows the independence of the solution from the mesh size.

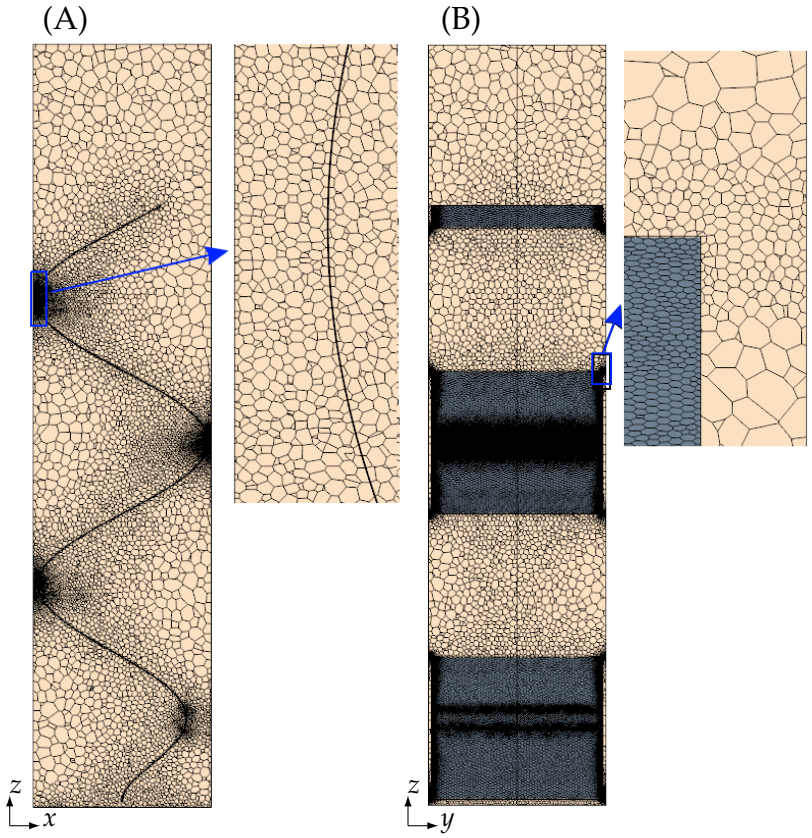

Fig. C.8: Mesh resolution in the gaps between the flagellum edges and the collar in the xy-plane (A) and the yz-plane (B).

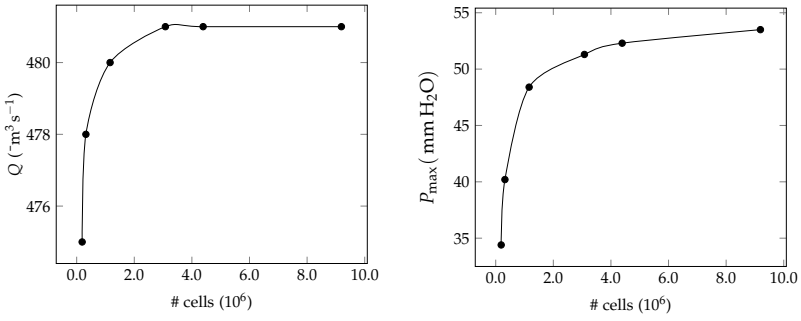

Fig. C.9: Mesh size independence of the volume flow rate Q and pressure rise P_{max} at two extreme conditions, i.e. free delivery condition (A) and shut-off condition (B).

References

[1] H. U. Riisgård and P. S. Larsen, "Filter-feeding in marine macroinvertebrates: Pump characteristics, modelling and energy cost," *Biol. Rev.*, vol. 70, no. 1, pp. 67–106, 1995.

[2] H. U. Riisgård, L. Kumala, and K. Charitonidou, "Using the F/R-ratio for an evaluation of the ability of the demosponge *Halichondria panicea* to nourish solely on phytoplankton versus free-living bacteria in the sea," *Mar. Biol. Res.*, vol. 12, no. 9, pp. 907–916, 2016.

[3] D. A. Ludeman, M. A. Reidenbach, and S. P. Leys, "The energetic cost of filtration by demosponges and their behavioural response to ambient currents," *J. Exp. Biol.*, vol. 220, no. 6, pp. 995–1007, 2017.

[4] H. U. Riisgård, S. Thomassen, H. Jakobsen, J. M. Weeks, and P. S. Larsen, "Suspension feeding in marine sponges *Halichondria panicea* and *Haliclona urceolus*: effects of temperature on filtration rate and energy cost of pumping," *Mar. Ecol. Prog. Ser.*, pp. 177–188, 1993.

[5] P. S. Larsen and H. U. Riisgård, "The sponge pump," *J. Theor. Biol.*, vol. 168, pp. 53–63, 1994.

[6] S. Vogel, *Life in Moving Fluids. The Physical Biology of Flow*, 2nd ed. Princeton, N. J.: Princeton University Press, 1994.

[7] S. P. Leys, G. Yahel, A. Reidenbach, V. Tunnicliffe, U. Shavit, and H. Reiswig, "The sponge pump: the role of current induced flow in the design of the sponge body plan," *PLoS One*, vol. 6, no. 12, p. e27787, 2011.

[8] J. L. Mah, K. K. Christensen-Dalsgaard, and S. P. Leys, "Choanoflagellate and choanocyte collar-flagellar systems and the assumption of homology," *Evol. & Develop.*, vol. 16, no. 1, pp. 25–37, 2014.

[9] N. Weissenfels, "The filtration apparatus for food collection in freshwater sponges (Porifera, Spongillidae)," *Zoomorph.*, vol. 112, no. 1, pp. 51–55, 1992.

[10] S. P. Leys and D. I. Eerkes-Medrano, "Feeding in a calcareous sponge: particle uptake by pseudopodia," *Biol. Bull.*, vol. 211, no. 2, pp. 157–171, 2006.

[11] E. J. Fjerdingstad, "The ultrastructure of choanocyte collars in *Spongilla lacustris* (l.)," *Z. Zellforsch.*, vol. 53, no. 5, pp. 645–657, 1961.

[12] G. Imsiecke, "Ingestion, digestion, and egestion in *Spongilla lacustris* (Porifera, Spongillidae) after pulse feeding with *Chlamydomonas reinhardtii* (Volvocales)," *Zoomorph.*, vol. 113, no. 4, pp. 233–244, 1993.

[13] P.-F. Langenbruch and N. Weissenfels, "Canal systems and choanocyte chambers in freshwater sponges (Porifera, Spongillidae)," *Zoomorph.*, vol. 107, no. 1, pp. 11–16, 1987.

[14] D. Mehl and H. M. Reiswig, "The presence of flagellar vanes in choanomeres of Porifera and their possible phylogenetic implications," *J. Zoo. Sys. Evol. Res.*, vol. 29, no. 4, pp. 312–319, 1991.

[15] J. B. Keller, "Viscous flow through a grating or lattice of cylinders," *J. Fluid Mech.*, vol. 18, no. 1, pp. 94–96, 1964.

[16] N. R. Silvester, "Some hydrodynamic aspects of filter feeding with rectangular-mesh nets," *J. Theor. Biol.*, vol. 103, no. 2, pp. 265–286, 1983.

[17] L. T. Nielsen, S. S. Asadzadeh, J. Dölger, J. H. Walther, T. Kiørboe, and A. Andersen, "Hydrodynamics of microbial filter feeding," *Proc. Natl. Acad. Sci. USA*, vol. 114, no. 35, pp. 9373–9378, 2017.

[18] A. C. Walshaw and D. A. Jobson, *Mechanics of fluids*. Longmans, Green, 1962.

[19] J. Happel and H. Brenner, *Low Reynolds number hydrodynamics*, 2nd ed. Kluwer Academic Publishers, 1983.

[20] S. P. Leys, "The choanosome of hexactinellid sponges," *Invert. Biol.*, vol. 118, no. 3, pp. 221–235, 1999.

[21] S. S. Asadzadeh, L. T. Nielsen, J. Dölger, A. Andersen, T. Kiørboe, P. S. Larsen, and J. H. Walther, "Hydrodynamic functionality of the lorica in choanoflagellates," *J. Roy. Soc. Inter*, vol. 16, no. 150, p. 20180478, 2019.

[22] F. Lüskow, H. U. Riisgård, V. Solovyeva, and J. R. Brewer, "Seasonal changes in bacteria and phytoplankton biomass control the condition index of the demosponge *Halichondria panicea* in temperate danish waters," *Mar. Ecol. Prog. Ser.*, vol. in press, 2018.

Article D

Hydrodynamic interactions with surfaces in choanoflagellate swimming

Seyed Saeed Asadzadeh[1], Mimi A. R. Koehl[2], Jens Honoré Walther[1,3]

[1]Section for Fluid Mechanics, Coastal and Maritime Engineering, Department of Mechanical Engineering, Technical University of Denmark, Nils Koppels Allé, 2800 Kgs. Lyngby, Denmark.
[2]Department of Integrative Biology, University of California, Berkeley, CA 94720, USA
[3]Computational Science and Engineering Laboratory, ETH Zürich, Clausiusstrasse 33 ETH-Zentrum, CH-8092 Zürich, Switzerland

This chapter is an unpublished work but it is written in a paper format

Contributions

Major contributions to the work:

- Conducting experimental observation of choanoflagellates near surfaces.
- Developing a new method to simulate force and torque free organism near surfaces.
- Carrying out presented CFD simulations.
- Writing the text.

Abstract

Choanoflagellates are unicellular eukaryotes and are united with animals by shared ancestry. They often have a collar filter composed of tentacles extending from the cell, and a flagellum which creates a flow or propel the cell. Some choanoflagellates have different and distinct life forms, among which are fast swimmers which lack the collar filter. Fast swimmers are believed to be dispersal form, but it remains yet unknown whether this dispersal form is used in conjunction with physical or chemical sensing. Fast swimmers attach themselves onto surfaces and differentiate into thecate cells. Here, we study trajectory of fast swimmers in the vicinity of surfaces both experimentally and numerically and explore how hydrodynamic interaction with surfaces impacts their trajectory. We find that unless very close to a surface, hydrodynamic interaction does not substantially affect their trajectory, but rather their initial swimming direction (and possible flicks) are the determining factor in directing them toward surfaces. However, we frequently observe that fast swimmers swim close to surfaces, arguably looking for a suitable spot to attach themselves. The hydrodynamics then will be beneficial in keeping the fast swimmers close to a surface while they navigate. Finally, we observe that after attachment to a surface and remaining there for approximately 45-60 minutes, fast swimmers detach themselves from the surface and swim away. This observation happens in the absence of bacteria, while it has been previously reported that in the presence of bacteria, attached fast swimmers differentiate into thecate cell after 45 minutes. These two observations suggest that the fast swimmers are not just stuck to a surface that they encounter, but rather retaining their position is purposeful with the presence of bacteria as a determining factor.

1 Introduction

Choanoflagellates are single-celled microeukaryotes and share ancestry with choanocytes of sponges. Both cells are equipped with a flagellum that drives the flow through the collar filter where the prey is captured [1–3]. Some choanoflagellates are able to differentiate into different forms, the prime example of which is choanoflagellate *Salpingoeca rosetta* which has five distinct cell types [4]. These types include two colonial and three solitary forms. Solitary *S. rosetta*, in response to environmental cue, can form slow swimmers, fast swimmers, and thecate cells. Slow swimmers and thecate cells are morphologically similar and have a relatively long collar filter. However, fast swimmers have a very short collar and it is believed they are dispersal life form of choanoflagellates, but it remains yet unknown whether this dispersal form is used in conjunction with physical or chemical sensing.

The waters of the ocean were assumed for decades to be a homogeneous environment, but recent work has shown the water column to be a very dynamic and heterogeneous environment [5]. Microorganisms, including choanoflagellates, experience and interact with a world full of physical

and chemical gradients either in unbounded flows or in the vicinity of surfaces. Many motile microorganisms are capable of directed motion toward attractants or away from repellents, a process called "taxis". For example, bacteria and spermatozoa use chemotaxis to move up or down a concentration gradient of a chemical cue. It has also recently been discovered that fast swimmers are capable of taxis toward PH 6-7, which could correspond to an acidic environment caused by a concentrated patches of bacteria [6].

Choanoflagellates' natural habitat in vicinity of surfaces (such as the surface of a real substratum in an estuary or a marine snow particle, organic detritus falling from the upper layers of the water column) is markedly different from an unbounded flow. In such environment, different physical and chemical environmental cues might interfere with each other resulting in an impaired or even improved taxis [7]. Therefore, it is of interest to study how different physical and chemical cue might contribute in taxis. One important physical interaction is hydrodynamic interactions in the vicinity of surfaces. It is known that based on far-field flow model, presence of a no-slip boundary surface results in attraction or change in trajectory of the microswimmer [8, 9]. However, this simplification does not account for other components of the flow in the near field where the attraction is higher.

In this report, we first experimentally study the effect of a no-slip wall on the trajectory of fast swimmer choanoflagellates at different distances from the wall. We will then, using computational fluid dynamics (CFD), study how presence of a surface changes the swimming velocity and rotation rate of fast swimmers.

2 Morphology

We use the same morphology for the fast swimmer as in [10]. The fast swimmer has oval cell, with a short collar (0.6 μm), with a flagellum that beats in plane (Fig. D.1). The cell has a length of 4.4 μm and width of 2.5 μm. The displacement of the flagellum is modeled in the x direction (in a local reference frame moving with the prey) as a simple traveling wave:

$$d(y,t) = (1 - e^{x/\delta})(ax + b)\sin\left(\frac{2\pi}{\lambda}(x - Vt)\right) \tag{D.1}$$

where d is the lateral displacement of the flagellum, $\delta = -3.3\,\mu$m the characteristic length scale of the amplitude modulation, $a = 0.13$ and $b = 0.61\,\mu$m are the wave parameters, $V = \lambda f$ the wave speed, in which $f = 24.3$ Hz is the frequency and $\lambda = 34.9\,\mu$m the wavelength, y the centerline axis of the collar, and t time.

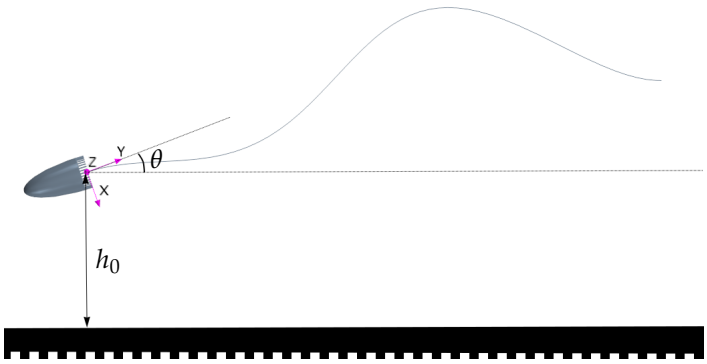

Fig. D.1: CFD model of fast swimmer choanoflagellate *S. rosetta* positioned at distance h_0 from the wall with orientation angle θ with respect to the wall.

3 Method

In this section we first describe the experiments and then numerical approach for simulating the freely swimming choanoflagellate.

3.1 Experiments

Experiments were conducted at the Koehl Lab [1]. The choanoflagellate *S. rosetta* was cultured and prepared by the King lab [2] as described in [4]. In the first days (day 1 to day 3) the culture had only slow swimmers. In the lack of bacteria and nutrients, the slow swimmer then begin to differentiate into fast swimmers, such that in day 5 the density of fast swimmers is the highest. Later, density of both slow and fast swimmers degrades. Therefore it is important to have cultures with different 'ages' to have suitable density of fast swimmers to continuously perform the experiment.

3.2 Computational fluid dynamics

The governing equations of an incompressible Newtonian fluid with density ρ and viscosity μ are the continuity and Navier-Stokes equations:

$$\nabla \cdot \mathbf{u} = 0 \tag{D.2}$$

[1] https://ib.berkeley.edu/labs/koehl/
[2] https://kinglab.berkeley.edu/

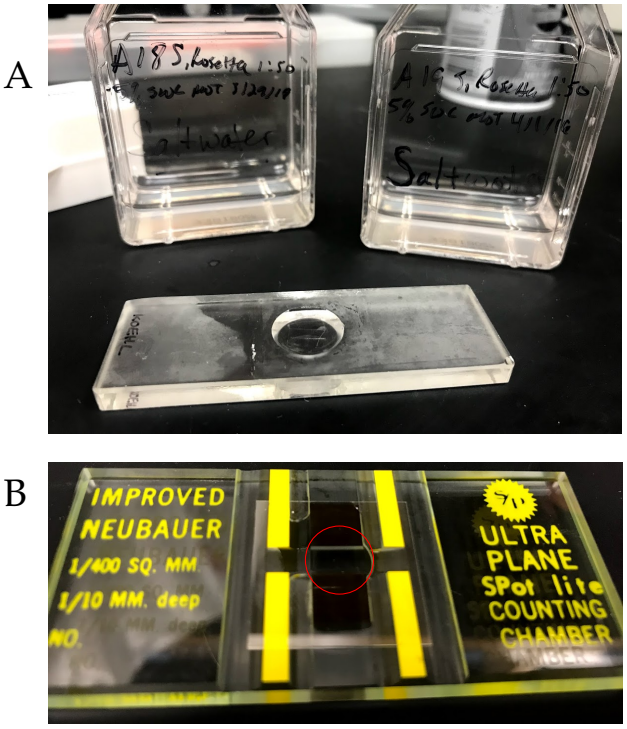

Fig. D.2: Culture of choanoflagellates and slides used in the experiments. A) A slide with a 5 *mm* deep well next two *S. rosetta* samples cultured at two different days. B) A cell counting chamber (Type: Improved Neubauer Ultra Plane SPot 1/10mm Deep 1/400 Sq MM) used for recording fast swimmer near a vertical surface. Red circle shows the position of vertical wall.

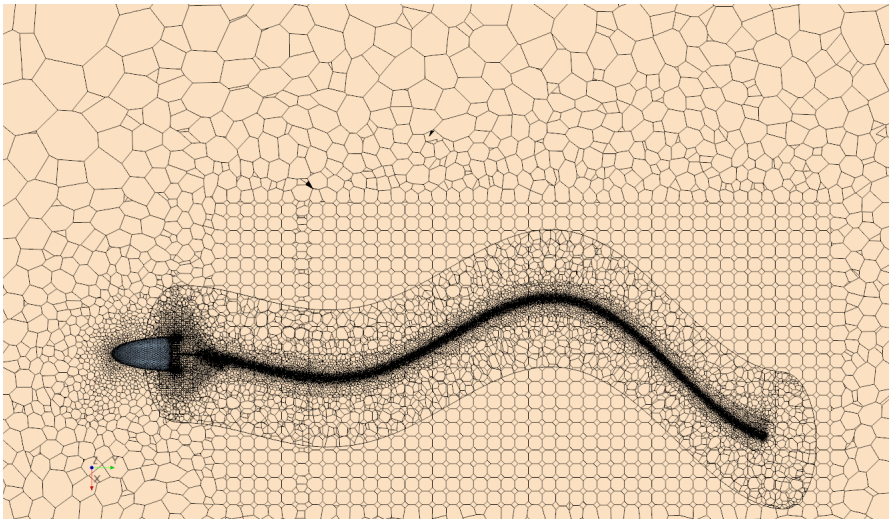

Fig. D.3: Discretized domain with overset mesh including only the flagellum and a stationary mesh that includes the cell and the short collar with background domain.

$$\rho\left(\frac{\partial \mathbf{u}}{\partial t} + (\mathbf{u}\cdot\nabla)\mathbf{u}\right) = -\nabla p + \mu\nabla^2\mathbf{u} \tag{D.3}$$

where $\mathbf{u}$ and p denote the velocity and pressure, respectively.

We employ finite volume to discretize the governing equations using the commercial CFD code STAR-CCM+(14.02.011-R8). We use overset technique to model the flagellum beat. Overset meshes are used to discretize a computational domain with several different meshes that overlap each other. To reduce the computational cost, we make an overset mesh which includes only the flagellum and a stationary mesh that includes the cell and the short collar with background domain (Fig. D.3). In the overset mesh, we use morphing technique to move the mesh in the overset region. Morphing redistributes the mesh vertices in response to the movement of the flagellum.

A freely swimming organism is force and torque free [8]. To simulate the freely swimming fast swimmer, we have developed an iterative method which at the end of iterations ensures a force and torque free swimmer. In so doing, the swimmer is fixed with respect to a local frame which has a translational ($\mathbf{U}$) and rotational (Ω) velocity. The iterative method will find the $\mathbf{U}$ and Ω such that at the end of each time step, the total forces and torques on the swimmer converge to zero. Fig **??** shows the procedure for finding $\mathbf{U}$ and Ω during the iteration process. In this process, the constants C_F and C_L are arbitrary and much smaller (typically 2-3 order of magnitudes) than $(6\pi\mu D)^{-1}$ and $(8\pi\mu D^3)^{-1}$, respectively, given D is the mean length scale of

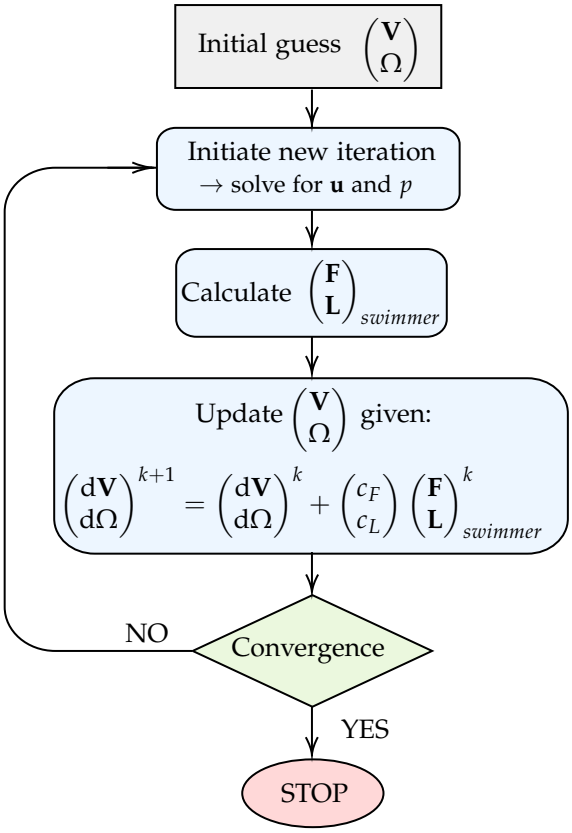

Fig. D.4: Procedure for finding tranlational and rotational velocities (**U** and Ω, respectively) of the local frame moving with the swimmer during the iterative process.

the swimmer.

To simulate the fast swimmer near a surface, the swimmer is initially positioned parallely (central axis, y-direction parallel to the wall) at an arbitrary distance h_0 from the wall (Fig. D.1). The swimmer has three degrees of freedom; translation velocity in x and y directions, and rotation rate ω in z direction. Once the flagellum beats, the swimmer will rotate (θ degrees, the angle between the central axis and the wall, Fig. D.1) and its distance from the wall changes. At any instant of time, the tranlational and rotational velocity of swimmer is then a function of h, θ, and the beat cycle phaseϕ (indicating the position of the flagellum during the beat cycle):

$$V = [Vx, Vy, \omega] = f(h, \theta, \phi) \tag{D.4}$$

In order to reduce the computational costs of simulating the swimmer for

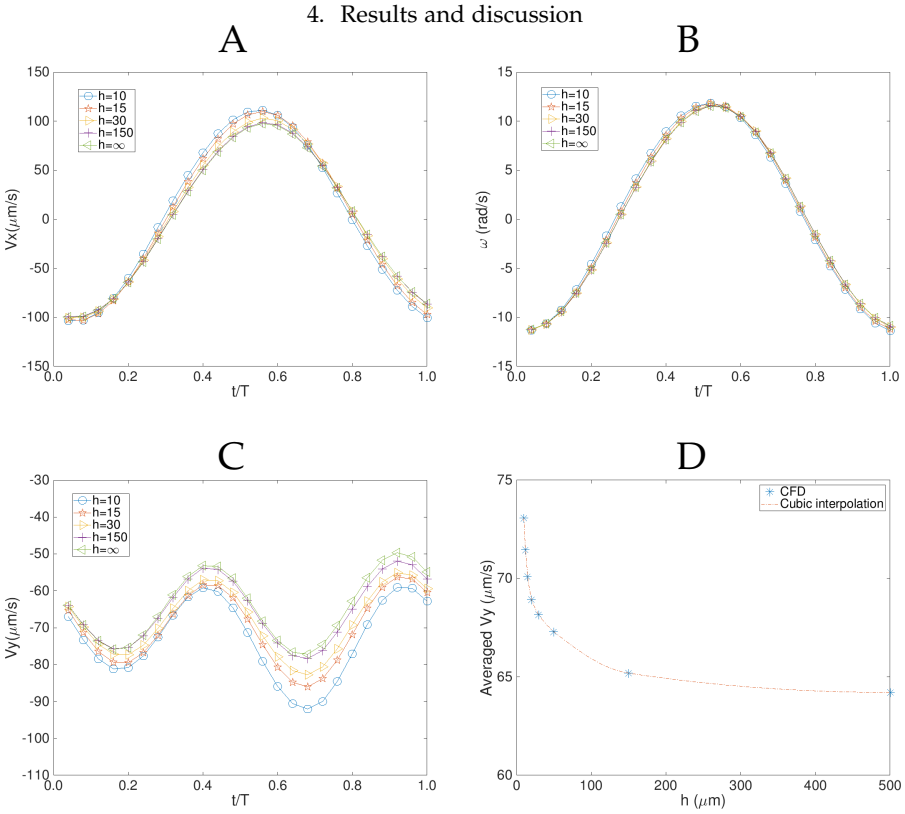

Fig. D.5: Translational and rotational velocity (A-C), and decay of the averaged swimming velocity (D) at different distances (in μm) from the wall over one beat cycle. The presence of the wall has an insignificant impact on the lateral and rotational velocity, but it increases the magnitude of the swimming velocity. The effect of wall on the swimming velocity is most significant very close to the wall.

many beat cycles in order to construct the trajectory, the swimmer is, instead, simulated at some discrete h and θ for a complete beat cycle ($\phi \rightarrow 0$ to 2π). With these sets of simulations, a table is generated base on Eq. D.4. Now, starting from any position with some arbitrary h, θ and ϕ, the velocity vector of swimmer V is interpolated from the table and with the corresponding time step, the new position and angle (h, θ and ϕ) of the swimmer is iteratively updated. With this procedure the trajectory of the swimmer will be constructed from any arbitrary position.

4 Results and discussion

4.1 Hydrodynamic attraction

We first simulate the fast swimmer in the absence of any nearby surfaces. This allows us to choose the appropriate constants as explained in the flowchart in the previous chapter. For the swimmer in the free space, the swimming velocity is calculated as $65\,\mu$m/s in a good agreement with what Nguyen et al. found ($64\,\mu$m/s) [10] where there the authors used another CFD method, the Regularized Stokeslet method.

Figure D.5 show the translational and rotational velocity at different distances from the wall over one beat cycle. The effect of the wall is an increased swimming velocity, and the effect is stronger in the second half period. However, the presence of the wall does not impact significantly the lateral velocity, with a negligible effect on the rotational velocity. The net impact of the wall is then an attraction toward the wall and an increase in the mean swimming velocity. According to Figure D.5C, in the first half beat period, the fast swimmer is oriented away from the wall, while in the second half period it is oriented toward the wall. Now, in the second half period the organism swim faster than the first half period resulting in a net attraction to the wall during the complete beat cycle. Figure D.6A shows the constructed trajectory of the fast swimmer starting from three different distances from the wall. The more the fast swimmer close to the wall, the stronger hydrodynamic attraction is experienced as a result of an increased mean swimming velocity (Fig. D.5D). Figure D.6B shows the observed trajectory of one fast swimmer swimming parallel to a surface (entering the scene from the right) which becomes closer to the surface when exiting the scene.

The above attractions are for a swimmer initially positioned parallel to the wall. But what happens if the swimmer is not initially parallel to the wall? As it is shown in Figure D.6A, at a distance of $h = 15\,\mu$m from the wall, the attraction angle, the angle between swimming trajectory and the wall is approximately 3°, a relatively small angle. This means if the fast swimmer is initially oriented (away from the wall) with some angle bigger than the attraction angle, it will swim away from the wall. In addition, the attraction is effective only in a very short range and becomes weaker as distance from the wall increases (Fig. D.5D). At a distance above $h > 150\,\mu$m, even the swimming velocity is effectively unaffected by the presence of the wall. Consequently, assuming that the fast swimmers swim almost on a straight line with no flicks (as apposed to the run and tumble swimming pattern in bacteria), it is dominantly the fast swimmer initial swimming direction that is the determining factor in becoming closer to or away from the wall. Therefore, unless very close to the wall, trajectory of the fast swimmers is unaffected by the presence of the wall. Figure D.7 show the observed trajectory of many

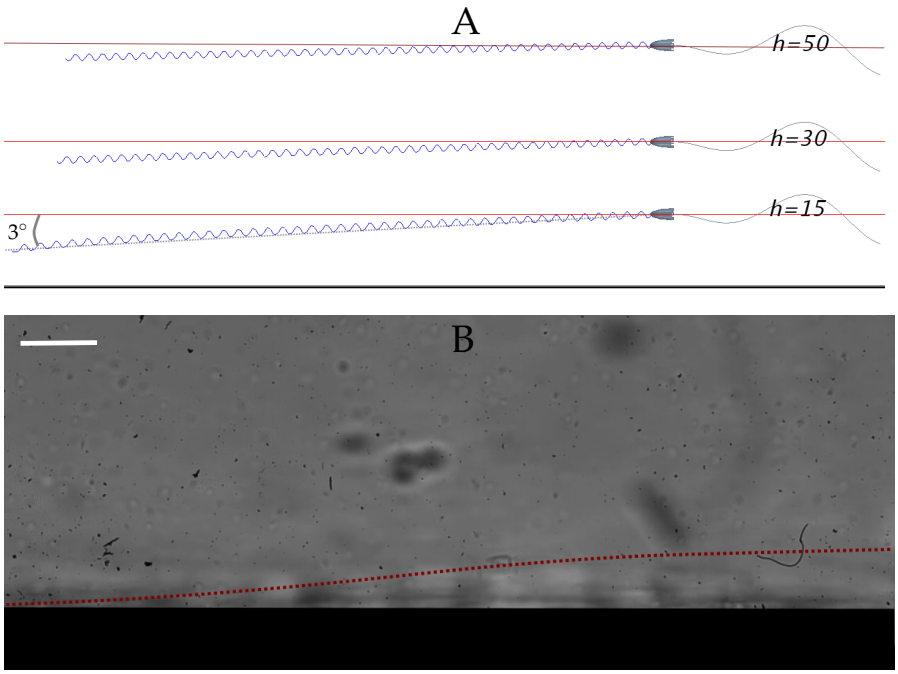

Fig. D.6: Trajectory of a fast swimmer. A) Three constructed trajectories based on the CFD simulation results at three different initial h given in μm. B) The observed trajectory (red dashed line) of a fast swimmer near a surface (black color). The oscillations in the observed trajectory are smoothed. Scale bar, 20 μm.

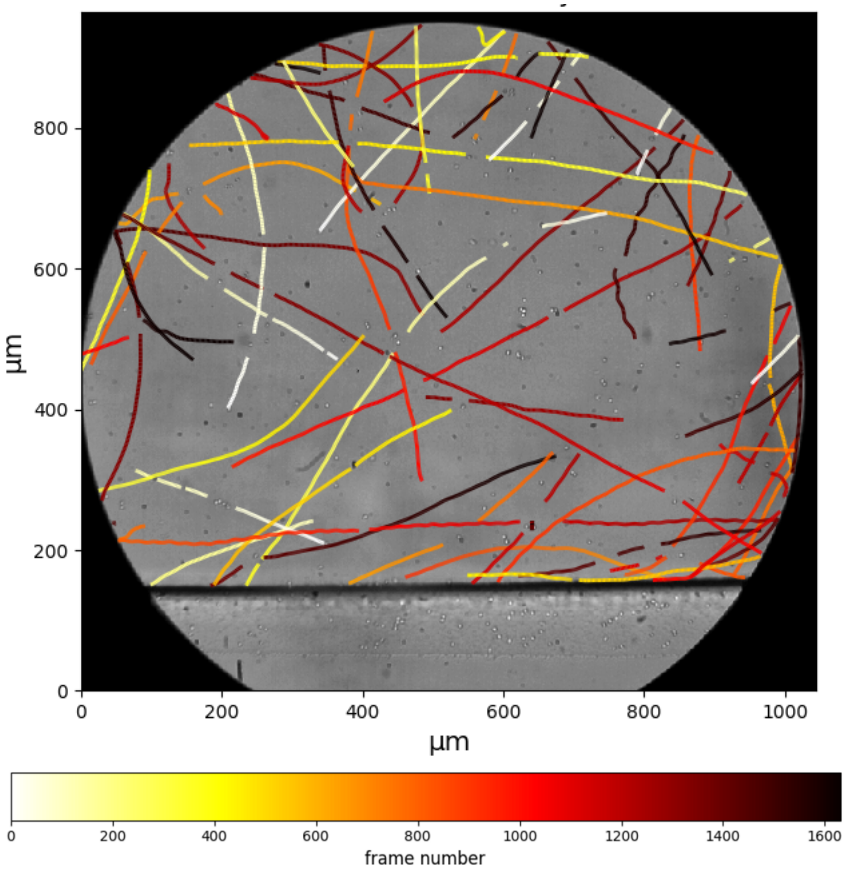

Fig. D.7: Trajectory of fast swimmers near a surface. To show the direction of swimming, trajectories are colored by frame number. The darker colors are later in the video.

fast swimmers near a surface which does not show an effect from the wall on the trajectory of the swimmers.

4.2 Swimming close to surfaces

Thus far both the experimental and the CFD results indicate that hydrodynamic effects do not result in a strong attraction of fast swimmers to surfaces. However, once swimming close to the surface, hydrodynamic attraction becomes stronger. It has been directly observed that fast swimmers settle on surfaces and then differentiate into thecate cells [4]. In addition, looking at the number of fast swimmers at different depth below the cover slip revealed that their presence is much higher right below the cover slip than the depth of the well. There are often some fast swimmers attached to the surface of

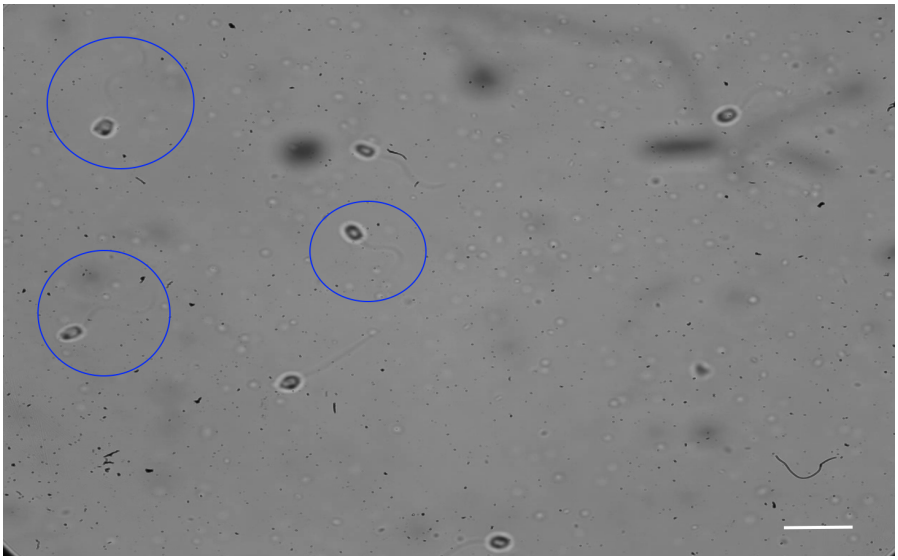

Fig. D.8: Snapshot of a video recording showing seven fast swimmers right below the coverslip where three of them are swimming (shown inside blue circles) and four are stationary, attached to the cover slip. Scale bar, 20 μm.

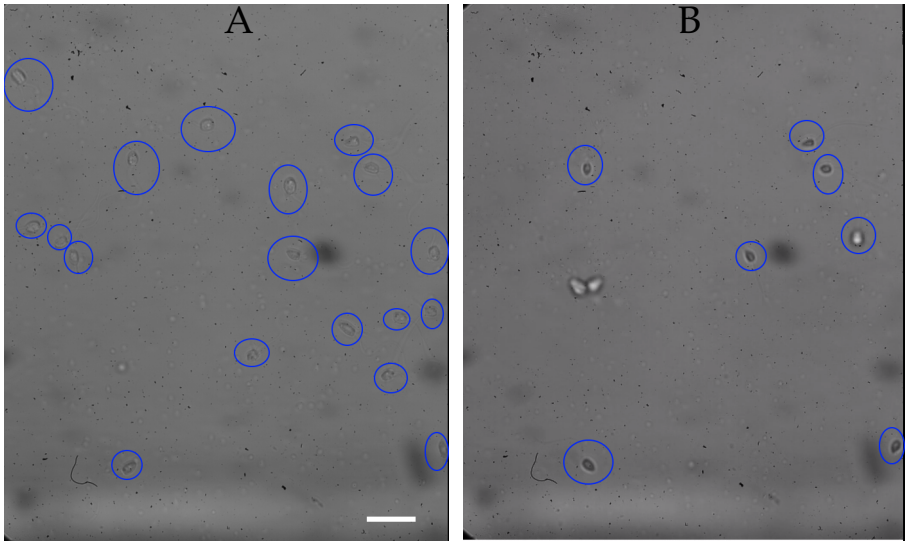

Fig. D.9: Escaping the surface in the absence of bacteria. A) Initially there are 18 fast swimmers attached to the surface(and here marked with a blue) in the view field. B) After 60 minutes 9 fast swimmers detach themselves from the surface and swim away. Scale bar, 20 μm.

the cover slip or are freely swimming just underneath and parallel to the cover slip (Fig D.8). Therefore, the fact that they are usually swimming underneath the cover slip might indicate that they are looking for a 'suitable' location to attach themselves, so they later can differentiate into the thecate cells. Consequently, if swimming near surfaces is of interest to the fast swimmers, hydrodynamic interaction is playing a substantial role by keeping them close to the surface.

Finally, it has been reported that once a fast swimmer attaches to a surface, in the present of bacteria in the media, it takes approximately 45 minutes while the cell differentiate into a bacteria-absorbing thecate cell [4]. In our experiment though, the culture was free of bacteria, and we have observed that once attached to the surface, the fast swimmers remain there for about 40-60 minutes, but then they begin detaching themselves from the surface and swim away (Fig D.9). Therefore, it is possible that fast swimmers are looking for surfaces in order to differentiate into the feeding thecate cells only in the absence of bacteria, otherwise it would be a futile differentiation.

References

[1] B. S. Leadbeater, *The Choanoflagellates: Evolution, Biology and Ecology*, 1st ed. Cambridge: Cambridge University Press, 2015.

[2] S. S. Asadzadeh, P. S. Larsen, H. U. Riisgård, and J. H. Walther, "Hydrodynamics of the leucon sponge pump," *J. Roy. Soc. Inter*, vol. 16, no. 150, p. 20180630, 2019.

[3] S. S. Asadzadeh, L. T. Nielsen, J. Dölger, A. Andersen, T. Kiørboe, P. S. Larsen, and J. H. Walther, "Hydrodynamic functionality of the lorica in choanoflagellates," *J. Roy. Soc. Inter*, vol. 16, no. 150, p. 20180478, 2019.

[4] M. Dayel, R. Alegado, S. Fairclough, T. Levin, S. Nichols, K. McDonald, and N. King, "Cell differentiation and morphogenesis in the colony-forming choanoflagellate *Salpingoeca rosetta*," *Develop. Biol.*, vol. 357, no. 1, pp. 73–82, 2011.

[5] R. Stocker, "Marine microbes see a sea of gradients," *Science*, vol. 338, no. 6107, pp. 628–633, 2012.

[6] G. L. Miño, M. A. R. Koehl, N. King, and R. Stocker, "Finding patches in a heterogeneous aquatic environment: pH-taxis by the dispersal stage of choanoflagellates," *Limnology and Oceanography Letters*, vol. 2, no. 2, pp. 37–46, 2017.

[7] H. Marcos, Fu, T. Powers, and R. Stocker, "Bacterial rheotaxis," *Proc. Natl. Acad. Sci. USA*, vol. 109, no. 13, pp. 4780–4785, 2012.

[8] E. Lauga and T. R. Powers, "The hydrodynamics of swimming microorganisms," *Rep. Prog. Phys.*, vol. 72, no. 9, p. 096601, 2009.

[9] E. Lauga, "Bacterial hydrodynamics," *Annu. Rev. Fluid Mech.*, vol. 48, pp. 105–130, 2016.

[10] H. Nguyen, M. A. R. Koehl, C. Oakes, G. Bustamante, and L. Fauci, "Effects of cell morphology and attachment to a surface on the hydrodynamic performance of unicellular choanoflagellates," *J. Roy. Soc. Inter*, vol. 16, no. 150, p. 20180736, 2019.

DTU Mechanical Engineering
Section of Fluid Mechanics, Coastal and Maritime Engineering
Technical University of Denmark

Nils Koppels Allé, Bld. 403
DK-2800 Kgs. Lyngby
Denmark

Tlf.: +45 4525 1360
Fax: +45 4525 1961

www.mek.dtu.dk

August 2019

ISBN: 978-87-7475-574-6

DCAMM
Danish Center for Applied Mathematics and Mechanics

Nils Koppels Allé, Bld. 404
DK-2800 Kgs. Lyngby
Denmark
Phone (+45) 4525 4250
Fax (+45) 4525 1961

www.dcamm.dk

DCAMM Special Report No. S266

ISSN: 0903-1685